MINISTRY OF HIGHER EDUCATION AND SCIENTIFIC RESEARCH
UNIVERSITY OF BABYLON
COLLEGE OF ENGINEERING
DEPARTMENT OF CIVIL ENGINEERING

Nonlinear Finite Element Analysis of steel fibrous Reinforced Concrete beams subjected to Combined Shear, Bending and Torsion with Opening

A THESIS
SUBMITTED TO THE COLLEGE OF ENGINEERING OF UNIVERSITY OF BABYLON IN FULFILLMENT OF THE PARTIAL REQUIREMENTS FOR THE DEGREE OF MASTER OF SCIENCE IN STRUCTURAL ENGINEERING

By

Isra'a Hassan Nile

Supervised by

Asst. Prof. Dr. **Mustafa B. Dawood**
Prof. Dr. **Ammar Y. Ali**

Rabea' al awaal 1428 **November 2009**

جمهورية العراق
وزارة التعليم العالي والبحث العلمي
جامعة بابل
كلية الهندسة
قسم الهندسة المدنية

التحليل غير الخطي ثلاثي الابعاد بواسطة العناصر المحددة للأعتاب الخرسانية المسلحة بالألياف الحديدية والمعرضة لحمل مركب من عزمي القص ,الانحناء و اللي والمزودة بفتحات

رسالة

مقدمة الى كلية الهندسة ـــ جامعة بابل

كجزء من متطلبات نيل شهادة ماجستير

علوم في الهندسة الإنشائية

من قبل

أسراء حسن نايل

بإشراف

أستاذ مساعد

د. مصطفى بلاسم داوود

أستاذ

د. عمار ياسر علي

تشرين الثاني 2008

ربيع الأول 1429

بسم الله الرحمن الرحيم

{قَالُوا سُبْحَانَكَ لَا عِلْمَ لَنَا إِلَّا مَا عَلَّمْتَنَا إِنَّكَ أَنْتَ الْعَلِيمُ الْحَكِيمُ}

صدق الله العلي العظيم

سورة البقرة

الآية (32)

الخلاصة

تم في هذا البحث استقصاء سلوك العتبات الخرسانية المسلحة بالالياف الحديدية اكانت مزودة بالفتحات ام لا والمتعرضة الى احمال مركبة ومتكونة من عزمي الانحناء واللي بالاضافة الى قوة القص وذلك باستعمال طريقة العناصر المحددة الثلاثية الابعاد لاجراء التحليل اللاخطي الناتج من تصرف مادة الخرسانة.

تم تمثيل الخرسانة باستخدام عناصر طابوقية ثلاثية الأبعاد ذات العشرين عقدة، أما قضبان حديد التسليح فقد تم تمثيله كعناصر محورية مطمورة داخل العنصر الطابوقي للخرسانة، مع فرض وجود ترابط تام بين الخرسانة وحديد التسليح. سلوك الخرسانة تحت تأثير اجهادات الانضغاط تم تمثيله بنموذج مرن - لدن يتبعه تصرف لدن تام ينتهي عند بداية تهشم الخرسانة. بينما سلوك الخرسانة تحت تأثير اجهادات الشد فقد مثل باستخدام نموذج الشق المنتشر والذي يكون عموديا على محاور الإجهاد الرئيسية مع اعتماد نموذج تصلب الشد لتمثيل الاجهادات المتبقية، نموذج بقاء القص لتمثيل تدهور مقاومة القص نتيجة التشقق، ونموذج التطرية لتمثيل الانخفاض الحاصل في مقاومة الخرسانة نتيجة التشققات المتعامدة.

تم حل معادلات التوازن اللاخطية باستخدام طريقة تزايدية - تكرارية اعتمادا على طريقة نيوتن - رافسون المعدلة. تمت التكاملات العددية باستخدام قاعدة التكامل المختزلة ذات السبع والعشرون.

تم تحليل العديد من الأعتاب الخرسانية المسلحة بالالياف الحديدية المعرضة إلى عزوم اللي والأحمال المركبة من قوى القص, الانحناء والالتواء. أظهرت نتائج التحليل توافق جيد مع النتائج العملية بالنسبة لعزم اللي الاقصى بفارق يتراوح بين (% 10- 8.4%). تم إجراء دراسات لبحث تأثير معاملات مختلفة على سلوك الأعتاب. كذلك تم دراسة تاثير موقع الفتحة,شكل الفتحة,مساحة الفتحة, نسبة الالياف الحديدية و تأثير الحمل المركز(P) على سعة عزم اللي (T). وقد وجد ان زيادة نسبة الألياف الحديدية تزيد من عزم اللي الاقصى بنسبة (34.96% و39.54%) بالنسبة للاعتاب المزودة و الغير مزودة بالفتحات. ايضا قد تم التوصل الى ان موقع الفتحة هو من اهم العوامل التي يجب ان تؤخذ بنظر الاعتبار عند التصميم. فعندما تكون الفتحة في منطقة الشد فانها سوف تحدث انخفاظا كبيرا بقيمة عزم اللي بمقدار (27.58%) للعتبات تحت تاثير الاحمال المركبة.

Acknowledgement

Praise be to ***ALLAH***, most gracious, most merciful, who has given me the ability and desire to complete this research work.

I would like to express my sincere thanks and gratitude to my supervisors ***Dr. Mustafa B. Dawood*** and ***Dr. Ammar Y. Ali*** for their valuable advice and guidance throughout the research work. Thanks are also expressed to ***Mr. Amir Toama*** and the staff of civil engineering department for their appreciable assistance.

I wish to thank ***my parents*** for their constant support, assistance and understanding.

Also special thanks are extended for ***my husband*** for his support.

Finally, special thanks are devoted to ***my sisters and family*** for their care, encouragement and assistance during this work.

Assra Hassan Nile

2008

List of Tables

Table		page
(1-1)	Physical Property of Steel fibers.	4
(3-1)	Shape Functions for the 20-Nodded Brick Element.	31
(3-2)	Weights and Locations of Sampling Points for the 15 and 27 – Point Integration Rules	38
(4-1)	Calculation of Parameters and C for Different fiber content	59
(5-1)	Material Properties and Material Parameters for Wafa Beams [B- B1].	79
(5-2)	Comparison between the Experimental and Predicted Ultimate and cracking Torque of Wafa Beams [B-B1].	84
(5-3)	Material properties and material parameters for Mansur Beams [H] and [F].	87
(5-4)	Comparison between the experimental and predicted Ultimate and cracking Torque for Groups (H) and (F) Beams	91
(5-5)	Open Notation.	94
(5-6)	Comparison between the Ultimate Torque for Beam F and Ultimate Torque of (A2, A3, and A4) Beams.	97
(5-7)	Comparison between the Ultimate Torque for Beam F and Ultimate Torque of (A1, A3, and A5) Beams.	99
(5-8)	Comparison between the Ultimate Torque for Beam F and Ultimate Torque of (A5, and A6) Beams.	100
(5-9)	Ultimate Torque and Ultimate Load for Different Values of (T/P) Ratio of Beam (A2).	109
		110

CONTENT

SUBJECT **Page**

Acknowledgement

Abstract ……. I

Content ……. II

List of tables ……. III

List of figures …… VI

Notations …… VII

Chapter One : Introduction

1.1 General …… 1

1.2 Fiber Reinforced concrete ……... 2

1.3 Objectives and Scope …… 6

1.4 Layout of the Thesis …… 6

Chapter Two : Review of Literature

2.1 Introduction ……. 8

2.2 Experimental Works……. 9

2.3 Theoretical and Analytical Studies …….. 12

2.3.1Torsion Theory ……. 12

2.3.1.1 Skew Bending Theory …… 12

2.3.1.2 Space Truss Analogy …… 15

2.3.2 Analytical Studies ……. 17

2.4 Summary …….. 22

Chapter Three : Finite Element Method and Nonlinear Solution Technique

3.1 Introduction ……. 23

3.2 Finite Element Formulation ……. 24

3.3 Structural Idealization of Reinforced Concrete …….. 27

3.3.1 Concrete Idealization …….. 27

3.3.2 Reinforcement Idealization ……. 31

3.4 Numerical Integration …….. 35

3.5 Nonlinear Solution Techniques ……... 38

3.6 Convergence Criteria ……... 42

3.7 Equivalent Nodal Forces ……. 42

Chapter Four : Modeling of Material Properties

4.1 Introduction ……. 44

4.2 Behavior of Steel Fiber Reinforced Concrete ……. 45

4.2.1 Unixial Compressive Behavior of Concrete ……...…… 45

4.2.2 The Modulus of Elasticity and Poisson's Ratio of Concrete …….. 47

4.2.3 Unixial Tensile Behavior of Concrete …….. 48

4.2.4 Biaxial Behavior of Fibrous Concrete …… 52

4.2.5 Triaxial Behavior of Fibrous Concrete …… 54

4.3 Stress- Strain Models of Concrete in Compression …… 56

4.3.1 The Yield Criterion …… 56

4.3.2 The Hardening Rule ……... 58

4.3.3 The Flow Rule ……... 60

4.3. 4 The Incremental Stress – Strain Relationship …… 61

4.3. 5 Crushing Condition …… 62

4.4 Behavior of Concrete in Tension..... 63

4.4.1 Cracking Criterion ……. 66

4.4.2 Tension- Stiffening Model ……... 70

4.4.3 Closing and Re-opening of Cracks …… 72

4.4.4 Shear Retention Model …….. 72
4.4.5 Modeling the Compressive Strength Reduction Due to Orthogonal Cracks …… 73
4.5 Modeling of Reinforcement ……. 75

Chapter Five : Applications and Discussion

5.1 Introduction ……. 76
5.2 Case One: Reinforced Concrete Beams under Pure Torsion …….. 76
5.2.1 Wafa Reinforced Concrete Beams [B] and [B1] ……... 76
5.2.2 Description and Material Properties of Wafa Beams [B] and [B1] … 77
5.2.3 Finite Element, Boundary Conditions and Equivalent Nodal Forces Of Wafa Beams [B] and [B1] ……..……. 79
5.2.4 Results of Analysis of Wafa Beams [B] and [B1] ……..... 81
5.3 Case Two: Reinforced Concrete Beams under Combined Shear Bending and Torsion ……..……..... 84
5.3.1 Mansur Reinforced Concrete Beams [H] and [F] ……..... 84
5.3.2 Description and Material Properties of Groups (H) and (F) Beams ……..... 84
5.3.3 Finite Element, Boundary Conditions and Equivalent Nodal Forces of the Tested Beams ……..... 87
5.3.4 Results of Analysis of the Tested Beams ……..... 89
5.4 Parametric Study ……..... 91
5.4.1 Effect of opening location through the depth of the beam…… 95
5.4.2 Effect of opening shape …… 96
5.4.3 Effect of opening Size ……..... 98
5.4.4 Effect of fiber ratio ……..... 99
5.4.5 Effect of Tension Stiffening Parameter (α_1 and α_2)…….. 100
5.4.6 Effect of Shear Retention Parameter (γ_1, γ_2 And γ_3)……. 102

5.4.7 Effect of Poisson's Ratio (υ)…… 105
5.4.8 Effect of Integration Rule …… 106
5.4.9 Effect of (T/P) Ratio on the Ultimate Capacity……. 107
5.5 Outline of the Computer Program …… 107

Chapter Six : Conclusions and Recommendations for Future Works

6.1 Introduction ……. 109
6.2 Conclusions ……. 109
6.3 Recommendations for Future Works ……. 111
References ……... 112

ABSTRACT

This research is implemented to study the effects of adding a small amount of discrete steel fibers on the behavior of reinforced concrete beams with openings, subjected to combined shear, bending and torsion. The three dimensional non-linear finite element models are presented to carry out the analysis throughout this work. The 20-noded isoperimetric brick elements have been used to model the concrete.

The steel bars are idealized as axial members embedded within the concrete elements. Perfect bond between the concrete and the reinforcement has been assumed. An elasto-plastic work hardening model followed by a perfectly plastic response, which terminated at the onset of crushing, has been considered to simulate the behavior of concrete in compression. The behavior of concrete in tension is simulated by a smeared crack model with fixed orthogonal cracks in connection with using a tension stiffening model to account for the retained post-cracking stresses, shear retention model to account for the reduced shear modulus, and a softening model to account for the reduction in compressive strength due to orthogonal cracks.

An incremental-iterative technique based on the modified Newton-Raphson method has been considered to solve the nonlinear equations of equilibrium. The numerical integration has been carried out using the reduced integration 27-point Gaussian rule.

Many reinforced concrete beams with steel fiber subjected to pure torsion and combined shear, bending and torsion loads have been analyzed. The results of the analysis show a good agreement with the available experimental results with

difference for ultimate torque a bout (10% and 8.9%) for pure torsion and combined shear and torsion, respectively.

Parametric study is considered to deal with the effect of some selected parameters such as openings location, openings shape, opening size, tension stiffing, shear retention, poison's ratio and fiber ratio. It can be noticed that the ultimate torque increases with increasing of fiber ratio by about (34.96% and 39.54%) for beams without and with opening, respectively. It is found that providing an opening at the tension zone of the beam causes sharp decrease in ultimate torque by about (27.58%) for beam under combined loading.

NOTATION AND SYMBOLS

The major part of the symbols used in the text is listed below; others are defined with their equations where they first appear.

General Symbols

$[A]^T$,$\{a\}^T$	Transpose of matrix [A] and vector {a}.
$[A]^{-1}$	Inverse of matrix [A].
d, ∂	Differential symbols.
$\lvert\ \rvert$, det	Determinate of matrix or absolute value.
Δ	Denotes incremental quantity.
{ }	Vector.
[ ]	Matrix.

Scalar

C_p	Plasticity coefficient.
d	Non- dimensional bond factor for fiber.
d_f	Diameter of fiber.
$d\lambda$	Plastic multiplier.
E_c	Modulus of elasticity of concrete.
E_f	Modulus of elasticity of the fiber.
E_m	Modulus of elasticity of matrix.
E_s	Modulus of elasticity of ordinary steel bar.
f	Function.
f_c'	Uniaxial compressive strength of concrete.
f_{cf}	Uniaxial compressive strength of fiber reinforced concrete.
f_r	Modulus of rupture of concrete.
f_t	Uniaxial tensile strength of concrete.

f_y	Yield strength of ordinary steel bar.
G	Shear modulus of concrete.
Gf	Fracture energy.
H'	Hardening parameter.
h	Height of a cross- section
I_1	First stress invariant.
I_1'	First strain invariant.
I_2	Second stress invariant.
I_3	Third stress invariant.
J	Jacobian.
J_2	Second deviatoric stress invariant.
J_2'	Second deviatoric strain invariant.
J_3	Third deviatoric stress invariant.
k	Ratio of average concrete compression stress to the peak stress.
l, m, n	Direction cosine of principal stresses.
k_1	Concrete compressive strength reduction parameter.
I_c	Crack characteristic length, critical fiber length.
N_f	Number of fiber per unit cross-sectional area.
q	Shear flow path.
p	Perimeter of the center line of the stirrups.
P	Concentrated applied load.
C ,S	Direction cosine of in-plane principal stresses.
s	Spacing of transverse reinforcement.
T	Applied torque.
T_c	Torsional moment contributed by concrete.
T_{cr}	Cracking torsional moment of concrete.
T_s	Torsional moment contributed by reinforcement bars.
T_n	Nominal torsional strength.
u, v, w	Displacement components.
V	Volume.

Vf	Volume fraction of fiber.
V_m	Volume fraction of matrix.
W	Weight of a sampling point.
X, Y, Z	Global coordinate system.
x, y, z	Local coordinate system.
x_1, y_1	Smaller and longer length of the stirrups.
α	Material parameter.
α_1, α_2	Tension stiffening parameters.
β	Shear retention factor or material constant.
γ	Shear strain.
$\gamma_1, \gamma_2, \gamma_3$	Shear retention parameters.
ε	Strain.
ε_{cu}	Ultimate strain of concrete.
ε_e	Elastic strain.
ε_o	Strain corresponding to peak Uniaxial concrete compressive stress.
$\boldsymbol{\varepsilon_o'}$	Total strain corresponding to the parabolic part of uniaxial compressive strength stress-strain curve.
ε_p	Plastic strain.
ε_{tf}	Tensile strain at peak tensile stress for fiber reinforced concrete.
ε_{cr}	Uniaxial cracking strain.
λ_1	Compression strength reduction factor of concrete.
υ	Poisson's ratio.
σ	Stress.
σ_{tu}	Ultimate fiber tensile stress.
$\boldsymbol{\sigma_o}$	Effective stress at onset of plastic deformation.
$\bar{\boldsymbol{\sigma}}$	Effective stress.
τ	Shear stress.
ξ,η,ζ	Natural coordinates system.

Matrices

[A]	Displacement gradient matrix of concrete element.
[B]	Strain-displacement matrix.
[D]	Material constitutive matrix.
[D$^{'}$]	Constitutive matrix for steel bar.
[J]	Jacobian matrix.
[K]	Stiffness matrix of concrete element.
[K$^{'}$]	Stiffness matrix of bar element.
[N]	Shape function of concrete element.
[T]	Transformation matrix.

Vectors

{a}	Nodal displacement or flow vector.
{B$^{'}$}	Strain-displacement vector of the bar element.
{b}	Body forces.
{f}	External nodal forces.
{P}	Internal load vector.
{r}	Residual load vector.
{t}	Surface traction.
{u}	Displacement vector.
{σ}	Stress vector.
{ε}	Strain vector.

Subscripts and superscripts

c	Concrete.
cf	Fiber reinforced concrete.
cr	Cracking.
e	Elastic component.
ep	Elasto-plastic.
f	Fiber.
n	Number.
m	Cement matrix.
n`	Normal.
p	Plastic component.
s	Steel.
T	Tangential.
t	Tension.
tf	Tension in fiber reinforced concrete.
tu	Ultimate tensile.
y	Yielding.
x,y,z	Denotes Cartesian coordinate.
1,2,3	Denotes the principal directions.

REFRENCES

1) Abdull- Ahad, R. B., and Abbas, J.M., (1989) ***"Behaviour of Steel Fiber Reinforced Concrete Under Biaxial Stresses"***, Proc. of the Inter. Conf. on Research Developments in Fiber Reinforced Cement and Concrete, 18-20 Sept., Cardiff (U.K.) Eds. Swamy and Barr, Elsvier Applied Science, pp.126-135.

2) Abdul-Razzak, A.A., (1996) ***"Nonlinear Finite Element Analysis of Fibrous Reinforced Concrete Structural Members"***, Ph.D. Thesis, University of Mosul.

3) ACI Committee 318-89, (1989) ***"Building Code Requirements for Reinforced Concrete"***, ACI Committee 318, American Concrete Institute, Detroit, 353 pp.

4) ACI Committee 318-02, (2002) ***"Building Code Requirements for Structural Concrete (ACI 318M-02) and Commentary (ACI 318RM-02)"***, American Concrete Institute, Detroit, 443 pp.

5) Al-Mousely, B.S.T., (1998) ***"Three Dimensional Nonlinear Finite Element Analysis for Steel Fiber Reinforced Concrete Beams Subjected to Combined Bending and Torsion"***, M.Sc. Thesis, University of Technology.

6) Allose, L.E.H., (1995) ***"Three Dimensional Nonlinear Finite Element Analysis of Steel Fiber Reinforced Concrete Beams in Torsion"***, M.Sc. Thesis, University of Technology, Baghdad.

7) Al-Shaarbaf, I.A.S., (1990), ***"Three Dimensional Non-Linear Finite Element Analysis of Reinforced Concrete Beam in Torsion"***, Ph.D. Thesis, University of Bradford, 320 pp.

8) Al Ta'an, S. A. (1992). "***Flexural Analysis of Reinforced Fibrous Concrete Beams***" Journal of Engineering and Technology, Vol. 11, No. 3, pp. 7-19.

9) Al Ta'an, S. A. (1978). "***Structural Behaviour of Conventionally Reinforced Concrete Beams with Steel Fiber*** " , Ph. D. Thesis, Sheffield University U.K.

10) Batson, G.,Terry, T., and Ming-Sung, C., ***"Fiber Reinforced Concrete Beams Subjected to Combined Bending and Torsion"***, Fiber Reinforced Concrete, International Symposium, Sp-81, American Concrete Institute, Detroit, pp. 51-68.

11) Belarbi, A., and Hsu, T.T., (1995) ***"Constitutive Laws of Softened Concrete in Biaxial Tension – Compression"***, ACI Structural J., Sec.-Oct., pp. 562-573.

12) Collins, M.P., and Mitchell, D., (1980) ***"Shear and Torsion Design of Pre stressed and Non-Pre stressed Concrete Beams"***, PCI Journal, September-October, pp. 32-100.

13) Chern, J. C., Yang, H. J., and Chen, H. W. (1992). "***Behavior of Steel Fiber Reinforced Concrete in Multiaxial Loading***", ACI Materials Journal, Vol. 89, No. 1, pp.32-40.

14) Chen, W. F. (1982). "***Plasticity in Reinforced Concrete***" McGrawHill Book Co., New York.

15) Chen and Carson, J.L., (1971) ***"Stress-Strain Properties of Random Wire Reinforced Concrete"***, ACI J. Proc., Vol.68, No. 12, Dec, pp.a33-a36.

16) Cervenka, V., (1985) ***"A Constitutive Model for Reinforced Concrete"***, Journal of ACI, Vol. 82, Nov.-Des., pp. 877-882.

17) Dawe, D.J., (1984) ***"Matrix and Finite Element Displacement Analysis of Structures"***, Claredon Press, Oxford, U.K.

18) Diab, M.I.M., (1998) ***"Three-Dimensional Non-Linear Finite Element Analysis of High Strength Concrete Panels under Combined Loadings and Beams in Torsion"***, Ph.D. Thesis, University of Technology, 182 pp.

19) Faisal F.Wafa, Abul-Hasnat and Osama F. Tarabolsi, (1992) ***"Prestressed Fiber Reinforced Concrete Beams Subjected to Torsion"***, ACI Structural Journal, Vol. 26, No. 89, June, pp. 272-283.

20) Gençoglu, M., and Eren, İ. (2002). "***An Experimental Study on the Effect of Steel Fiber Reinforced Concrete on the Behavior of the Exterior Beam-Column Joints Subjected to Reversal Cyclic Loading***", Turkish Journal Eng. Env. Sci., 26, pp.493-502.

21) Gebman, M. (2001). "***Application of Steel Fiber Reinforced Concrete in Seismic Beam- column Joints***", M.Sc. Thesis, San Diego State University, USA.

22) Hartmann, T. (1999). "***Steel Fiber Reinforced Concrete***", This Thesis was prepared and conducted at the Department of Structural Engineering at the Royal Institute of Technology in Stockholm.

23) Hinton, E., (1988) ***"Numerical Methods and Software for Dynamic Analysis of Plates and Shells"***, Pineridge Press, Swansea, U.K., 260 pp.

24) Karij, N., and Pal, A.K, (1972) ***"Strength of Fiber Reinforced Concrete"***,Proc., ASCE, Vol.98, No. ST5, May.pp. 1053-1068.

25) Kupfer, H.B., Hilsdorf, H.K., and Rusch, H., 1969 ***"Behavior of Concrete under Biaxial Stresses"***, Journal of ACI, Vol. 66, No. 8, August, pp. 656-666.

26) Kwak, H.G., and Filippou, F.C., (1997) ***"Nonlinear F.E. Analysis of R/C Structures under Monotonic Loads"***, Journal of Computers and Structures, Vol. 65, No. 1, pp. 1-16.

27) Lampert, P., and Thurliman, B., (1968) ***"Torsional Tests of Reinforced Concrete Beams"***, Report No. 6506-2, Institute for Baustatik, Zurich, June.

28) Lee, I., Punurai, W., and Hsu, C.T.T. (2002). "***Complete Stress-Strain Behavior of High Preformance Fly Ash Concrete***", ASCE Engineering Mechanics Conference June 2 – 5, 2002, Columbia University, New York, NY.

29) Lessig, N.N., (1959) ***"Determination of Carrying Capacity of Reinforced Concrete Elements with Rectangular Cross-Section Subjected to Flexural with Torsion"***, Concrete and Reinforced Concrete Institute, Moscow, No.5, pp. 5-28.

30) Mansur, M.A., (1982) ***"Bending- Torsion Interaction for Concrete Beams Reinforced with Steel Fibers"***, Magazine of Concrete Research, V.34, No.121, Dec., pp.182-190.

31) Mansur, M.A., and Paramavisam, p., (1985) ***"Fiber Reinforced Concrete Beams in Torsion, Bending and Shear"***, ACI Journal, Proceedings V.82, No.1, Feb., pp.33-39.

32) Mindess, S. (1980). "***Torsion Tests of Steel-Fiber Reinforced Concrete***", the International Journal of Cement Composites, Vol. 2, No. 2, pp. 85-89.

33) Murugappan, K., Paramasivam, P., and TAN, k.H., (1992) ***"Shear Response of Reinforced Fibous Concrete Beam Using Finite Element Method"*** proc. of the 4th. Inter. RLLEM Symp. On Fiber Reinforced Cement and Concrete, Sheffield 20-23, July, E.&FN SPON, London, pp.447-463.

34) Narayana, R. and Toorani, G.Z., (1979) ***"Fiber Reinforced Concrete Beams in Torsion and in Combined Bending and Torsion"***, Proceedings, Institution of Civil Engineers (London), Part2, V.67, Dec., pp.987-1001.

35) Nogabai, K. (2000). "***Beams of Fibrous Concrete in Shear and Bending: Experiment and Model***", Journal of Structural Engineering, ASCE, Vol. 126, No. 2, pp.243-246.

36) Owen, D. R. J., and Hinton, E. (1980). "***Finite Element in Plasticity : Theory and Practice***", Pinneridge Press, Swansea, U.K.

37) Rausch, E., (1929) ***"Design of Reinforced Concrete in Torsion"***, Techniche Hochschule, Berlin, Second Edition, 1938, 53 pp.

38) Radmix ™ "***Web:http://www.radmix.com***".

39) Soroushian, P., and Lee, C. D. (1989). "***Constitutive Modeling of Steel Fiber Reinforced Concrete under Direct Tension and Compression***", Recent Developments in Fiber Reinforced Cements and Concretes, Elevier Scinece Publishers Ltd., Essex, pp. 363-377.

40) Soroushian, P., and Bayasi, Z. (1991). "***Fiber-Type Effects on the Perfarmance of Steel Fiber Reinforce Concrete***", ACI Materials Journal, Vol. 88, No. 2, pp 129-134.

41) Swamy, R.N., Mangat, P.S., and Rao, C.V.S.K. (1974). "***The Mechancs of Fiber Reinforced of Cement Material***", Fiber Reinforced Concrete ACI SP-44, Detroit, Michigan, pp. 1-28.

42) Yin, W. S., Eric, C. M. SU, Mansur, M. A. and Thomas, T. C. Hsu., (1989) "***Biaxial Tests of Plain and Fiber Concrete***" ACI Material J., Vol. 86, No.3, May- June, pp. 236-243.

Chapter one

INTRODUCTION

Chapter two

REVIEW OF LITERATURE

Chapter three

FINITE ELEMENT METHOD

AND NONLINEAR SOLUTION TECHNIQUE

Chapter Four

MODELING OF MATERIAL PROPERTIES

Chapter six

CONCLUSION AND RECOMMENDATIONS FOR FUTURE WORKS

Chapter Five

APPLICATION AND DISCUSSION

LIST OF FIGURES

FIG. NO.	TITLE	Page
(1-1)	Shape of steel fibers……	5
(1-2)	Bridging action of steel fibers…….	5
(2-1)	Skew bending failure and forces acting on a skew plane at failure of reinforced concrete beam ……	14
(2-2)	Space truss model for hollow rectangular reinforced concrete beam ……	16
(2-3)	Thin – walled tube analogy …….....	17
(2-4)	Bending behavior of SFRC beams ……	20
(2-5)	Normalized stress-strain curve for steel fiber concrete, 20% fly ash replacement ……	21
(3-1)	The 20-noded isoparametric brick element …….……...	28
(3-2)	Representation of steel reinforcement …….……...	34
(3-3)	Distribution of sampling points over the element in 15 and 27- Gaussian point integration rules ……..…….	37
(3-4)	Non-linear solution techniques ……..…….	41
(4-1)	Stress-strain curves in compression for SFRC ……..	47
(4-2)	Tensile stress-strain curve of steel fiber reinforced concrete...	50
(4-3)	Interaction of micro-cracks with steel fibers ……..	51
(4-4)	Debonding and pull-out of fibers under tension …….	52
(4-5)	Failure envelope of concrete in biaxial stress space ……..….	54
(4-6)	Typical traixial failure envelope of concrete ……..……	56
(4-7)	Typical Unaixial failure envelope of concrete ……..……	56
(4-8)	Uniaxial stress-strain curve for concrete in compression ….....	60
(4-9)	Idealization of a single crack …….…….	66
(4-10)	Idealization of a discrete crack model …….……...	66

(4-11) Failure cracking for triaxially loaded concrete …….. 70
(4-12) Post-cracking model for concrete in tension …… 72
(4-13) Post-cracking model for concrete in tension for current study... 72
(4-14) Shear retention model for concrete ……. 74
(4-15) Stress-strain relationship of steel bars used in the analysis ….. 77

(5-1) Dimensions details of Wafa beams [B1] and [B1]……. 80
(5-2) Finite element mesh, boundary conditions and equivalent nodal forces for Wafa beams [B] and [B1] …….. 82
(5-3) Torque – twist curve of beam [B] (case one) ……..... 84
(5-4) Torque – twist curve of beam [B1] (case one) ……..… 85
(5-5) Torque – twist curve of beams [B] and [B1] (case one) ……. 85
(5-6) Dimensions details of Mansur beams [H] and [F] ……. 88
(5-7) Finite element mesh, boundary conditions and equivalent nodal forces for Mansur beams [F] and [H] …….. 90
(5-8) Torque – twist curve of beam (F) (case two) …..…..……. 92
(5-9) Torque – twist curve of beam (H) (case two) …..…..……. 92
(5-10) Simply supported reinforced concrete beam with openings geometry and loading arrangement …… 94
(5-11) Finite element idealization of beams F and A1 …….. 95
(5-12) Simply supported reinforced concrete beam with openings at different case …… 96
(5-13) Effect of positions for openings through the beam depth on the torque-twist behavior …… 98
(5-14) Effect of shape for openings on the torque-twist behavior …… 99
(5-15) Effect of decrease area for openings on the torque-twist behavior ……. 100

(5-16) Effect of fiber ratio on the torque-twist behavior for beam (F) ……...……..... 101
(5-17) Effect of fiber ratio on the torque-twist behavior for beam (A1) ……...……..... 102
(5-18) Effect of tension stiffening parameter (α_1) on the torque – twist behavior of beam (H) (case two) ……..…… 103
(5-19) Effect of tension stiffening parameter (α_2) on the torque – twist behavior of beam (H) (case two) ……..…… 104
(5-20) Effect of tension stiffening parameter (γ_1) on the torque – twist behavior of beam (H) (case two) ……..…… 105
(5-21) Effect of tension stiffening parameter (γ_2) on the torque – twist behavior of beam (H) (case two) ……..…… 106
(5-22) Effect of tension stiffening parameter (γ_3) on the torque – twist behavior of beam (H) (case two) ……..…… 106
(5-23) Effect of Poison's ratio (υ) on the torque – twist behavior of beam (H) ……. 107
(5-24) Effect of Integration Rule on the torque-twist behavior for beam (F) ……..... 108

ABSTRACT

This research work is implemented to study the effects of adding a small amount of discrete steel fibers on the behavior of reinforced concrete beams with openings, subjected to combined shear, bending and torsion. The three dimensional non-linear finite element models are presented to carry out the analysis throughout this work. The 20-noded isoperimetric brick elements have been used to model the concrete.

The steel bars are idealized as axial members embedded within the concrete elements. Perfect bond between the concrete and the reinforcement has been assumed. An elasto-plastic work hardening model followed by a perfectly plastic response, which terminated at the onset of crushing, has been considered to simulate the behavior of concrete in compression. The behavior of concrete in tension is simulated by a smeared crack model with fixed orthogonal cracks in connection with using a tension stiffening model to account for the retained post-cracking stresses, shear retention model to account for the reduced shear modulus, and a softening model to account for the reduction in compressive strength due to orthogonal cracks.

An incremental-iterative technique based on the modified Newton-Raphson method has been considered to solve the nonlinear equations of equilibrium. The numerical integration has been carried out using the reduced integration 27-point Gaussian rule.

Many reinforced concrete beams with steel fiber subjected to pure torsion and combined shear, bending and torsion loads have been analyzed. The results of the analysis show a good agreement with the available

experimental results with difference for ultimate torque a bout (10% and 8.9%) for pure torsion and combined shear and torsion, respectively.

Parametric study is considered to deal with the effect of some selected parameters such as openings location, openings shape, opening size, tension stiffing, shear retention, poison's ratio, fiber ratio, and effect of (T\P) ratio on the ultimate capacity. It can be noticed that the ultimate torque increases with increasing of fiber ratio by about (34.96% and 39.54%) for beam without and with opening, respectively. It was found that providing an opening at the tension zone of the beam causes sharp decrease in ultimate torque by about (27.58%) for beam under combined loading.

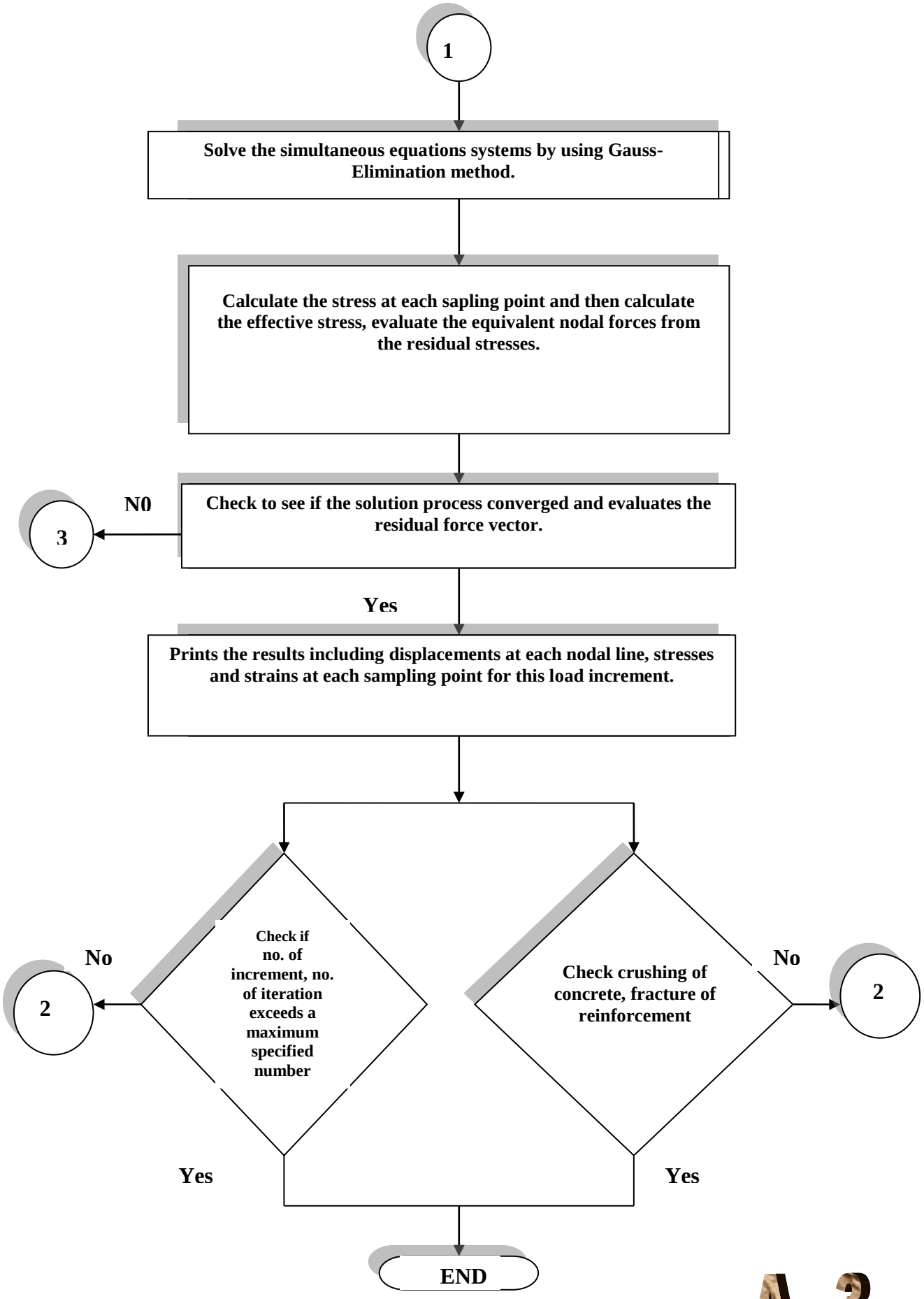
1
Solve the simultaneous equations systems by using Gauss-Elimination method.
Calculate the stress at each sapling point and then calculate the effective stress, evaluate the equivalent nodal forces from the residual stresses.
Check to see if the solution process converged and evaluates the residual force vector.
N0
3
Yes
Prints the results including displacements at each nodal line, stresses and strains at each sampling point for this load increment.
Check if no. of increment, no. of iteration exceeds a maximum specified number
No
2
Yes
Check crushing of concrete, fracture of reinforcement
No
2
Yes
END

APPENDIX A

tension- stiffening models

In this appendix the additional subroutine concerning the tension-stiffening models for reinforced concrete with steel fiber is presented.

A.1 Model TS

These subroutines are added to account for a tension-stiffening bilinear stress-strain curve for steel fiber reinforced concrete.

A.1.2 CRAK IN THE FIRST DIRECTION

```
SUBROUTINE MODTSR1 (ABSLNC, SCR, CHI, ALPH, PSTRN, ECR, SCONT)
IMPLICIT REAL*8(A-H, O-Z)
SCONT=0.00065
IF (PSTRN (1). GT. ABSLNC (1, KGAUSE). AND. PSTRN (1).LT.SCONT) THEN
ECR (1) = CHI*SCR (I, KGAUSC)/PSTRN (1)
ELSEIF (PSTRN (1).G.T.SCONT. AND. PSTRN (1). LT. (ALPH*ABSLNC (1, KGAUSC))) THEN ECR (1) = (CHI. SCR (1, KGAUSC)/PSTRN (1))*(ALPH – PSTRN (1) / ABSLNC (1, KGAUSC))/ ALPH – (SCONT/ ABSLNC (1, KGAUSC))
END IF
RETURN
END
```

APPENDIX A

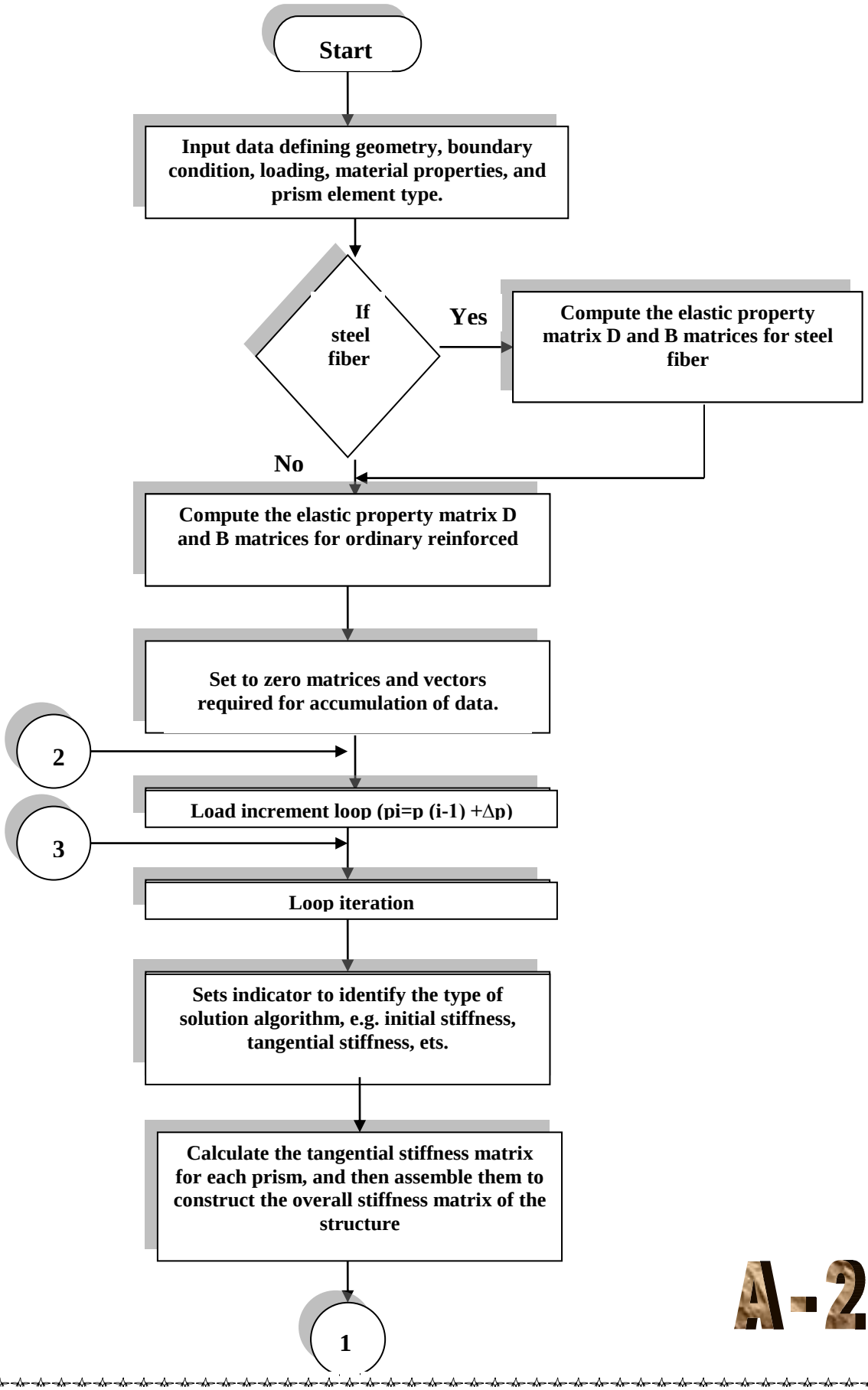
Start
Input data defining geometry, boundary condition, loading, material properties, and prism element type.
If steel fiber
Yes
Compute the elastic property matrix D and B matrices for steel fiber
No
Compute the elastic property matrix D and B matrices for ordinary reinforced
Set to zero matrices and vectors required for accumulation of data.
2
Load increment loop (pi=p (i-1) +Δp)
3
Loop iteration
Sets indicator to identify the type of solution algorithm, e.g. initial stiffness, tangential stiffness, ets.
Calculate the tangential stiffness matrix for each prism, and then assemble them to construct the overall stiffness matrix of the structure
1

Substituting equation (B-10) into equation (B-6)

$$\alpha.\sigma\circ+\beta.\sigma_{\circ}^{2}=-2.\gamma.\alpha.\sigma\circ+\beta.\gamma^{2}.\sigma_{\circ}^{2} \quad \text{..... (B-11)}$$

Re-arranging Eq. (B-11)

$$\text{..... (B-12)}\ \alpha=\frac{(\gamma^{2}-1)}{(2.\gamma-1)}\beta.\sigma\circ$$

Substituting into equation (B-6)

$$\text{..... (B-13)}\ \beta.\sigma_{\circ}^{2}=\frac{(\gamma^{2}-1)}{(2\gamma-1)}\beta.\sigma_{\circ}^{2}=\sigma_{\circ}^{2}$$

$$\text{..... (B-14)}\ \beta=\frac{1}{1-\dfrac{(\gamma^{2}-1)}{(2\gamma-1)}}$$

Substituting into Eq. (B-13) we get.

$$\text{..... (B-15)}\ \alpha\left[\frac{1}{1-\dfrac{(\gamma^{2}-1)}{(2\gamma-1)}}\right].\sigma\circ$$

And

$$\text{..... (B-16)}\ c=\frac{1}{2}\left[\frac{1}{1-\dfrac{(\gamma^{2}-1)}{(2\gamma-1)}}-1\right]$$

APPENDIX B

Material Parameters a, ß and C for Steel Fiber Reinforced Concrete

The yield condition presented in section 4.3.1

$$\sigma_o = f(\{\sigma\}) = cI_1 + \left[(cI_1)^2 + 3\beta J_2\right]^{1/2} \qquad \text{(E-1)}$$

Which represent the Von-Mises yield condition

To find **α** and **ß**

1- For uniaxial compressive state of stress:

$\sigma x = -\sigma\circ$ And $\sigma y\, \tau_{xy} = 0$ ..... (B-2)

$I = \sigma_x + \sigma_y = -\sigma\circ$ .....(B-3)

$J_2 = (1/3)(\sigma_x^2 + \sigma_y^2 - \sigma_x\sigma_y) + \tau_{xy}^2$ ..... (B-4)

$J_2 = (1/3)\,\sigma_\circ^2$ ..... (B-5)

Substituting into equation (B-1)

$-\alpha\sigma_\circ + \beta\sigma_\circ^2 = \sigma\circ^2$ ..... (B-6)

$\sigma_x = \sigma_y = -\lambda\sigma\circ$ And $\tau_{xy} = 0$ ..... (B-6)

2- For biaxial compressive state of stress:

$I1 = -\gamma\sigma_x - \gamma\sigma\circ = -2.\gamma.\sigma\circ$ ..... (B-8)

$J_2 = (1/3)\,\gamma^2\,\sigma_\circ^2$ ..... (E-9)

Substituting into equation (B-1)

$-2.y.a.a_o + ß.y2\,.\,\sigma_\circ^2 = \sigma_\circ^2$ ..... (B-1 0)

Chapter Four

MODELING OF MATERIAL PROPERTIES

4.1 INTRODUCTION

The efficiency and accuracy of the nonlinear finite element approach in the analysis of reinforced concrete structures depends mainly on the suitable modeling of material properties. The modeling implies choosing the suitable element type, simulation of the actual behavior of the material properties, choosing of sufficient number of the sampling points and selection of the proper integration technique (**Diab** 1998).

Cementations materials such as concrete, mortar and cement paste have a weakness in resisting tension, impact and other types of loading. This weakness is due to the material's inability to prevent small cracks, which can originate at flaws or voids, from becoming unstable under small tensile stresses. To overcome this weakness, steel, glass, polymer and other types of fiber have been added as reinforcement, thus producing a composite material. Even though the percentage by volume of the fibers is small, the mechanical behavior of the resulting composite material is substantially different from that of the matrix material. The composite generally possesses higher tensile strength, ductility and fracture toughness. For both design and research purposes, mathematical models have been formulated to predict the mechanical behavior of composite depending on the mechanical properties of the matrix and fibers.

Because non-linear finite element analysis is computationally expensive, simplified models to simulate material behaviour are required. However, these models should adequately predict the overall behaviour of the member. Realistic modeling of material behaviour is also needed to predict the effects caused by static loading at serviceability design load intensities, and to predict ultimate load. This chapter outlines the constitutive models for the fiber reinforced concrete and the reinforcing bars used in the present study.

4.2 BEHAVIOR OF STEEL FIBER REINFORCED CONCRETE

The behavior of steel fiber reinforced concrete material is discussed in the following sections.

4.2.1 UNIAXIAL COMPRESSIVE BEHAVIOR

Fibers do little to enhance the static compressive strength of concrete, with increases in strength ranging from essentially nil to perhaps 25%. Even in members that contain conventional reinforcement in addition to the steel fibers, the fibers have little effect on compressive strength. However, the fibers do substantially increase the post-cracking ductility, or energy absorption of the material.

This is shown graphically in the compressive stress-strain curves of SFRC in Fig. (4-1).The strain at peak compressive stress (ε_{pf}) can be expressed as (**Soroushian** and **Lee** 1989):

$$\varepsilon_{of} = 0.0021+0.0007\left[\frac{V_f . L_f}{D_f}\right] \qquad \text{....(4-1)}$$

where:

V_f The volume fraction of fibers.

L_f The fiber length.

D_f The fiber diameter.

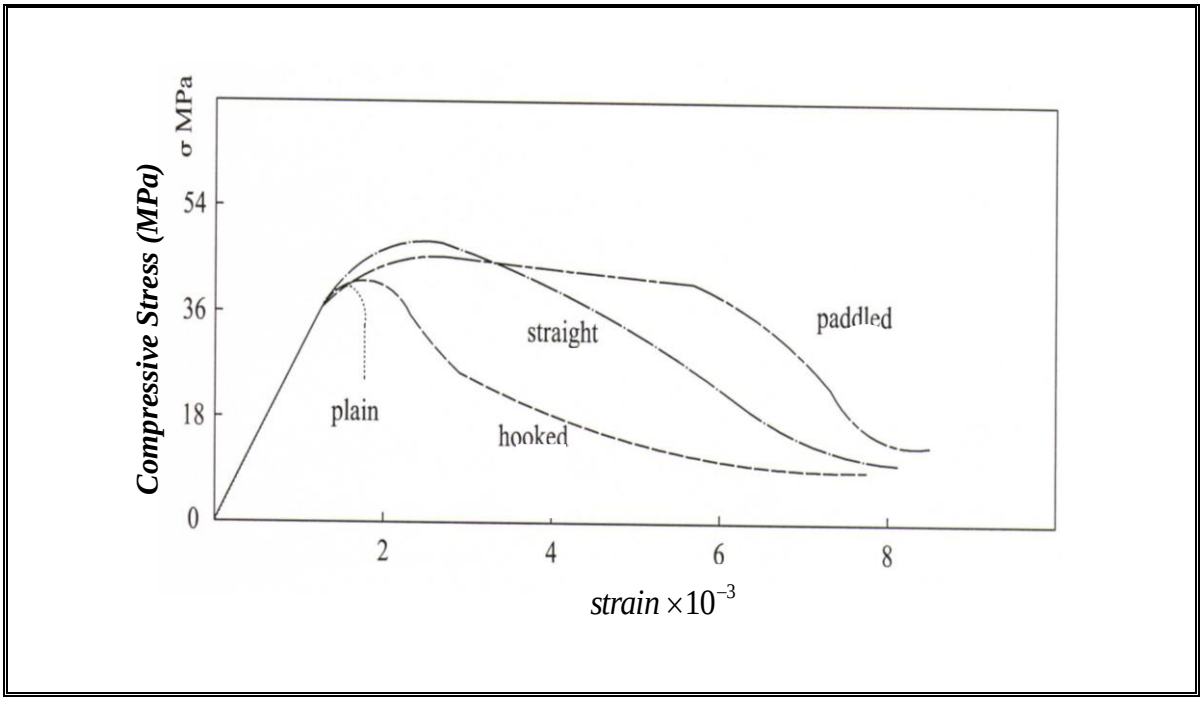

Fig.(4-1) Stress-Strain curves in compression for SFRC

(**Soroushian** and **Lee** 1989)

Also Fig.(4-1), shows that the stress-strain curve has a nearly elastic behavior up to about 30 percent of its maximum compressive strength f'_{cf} (like plain concrete). For stress beyond the level, the curve shows a gradual increase in the curvature up to about 0.8 f'_{cf}, where it bends more sharply and approaches the peak point at f'_{cf}. Beyond peak point, the stress-strain curve has a descending part. The shape of this descending part depends on the fiber parameters. Finally the crushing failure occurs at the ultimate strength ε_{cuf}.

An empirical equation to express the compressive strength of fibrous concrete material suggested by **(Soroushian and Lee** 1989) has been adopted throughout this research work:

$$f'_{cf} = f'_c + 3.6\frac{(Vf.Lf)}{Df} \qquad \text{…..(4-2)}$$

Test results indicate that the compressive strength of fibrous concrete depends on the method of fabrication, fiber geometry and fiber content (**Karij**

and **Pal** 1972). **Chen** and **Carson** (1972**)** concluded that the maximum increase in compressive strength of concrete is observed at volume fraction of fibers equals to 2% by using (0.46 ×13mm) steel fibers. Results of **(Pakotiprapha el.at.** (1974) show that the ultimate strength in axial compressive of the composite is smaller than the ultimate strength of the mortar. However, the presence of the fibers increases the ductility of the composite.

4.2.2 MODULUS OF ELASTICITY AND POISSON'S RATIO

For plain concrete, the modulus of elasticity E_c is highly dependent on the compressive strength f'_c. The modulus of elasticity E_c can be calculated with responsible accuracy from the empirical formula recommended by ACI committee-318 M02 as:

$$E_c = 43.W_c^{1.5}.f'^{0.5}_c.10^{-3} \quad .....(4\text{-}3)$$

Where W_c is concrete unit weight kg/m^3 and both E_c and f'_c are expressed in MPa.

It may be assumed that the steel fibrous concrete material behaves elastically up to the strain value required for crack propagation. During the elastic stage, the load carried by unit area of the composite is divided between the matrix and the fibers. The modulus of elasticity of the steel fiber reinforced material is given by:

$$E_m = E_c.V_m + \eta_\lambda.\eta_o.V_f.E_f \quad .....(4\text{-}4)$$

Where, E_c, is the modulus of elasticity of the matrix given by Eq.(4.3), and E_f, is the modulus of elasticity of the fibers. V_m and V_f are the volume fractions of the matrix and fibers respectively. While, η_o, is the orientation factor of fiber. The value of orientation factor depends on the distribution of fiber. For three-dimensional random orientation, this factor has been found to vary between 0.33 and 0.5. Also, η_λ is the length efficiency factor, to account

for the varying fibers stress at the end portions of fibers. The factor η_λ is defined as the ratio of the average fiber stress to the maximum fiber stress. Hence:

$$\eta_\lambda = \begin{cases} 0.5\dfrac{L_C}{L_f} & for L_f < L_c \\ 1 - L_c / L_f & for L_f > L_c \end{cases} \qquad \text{…..(4-5)}$$

Where, Lf and L_c are the actual and critical lengths of the fiber respectively. The critical length L_c is defined as the length required developing the ultimate fiber stress σ_{fu} when a uniform ultimate bond stress τ_u between the fiber and the matrix is assumed, to occur, therefore,

$L_c = 0.5.\ \sigma_{fu}.\ D_f / \tau_u$ …..(4-6)

Where, σ_{fu} is given by:

$$\sigma_{fu} = \eta_\lambda \eta_o\ V_f\ \frac{L_f}{2r}\ \tau_u \qquad \text{…..(4-7)}$$

And D_f is the diameter of the fiber and r is the ratio of the fiber cross section to its perimeter. The volume fraction of the matrix, V_m is given by:

$V_m = (1 - \eta_o V_f)$ …... (4-8)

Poisson's ratio (υ) for concrete under uniaxial compressive loading ranges from about (0.15 to 0.22). The ratio (υ) remains constant until approximately 80 percent of $f`_c$, at which stress the apparent Poisson's ratio begins to increase (**Chen** 1982).

4.2.3 UNIAXIAL TENSILE BEHAVIOR

In the case of tensile loading, very important change in the stress-strain curve can be achieved by the addition of a suitable amount of fiber reinforcement. A typical tensile stress-strain curve of steel fiber reinforced concrete is shown in Fig. (4-2)

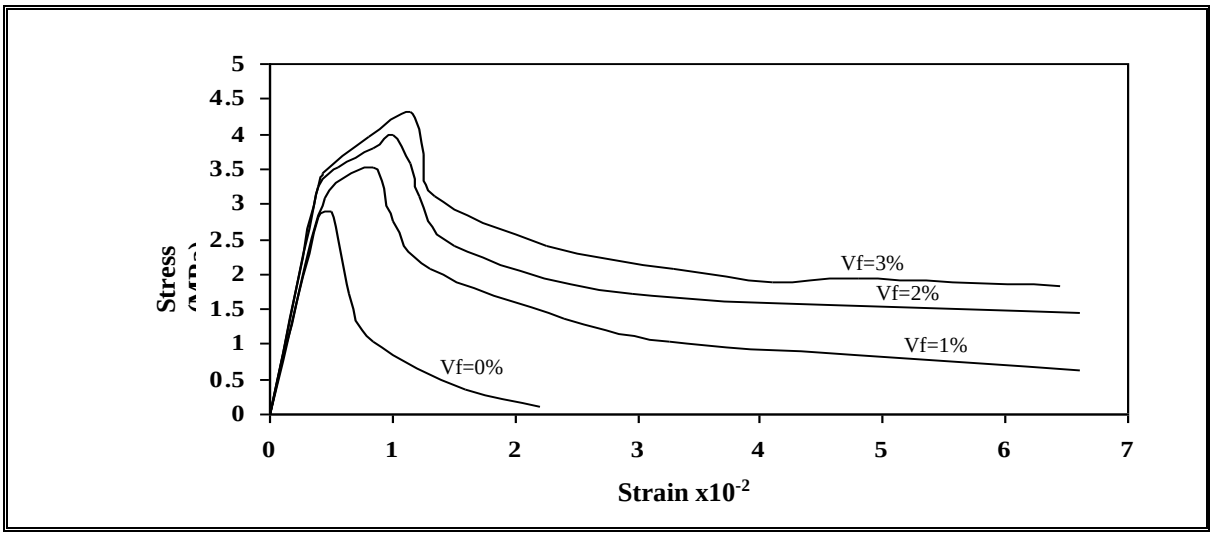

Fig. (4-2) Tensile stress-strain curve of steel fiber reinforced concrete (**Soroushian** and **Bayasi** 1987).

The ascending part of the curve, up to the first cracking, is similar to that of plain concrete, and then it tends to deviate from linearity due to the process of micro crack propagation in matrix prior to the formation of a continuous crack system at peak stress. This is followed by formation of an unstable micro crack system, which grows rapidly under the tensile stress bringing the material to its post-peak region.

The process of micro crack propagation tends to be influenced by the presence of fibers. Micro cracks encountering steel fibers may be shifted or branched out, (spacing concept) Fig. (4-3). Hence, the propagation of micro cracks in steel fiber reinforced concrete involves dissipation of additional energy form the stress-system due to the interaction of micro- cracks with fibers. This explains an important mechanism through which fibers increase the tensile strength of concrete.

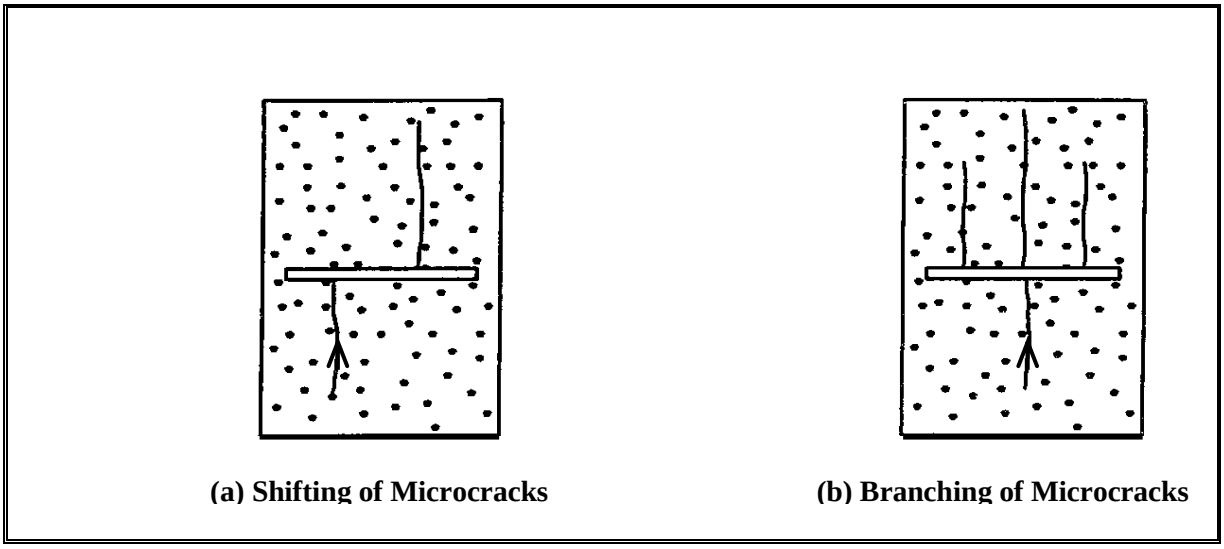

Fig. (4-3) interaction of micro-cracks with steel fibers (**Soroushion and Lee** 1989**)**.

On the other hand, the debonding and pull-out of fibers (composite concept), Fig. (4-4) enhances the tensile behavior of the steel fibrous concrete close to the peak tensile stress and at the post peak region. The pull-out action of the fibers would be mobilized when a crack tends to widen at critical sections, which transfers particularly all tensile stresses to the fibers bridging the crack by fractional forces.

This action starts to occur at peak load and largely provides the post-peak tensile resistance of the fibrous concrete. Therefore, the tensile stress-strain model of steel fiber concrete is divided into two regions, namely the pre-peak and post-peak regions (**Soroushian** and **Bayasi** 1987).

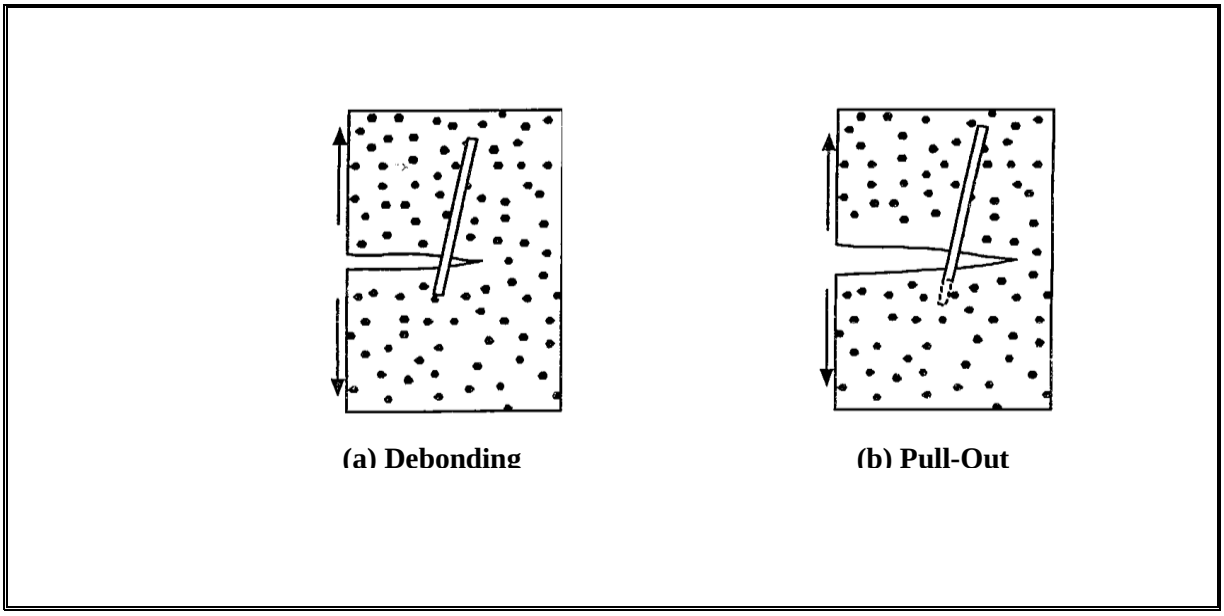

Fig.(4-4) debonding and pull-out of fibers under tension(**Soroushion and Lee** 1989**)**.

Many investigations simulate this region by a linearly elastic model up to its composite tensile strength f_{tf}. Either the "composite material concept", or the "spacing concept" has generally been used to predict the tensile strength of fibers, **(Soroushion** and **Lee** 1989) use the so called "interaction concept", which attributes the increase in tensile strength of fibrous concrete to microcrack-arrest of fibers as well as to the pull-out action of fibers which is only partially mobilized at the peak tensile stress of the material. In their study the following equations have been used to predict the tensile strength f_{tf} of steel fiber reinforced concrete.

$$f_{tf} = ft\left(1 + 0.016Nf^{\frac{1}{3}} + 0.05\pi.df.lf.Nf\right) \qquad \text{…..(4-9)}$$

And the composite tensile strain at peak tensile stress is given by:

$$\varepsilon_{tf} = \varepsilon_t\left(1 + 0.35Nf.df.lf\right) \qquad \text{….. (4-10)}$$

$$\varepsilon_t = \frac{lf.\tau_u}{df.Ef} \qquad \text{….. (4-11)}$$

Where:

Nf The number of fibers per unit cross-section area; given by:

$$Nf = \eta_0 \left[\frac{4vf}{\pi df^2} \right] \quad \text{….. (4-12)}$$

η_0 The orientation factor of fibers; $(\eta_0 = 0.5)$ for random distribution.

τ_u The shear stress between the fiber and the concrete given by:

$$\tau_u = \eta_b (2.26 - 0.0036 Nf) \quad \text{….. (4-13)}$$

η_b The bond efficiency factor ($\eta_b = 1.0$ or 0.75 for hooked or straight fiber respectively).

4.2.4 BIAXIAL BEHAVIOR OF FIBROUS CONCRETE

Michael et. al. (1976) carried out an experimental study for steel fiber reinforced mortar under biaxial compression. They found that the compressive strength was increased by about 72% as compared with the uniaxial compressive strength at a stress ratio (σ_1/σ_2) of 0.6. Fig. (4-5) illustrated a typical biaxial strength envelope for plain concrete subjected to proportional biaxial loading.

(**Abbas** 1989) tested steel fiber reinforced concrete, with different aspect ratios, under biaxial stresses by using sequential loading system. They divided the tested specimens into three groups according to the states of stress (biaxial compression, biaixil compression-tension and biaxial tension states). They concluded from the results that this effect of biaxial stress increased the strength of fibrous concrete under biaxial compression and tension states, whereas it decreased the strength under biaxial tension-compression state.

(**Yin et. al**. 1989) presented an experimental study to investigate the effect of biaxial compression stress on steel fibrous and plain concrete. The compressive stresses were applied through brush – type loading plate to eliminate frictional stresses between the concrete and the plates. The test program covered four principal compression stress ratios ranging from 0.0 to

1. Steel fibers with 25.4 mm diameter and 19 mm length, and volume fraction of 1.0 and 2.0 percent have been used. The test results showed that fiber content possesses higher strength than plain concrete in biaxial compression. The increase was as high as 35% in the case of 25.4 mm fiber length, 2% volume ratio, and a stress ratio of 0.2. Observation of failure modes reveals that splitting type failure occurs in plain concrete but faulting-type failure occurs in the fibrous concrete.

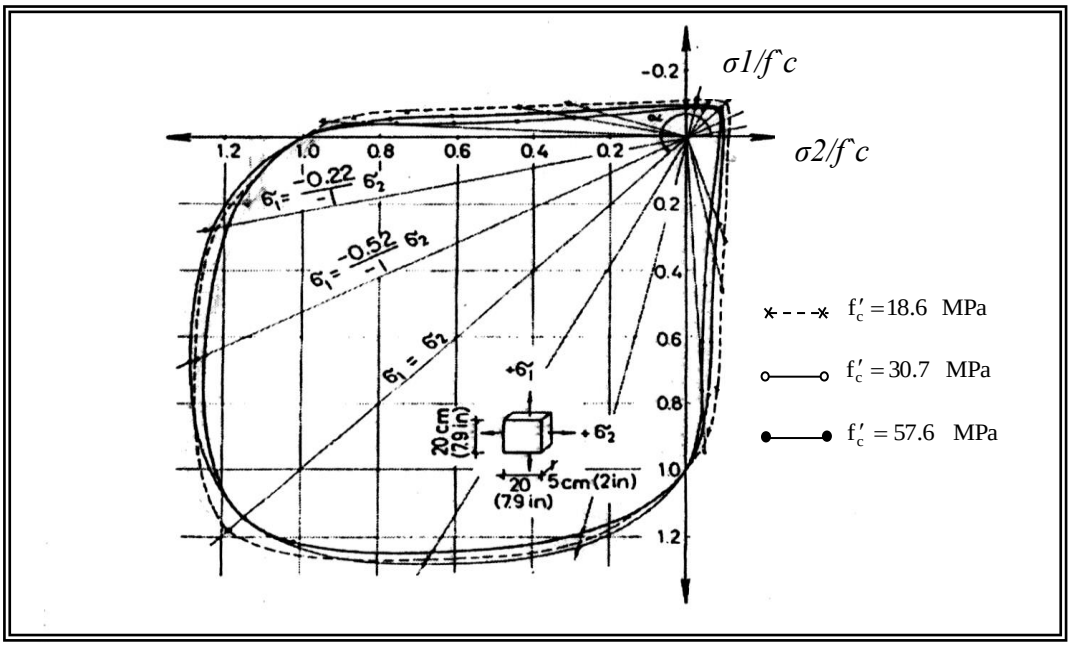

Fig. (4-5): Failure Envelope of Concrete in Biaxial Stress Space (**Chen** 1982)

4.2.5 TRIAXIAL BEHAVIOR OF FIBROUS CONCRETE

Experiments under triaxial loading indicate that the failure surface for concrete is a function of three principal stresses, Fig. (4-6). the deviatoric sections (plains perpendicular to the axial $\sigma_1=\sigma_2=\sigma_3$) of the failure surface are convex and non-circular, but for increasing hydrostatic compression they become more circular. No test of the response of concrete in hydrostatic tension has been reported, most triaxial tests on concrete have been concerned with ultimate failure. Generally, the maximum tensile strength is approximately equal to the tensile strength in the uniaxial tension and the failure mode corresponds to forming a crack plane perpendicular to the largest principal tensile stress direction. Under combination of compression and tension states, it is observed that the compressive strength decreases when the applied tensile stress increases.

Typical stress-strain curves are shown in Fig. (4-7). These curves show that the ultimate axial compressive strength of concrete increases with increasing hydrostatic (confining) stress, and the high stresses resisted by concrete under high confining compression are always accompanied by large deformation or ductility. Much of the deformation under triaxial loading is due to inelastic reduction of volume or a compaction of the concrete under stress. The amount of compaction varies considerably with the quality of concrete (less for high strength concrete). Different modes of failure have been observed for concrete under triaxial compression. The failure modes showed a distinct transion from splitting tension under low confinement, over shear faulting under intermediate confinement, to distribute plastic flow at high confinement.

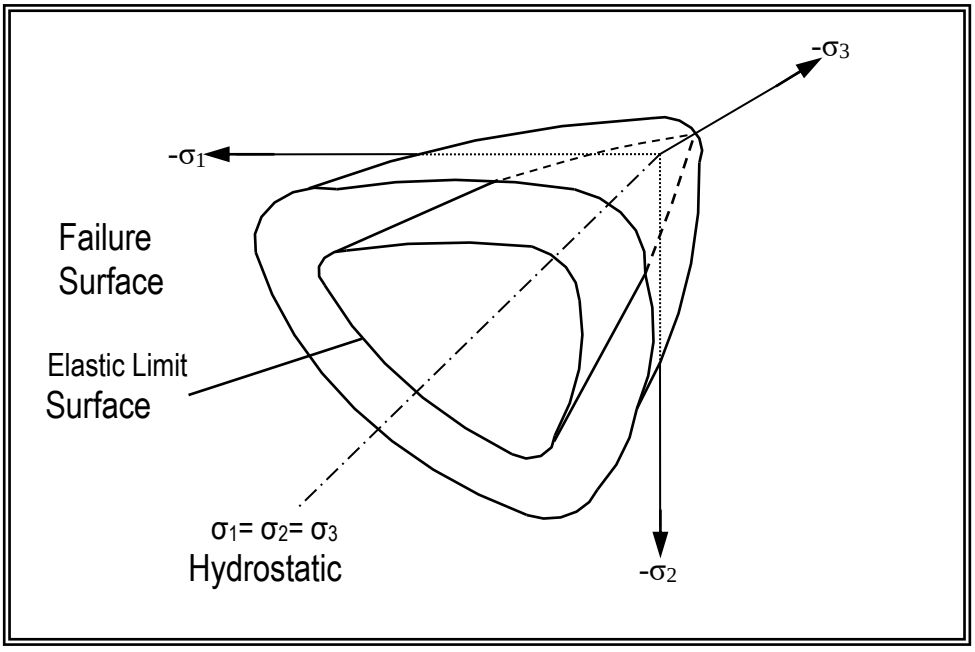

Fig.(4-6): Typical Triaxial Failure Envelope of Concrete (**Chen** 1982)

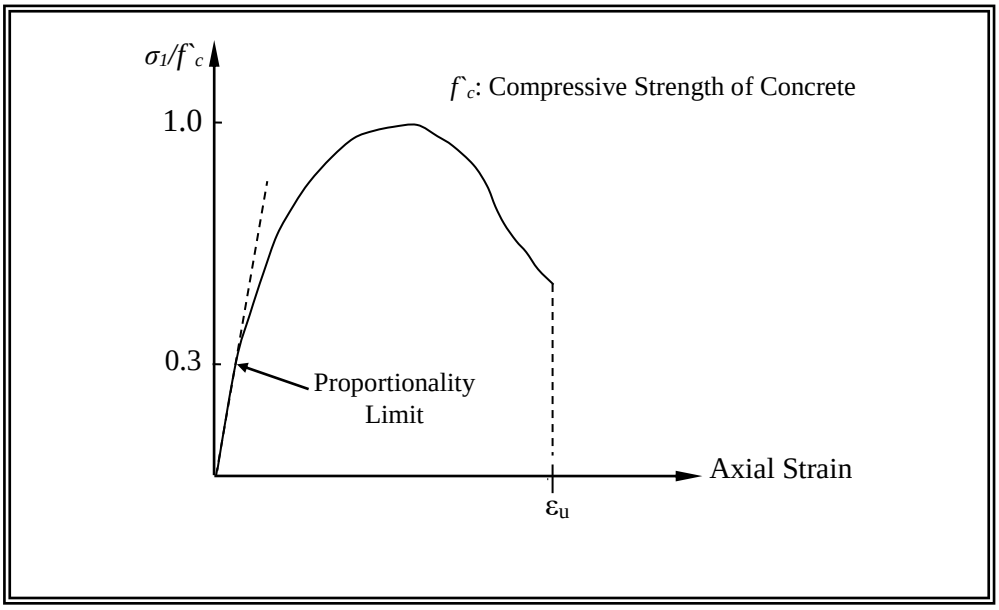

4.3 STRESS-STRAIN MODELS FOR CONCRETE IN COMPRESSION

The plasticity – based model has been used to describe the nonlinear behavior of concrete in compression. In this approach, the nonlinear deformations occur when concrete is stressed beyond its limit of elasticity. The total strain may be separated into recoverable and irrecoverable parts. The recoverable part represents the framework of elasticity, while the treatment of the irrecoverable part is based on the theory of plasticity. Under triaxial compression, concrete can flow like a ductile material on the yield or failure surfaces before reaching its crushing strains (**Chen** 1982).

In this study, the behavior of concrete in compression is simulated by an elasto-plastic work hardening model followed by a perfectly plastic response, which is terminated at the onset of crushing. The adopted plasticity model will be illustrated in terms of the following constituents:

a) The yield criterion.
b) The hardening rule.
c) The flow rule.
d) The incremental stress – strain relationship.
e) The crushing condition.

4.3.1 YIELD CRITERION

The meterial is assumed to behave elasticity until it reaches the yeild limit, until a certain function of the stress component reaches a prescribed value, which is known as the yeild surface. For isotropic material, the initial yield criterion should be independent of the orientation of the coordinate system in which the stress state is defined, and therefore, it should be a function of the stress invariants only. The yield criterion used in the present work has been successfully used by many researchers(**Chen** 1982, **Own** 1980 and **Al-Shaarbaf** 1990) . It can be expressed as:

$$\sigma_o = f(\{\sigma\}) = cI_1 + \left[(cI_1)^2 + 3\beta J_2\right]^{1/2} \quad \text{…..(4-14)}$$

where c and β are material parameters, I_1 is the first stress invariant given by:

$$I_1 = \sigma_x + \sigma_y + \sigma_z \quad \text{…..(4-15)}$$

and J_2 is the second deviatoric stress invariant given by:

$$J_2 = \frac{1}{3}\{\left[\sigma_x^2 + \sigma_y^2 + \sigma_z^2\right] - \left[\sigma_x\sigma_y + \sigma_y\sigma_z + \sigma_z\sigma_x\right]\} + \left[\tau_{xy}^2 + \tau_{yz}^2 + \tau_{zx}^2\right] \text{…..} \quad (4\text{-}16)$$

And σ_o is the equivalent effective stress at the onset of plastic deformation that can be determined from the uniaxial compression test as:

$$\sigma_o = C_p . f_c' \quad \text{.....} \quad (4\text{-}17)$$

Where, C_p is the plasticity coefficient which is used to mark the initiation of the plastic deformation.

The parameters c, andβ, are determined from the uniaxial and biaxial experimental results carried out by (**Kupfer** 1969) for plain concrete as:

$c = 0.17734$ And $\beta = 1.35468$

For steel fiber reinforced concrete, the parameters β and c are determined from the uniaxial and biaxial experimental results given in references ((**Allose** 1995, (**Yin**, **Mansur** and **Thomas** 1989)) taking into account the volume fraction of fibers. The value and procedure for calculation these parameters are given in Table (4-1) and Appendix [B].

Table (4-1) Calculation of parameters β and C for different fiber content.

((**Allose** 1995, (**Yin**, **Mansur**, **Thomas** 1989))

Fiber content V_f (%)	γ	α	β	C
0.0	1.16	0.3546798	1.3546798	0.1773399
0.5	1.39	1.0993042	2.0993042	0.596521
1.0	1.47	1.4900526	2.4900526	0.740263
2.0	1.52	1.760526	2.7960526	0.8980263

4.3.2 THE HARDENING RULE

The hardening rule is required to define the motion of the subsequent loading surfaces during plastic loading. To describe the growth of the subsequent loading surfaces for a strain-hardening material, many hardening rules have been proposed. The isotropic hardening rule is the simplest one to formulate and has been adopted in the present study to simulate concrete behavior. This rule assumes that the yield surface expands uniformly without distortion as plastic deformation occurs **(Al-Shaarbaf** 1990, **Diab** 1998)**)**. Therefore, the subsequent loading surfaces may be written as:

$$\bar{\sigma} = f(\{\sigma\}) = cI_1 + \left[(cI_1)^2 + 3\beta J_2 \right]^{1/2} \qquad \text{….. (4-18)}$$

Where the effective stress or equivalent uniaxial stress $\bar{\sigma}$ represents the stress level at which further plastic deformation will occur.

In the present model, a parabolic stress-strain curve is used for the equivalent uniaxial stress-strain relationship of steel fiber reinforced concrete beyond the limit of elasticity as shown in Fig. (4-8), $C_p f'_{cf}$. This parabolic curve represents the work-hardening stage of behavior. When the peak compressive stress is reached, a perfectly plastic response is assumed to occur **(Al-Shaarbaf** 1990**)**. These relationships are given by:

a) For $\varepsilon_{cf} \le C_p f'_{cf} \backslash E$

$$\bar{\sigma} = E.\varepsilon_{cf} \qquad \text{…..(4-19)}$$

b) For $C_p f'_{cf} \backslash E \le \varepsilon_{cf} \le f'_{cf} \backslash E$

$$\bar{\sigma} = C_p.f'_{cf} + E\left[\varepsilon_{cp} - \frac{C_p.f'_{cf}}{E}\right] - \frac{E}{2\varepsilon'_o}\left[\varepsilon_{cf} - \frac{C_p.f'_{cf}}{E}\right]^2 \qquad \text{….. (4-20)}$$

c) For $\varepsilon_{cf} \ge (2 - C_p).\frac{f'_{cf}}{E}$

$$\bar{\sigma} = f'_{cf} \qquad \text{…..(4-21)}$$

Where ε'_o is the total strain corresponding to the parabolic part of the curve given by:

$$\varepsilon'_o = 2(1 - C_p)\frac{f'_{cf}}{E} \qquad \text{….. (4-22)}$$

By substituting the value of the total strain component, which is the sum of the elastic and plastic strains into Eq. (4-20), the effective stress-plastic strain relationship can be expressed as:

$$\bar{\sigma} = C_p f'_c - E \cdot \varepsilon_{cp} + (2E^2 \cdot \varepsilon'_o \cdot \varepsilon_p)^{1/2} \qquad \text{….. (4-23)}$$

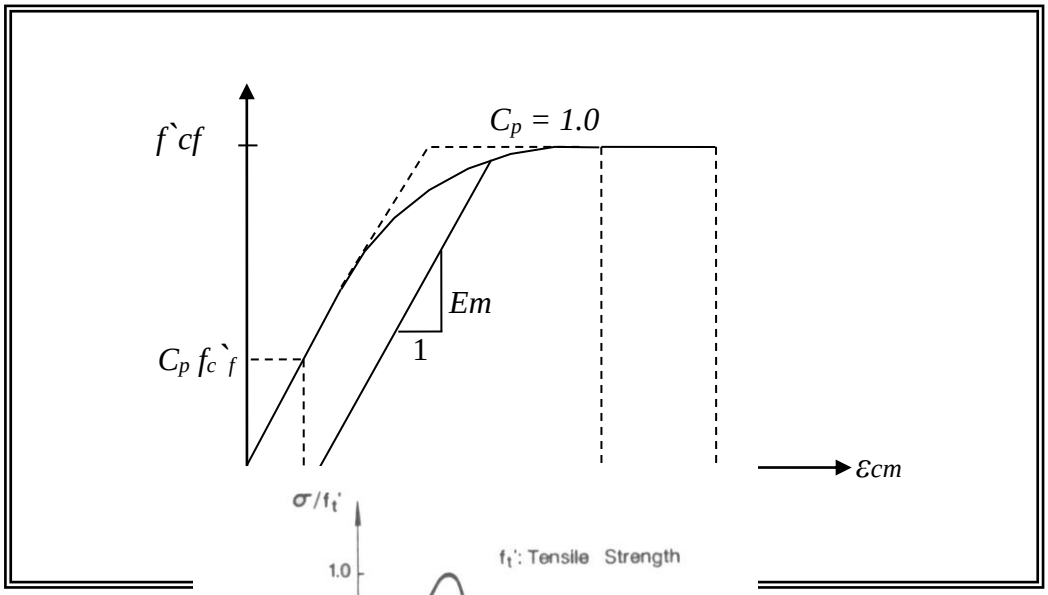

Fig. (4-8): Un e **(Al-Shaarbaf** 1990)

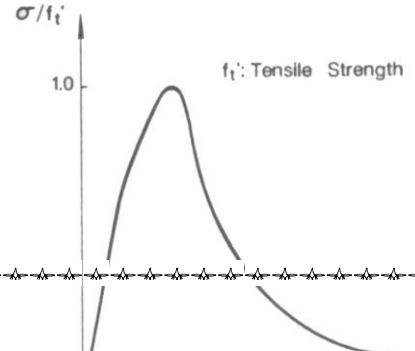

The hardening coefficient H', which is the slope of the effective stress-plastic strain curve, is used in the formulation of the elasto-plastic incremental stress-strain relationship. By differentiation of Eq. (4.23) with respect to the effective plastic strain, the hardening parameter can be expressed as:

$$H' = \frac{d\bar{\sigma}}{d\varepsilon_p} = E\left[\left(\frac{\varepsilon'_o}{2\varepsilon_p}\right)^{1/2} - 1.0\right] \qquad \text{….. (4-24)}$$

4.3.3 THE FLOW RULE

In the plasticity – based theory, when the current yield surface is reached, the material becomes in state of plastic flow upon further loading. The flow rule is usually employed to connect the loading function (*f*) and the stress – strain relation in the plastic range. This rule has been widely used for concrete models because of its simplicity **(Al-Shaarbaf** 1990 and **Chen** 1982).

The plasticity strain vector will be assumed to be normal to the yield surface; the plastic strain increment is given by:

$$d\{\varepsilon_p\} = d\lambda \frac{\partial f(\{\sigma\})}{\partial\{\sigma\}} \qquad \text{….. (4-25)}$$

Where $d\lambda$ is a positive scalar hardening parameter which can vary throughout the staining process. The normal to the current loading surface ($\frac{\partial f(\{\sigma\})}{\partial\{\sigma\}}$) is termed as the flow vector, which can be obtained by the derivatives the yield function with respect to the stress components, and given by:

$$\{a\} = \left[\frac{\partial f}{\partial\sigma_x}, \frac{\partial f}{\partial\sigma_y}, \frac{\partial f}{\partial\sigma_z}, \frac{\partial f}{\partial\tau_{xy}}, \frac{\partial f}{\partial\tau_{yz}}, \frac{\partial f}{\partial\tau_{zx}}\right] \qquad \text{….. (4-26)}$$

These derivatives can be evaluated from equation (b-2) with the use of equations (4-15) and (4-16) as:

$$\left.\begin{aligned}
\frac{\partial f}{\partial \sigma_x} &= C + \left[2(C^2+\beta)\sigma_x + (2C^2-\beta)(\sigma_y+\sigma_z)\right]/Q \\
\frac{\partial f}{\partial \sigma_y} &= C + \left[2(C^2+\beta)\sigma_y + (2C^2-\beta)(\sigma_x+\sigma_z)\right]/Q \\
\frac{\partial f}{\partial \sigma_z} &= C + \left[2(C^2+\beta)\sigma_z + (2C^2-\beta)(\sigma_x+\sigma_y)\right]/Q \\
\frac{\partial f}{\partial \tau_{xy}} &= 6\,\frac{\beta\,\tau_{xy}}{Q} \\
\frac{\partial f}{\partial \tau_{yz}} &= 6\,\frac{\beta\,\tau_{yz}}{Q} \\
\frac{\partial f}{\partial \tau_{zx}} &= 6\,\frac{\beta\,\tau_{zx}}{Q}
\end{aligned}\right\} \quad \text{….. (4-27)}$$

Where (C) and (β) are the material constants given in Table (4-1), and (Q) is given by:

$$Q = 2[(C^2+\beta)(\sigma_x^2+\sigma_y^2+\sigma_z^2) + (2C^2-\beta)(\sigma_x\,\sigma_y+\sigma_y\,\sigma_z+\sigma_z\,\sigma_x) + 3\beta(\tau_{xy}^2+\tau_{yz}^2+\tau_{zx}^2)]^{0.5} \quad \text{….. (4-28)}$$

4.3.4 THE INCREMENTAL STRESS – STRAIN RELATIONSHIP

The total incremental strain is composed of elastic and plastic strain, therefore:

$$d\{\varepsilon\} = d\{\varepsilon_e\} + d\{\varepsilon_p\} \quad \text{….. (4-29)}$$

Substituting equation (4-25) with equation (4-29) yields:

$$d\{\varepsilon\} = d\{\varepsilon_e\} + d\lambda\,\frac{df(\sigma)}{d(\sigma)} \quad \text{….. (4-30)}$$

the elastic strain increment is related to the stress increment by the elastic constitutive relation given by:

$$d\{\sigma\} = [D]\,d\{\varepsilon_e\} \quad \text{….. (4-31)}$$

Hence:

$$d\{\varepsilon_e\} = [D]^{-1}.d\{\sigma\} \qquad \text{….. (4-32)}$$

Where *[D]*, is the elastic constitutive matrix given by:

$$[D] = \frac{E}{(1+\nu)(1-2\nu)} \begin{bmatrix} 1-\nu & \nu & \nu & 0 & 0 & 0 \\ \nu & 1-\nu & \nu & 0 & 0 & 0 \\ \nu & \nu & 1-\nu & 0 & 0 & 0 \\ 0 & 0 & 0 & \frac{1-2\nu}{2} & 0 & 0 \\ 0 & 0 & 0 & 0 & \frac{1-2\nu}{2} & 0 \\ 0 & 0 & 0 & 0 & 0 & \frac{1-2\nu}{2} \end{bmatrix} \qquad \text{….. (4-33)}$$

Substituting equation (4-29) into equation (4-31) yields:

$$d\{\varepsilon\} = [D]^{-1}.d\{\sigma\} + d\lambda.\{a\} \qquad \text{….. (4-34)}$$

Pre-multiplying both sides of equation (4-34) by, *($\{a\}^T.[D]$)* and eliminating *($\{a\}^T.d\{\sigma\}$)*, the following expression for the plastic multiplier, dλ is obtained :

$$d\lambda = \left[\frac{\{a\}^T.[D]}{H' + \{a\}^T.[D].\{a\}} \right].d\{\varepsilon\} \qquad \text{….. (4-35)}$$

By substituting equation (4-35) with equation (4-29) and pre-multiplying both sides by *[D]*, the complete elasto – plastic incremental stress – strain relationship can be expressed as:

$$d\{\sigma\} = \left[[D] - \frac{\{a\}^T.[D]}{H' + \{a\}^T.[D].\{a\}} \right].d\{\varepsilon\} \qquad \text{….. (4-36)}$$

Where the second term in the brackets represents stiffness degradation due to the plastic deformation.

4.3.4 CRUSHING CONDITION

Crushing of concrete indicates the complete rupture and disintegration of the material under compression stress state. After crushing, the current stresses drop rapidly to zero and the concrete is assumed to lose its resistance completely against further deformation.

In the adopted model, the concrete crushing criterion is obtained when the strain reaches the ultimate strain. The crushing criterion is obtained by simply converting the yield criterion which is written in terms of stresses directly into strains, thus:

$$C.I_1' + \sqrt{(C.I_1')^2 + 3\beta.J_2'} = \varepsilon_{cu} \qquad \text{….. (4-37)}$$

Where ε_{cu} is the ultimate crushing strain of concrete, extrapolated from uniaxial test, I_1' and J_2' are the first strain invariant and the second deviatoric strain invariant that can be obtained by the following equations **(Al-Shaarbaf** 1990**)**:

$$I_1' = \varepsilon_x + \varepsilon_y + \varepsilon_z \qquad \text{….. (4-38)}$$

$$J_2 = \left(\frac{1}{3}\right)\left[\left(\varepsilon_x^2 + \varepsilon_y^2 + \varepsilon_z^2\right) - \left(\varepsilon_x\varepsilon_y + \varepsilon_y\varepsilon_z + \varepsilon_z\varepsilon_x\right)\right] + (\gamma_{xy})^2$$
$$+ (\gamma_{yz})^2 + (\gamma_{zx})^2 \qquad \text{….. (4-39)}$$

4.4 BEHAVIOR OF CONCRETE IN TENSION

The stress – strain curve of concrete in tension is linear up to about stress level of 60 percent of the uniaxial tensile strength f_t. above this level, the bond cracks start to grow and the nonlinearity of the curve starts to increase as the stress level increases until the peak stress. The term cracking indicates a partial collapse of the material across the plane of cracking under tensile stress states (**Chen** 1982).

After cracking, concrete changes from isotropic to orthotropic material. In the finite element analysis of concrete structures, three different approaches have been employed for crack modeling (**Chen** 1982):

1.) Smeared – cracking model.

2.) Discrete – cracking model.

3.) Fracture – mechanics model.

The particular cracking model to be selected depends upon the purpose of the analysis (**Kwak** 1997).

If the overall load – deflection behavior is desired without regard to completely realistic crack patterns and local stresses, the smeared – cracking model is probably the best choice. In this approach the cracked concrete is assumed to remain a continuum, and the concrete becomes orthotropic or transversely isotropic. After the first cracking has occurred, one of the material axes being oriented along the direction of the cracking as shown in Fig. (4-9). For most structural engineering applications, the smeared – cracking modeling is generally used (**Chen** 1982).

The discrete – cracking model represents a continuous smeared – cracking model; this is normally done by disconnecting the displacement at nodal points for adjoining elements as shown in Fig. (4-10). The difficulty in this approach is that the location and orientation of the cracks are not known. This approach is used to obtain details about the local behavior of concrete. While the applicability of fracture – mechanics model to reinforced concrete is still questionable (**Chen** 1982).

In the present study, the behavior of concrete in tension is simulated by linear elastic prior to cracking. The cracking criterion of concrete is expressed in terms of the principal tensile stress or strain. A smeared – cracking model with fixed orthogonal cracks is adopted to represent the fractured concrete.

The adopted model is desired in terms of **(Al-Shaarbaf** 1990**)**:

a.) Cracking criterion.

b.) Tension- stiffening model

c.) Closing and re- opening of cracks.

d.) Shear retention modal.

e.) Compressive strength reduction due to orthogonal crack mod

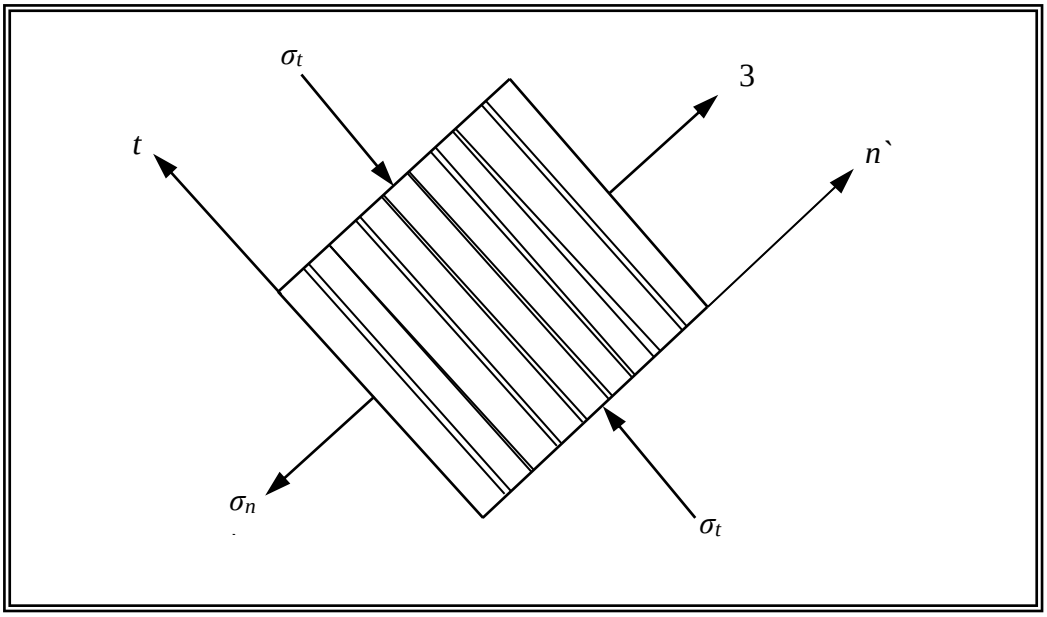

Fig. (4-9): Idealization of a Single Smeared Crack (**Chen** 1982)

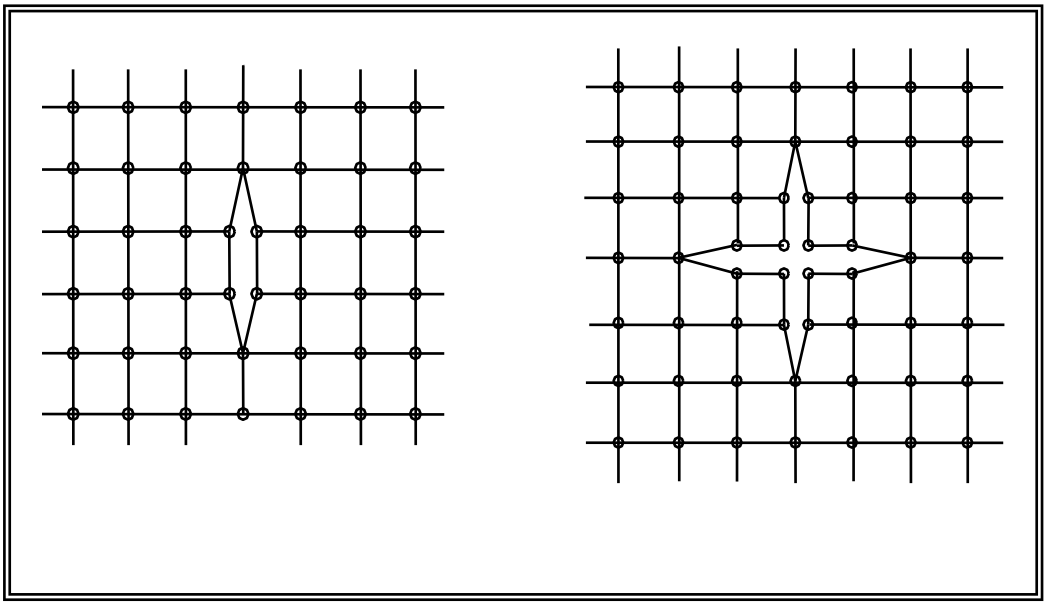

Fig. (4-10): Discrete Crack Model (**Chen** (1982)**)**

4.4.1 THE CRACKING CRITERION

In the present research, the onset of cracking is controlled by a maximum principal stress criterion. According to this criterion, cracking occurs when the principal tensile stress exceeds the limited tensile strength of concrete f_t, the limited tensile stress required to define the onset of cracking can be calculated for states of triaxial tensile stress and for combination of tension and compression principal stresses as **(Al-Shaarbaf** 1990**)**:

a.) For the triaxial tension zone ($\sigma_1 \geq \sigma_2 \geq \sigma_3 \geq 0$)

$$\sigma_i = \sigma_{cri} = f_{tf} \qquad \text{Where } i = 1, 2, 3 \qquad \text{….. (4-40)}$$

b.) For tension – tension – compression zone ($\sigma_1 \geq \sigma_2 > 0, \sigma_3 \leq 0$)

$$\sigma_i = \sigma_{cri} = f_{tf}[1.0 + \frac{0.75\sigma_3}{f'_{cf}}] \qquad i = 1,2 \qquad \text{….. (4-41)}$$

c.) For tension – compression – compression ($\sigma_1 > 0, \sigma_3 \leq \sigma_2 \leq 0$)

$$\sigma_i = \sigma_{cri} = f_t[1.0 + \frac{0.75\sigma_2}{f'_c}].[1.0 + \frac{0.75\sigma_3}{f'_c}] \quad i = 1 \qquad \text{….. (4-42)}$$

Where (σ_{cr}) is the cracking stress and both (ft) and ($f`_c$) are the tensile and compressive strengths of concrete substitute in positive values.

The last two equations (4-41) and (4-42) indicate that the presence of compressive stress in one direction favors the cracking in other directions and thus reduces the tensile capacity of the material.

After cracking, the modulus of elasticity in the direction of the maximum tensile stress (σ_1) is reduced because of the lack of interaction between orthogonal planes caused by cracking, Poisson's ratio (υ), is set to zero and a reduced shear modulus ($\beta_1.G$) is employed to model the shear strength deterioration. Therefore, the incremental stress – strain relationship in local material axes may be expressed as:

$$\begin{Bmatrix}\Delta\sigma_1\\ \Delta\sigma_2\\ \Delta\sigma_3\\ \Delta\tau_{12}\\ \Delta\tau_{23}\\ \Delta\tau_{31}\end{Bmatrix}=\begin{bmatrix}E_1 & 0 & 0 & 0 & 0 & 0\\ 0 & E/1-\nu^2 & \nu E/1-\nu^2 & 0 & 0 & 0\\ 0 & \nu E/1-\nu^2 & E/1-\nu^2 & 0 & 0 & 0\\ 0 & 0 & 0 & \beta_1 G & 0 & 0\\ 0 & 0 & 0 & 0 & G & 0\\ 0 & 0 & 0 & 0 & 0 & \beta_1 G\end{bmatrix}\begin{Bmatrix}\Delta\varepsilon_1\\ \Delta\varepsilon_2\\ \Delta\varepsilon_3\\ \Delta\gamma_{12}\\ \Delta\gamma_{23}\\ \Delta\gamma_{31}\end{Bmatrix} \quad \text{….. (4-43)}$$

Where (E_1) is the reduced modulus of elasticity in the direction of (σ_1) and (G) is the shear modulus of elasticity. Equation (4-43) can be written in a compact form as:

$$\{\Delta\sigma\}=[D_{cr}].\{\Delta\varepsilon\} \quad \text{….. (4-44)}$$

Where $[D_{cr}]$ is the material stiffness in the local axes. The stress increment in the global axes (x, y, and z) may be obtained by using the coordinate transformation matrix such that

$$\{\Delta\sigma\}=[T]^T.[D_{cr}].[T].\{\Delta\varepsilon\} \quad \text{….. (4-45)}$$

Where $[T]$, is the transformation matrix expressed in terms of the direction cosines as:

$$[T]=\begin{bmatrix} l_1^2 & m_1^2 & n_1^2 & l_1 m_1 & m_1 n_1 & n_1 l_1\\ l_2^2 & m_2^2 & n_2^2 & l_2 m_2 & m_2 n_2 & n_2 l_2\\ l_3^2 & m_3^2 & n_3^2 & l_3 m_3 & m_3 n_3 & n_3 l_3\\ 2l_1 l_2 & 2m_1 m_2 & 2n_1 n_2 & (l_1 m_2 + l_2 m_1) & m_1 n_2 + m_2 n_1 & n_1 l_2 + n_2 l_1\\ 2l_2 l_3 & 2m_2 m_3 & 2n_2 n_3 & (l_2 m_3 + l_3 m_2) & m_2 n_3 + m_3 n_2 & n_2 l_3 + n_3 l\\ 2l_3 l_1 & 2m_3 m_1 & 2n_3 n_1 & (l_3 m_1 + l_1 m_3) & m_3 n_1 + m_1 n_3 & n_3 l_1 + n_1 l_3\end{bmatrix} \quad \text{….. (4-46)}$$

Where l_i, m_i, and n_i represent the direction cosines with respect to x,y, and z directions respectively.

For both the tension – tension – compression and the triaxial tension states of stress, the cracking criterion may be violated by the major principal stress (σ_1) and the second principal stress (σ_2) simultaneously. Thus, two sets of orthogonal failure planes develop. These planes are perpendicular to the

principal axes 1 and 2 respectively as in Fig. ((4-11 (a and b)). In this case Poisson's ratio is set to zero in all directions and the constitutive matrix in the local material axis is reduced to the following form:

$$[D_{cr}]=\begin{bmatrix} E_1 & 0 & 0 & 0 & 0 & 0 \\ 0 & E_2 & 0 & 0 & 0 & 0 \\ 0 & 0 & E & 0 & 0 & 0 \\ 0 & 0 & 0 & \beta_1 G & 0 & 0 \\ 0 & 0 & 0 & 0 & \beta_2 G & 0 \\ 0 & 0 & 0 & 0 & 0 & \beta_1 G \end{bmatrix} \qquad \text{….. (4-47)}$$

In a fixed crack model, the rotation of the principal stresses after the formation of the first crack is ignored. However, if the second crack onsets at a subsequent stage of loading, rotation of the principal stresses within the planes perpendicular to direction of, $\sigma 1$ may be taken into account.

Magnitude and directions of the new second and minor principal stresses, $\sigma_1^{/}$ and $\sigma_3^{/}$, may be calculated from the original principal stresses, σ_2 and σ_3, and the shear stresses, τ_{23} accumulated during loading stages beyond the formation of the first crack. Thus:

$$\sigma_1^{/}=\frac{\sigma_2+\sigma_3}{2}\pm\left[\frac{(\sigma_2+\sigma_3)^2}{2}+\tau_{23}^2\right]^{0.5} \qquad \text{i=2, 3} \qquad \text{….. (4-48)}$$

For tension- tension-compression states, the onset of the second crack is expressed in terms of the new principal stresses as:

$$\sigma_2^{/}=\sigma_{cr}=f_{tf}\left[1+\frac{0.75\sigma_3^{/}}{f_{cf}^{/}}\right] \qquad \text{….. (4-49)}$$

Failure planes corresponding to the second crack are assumed to be perpendicular to the direction of the second principal stress, $\sigma_2^{/}$

Fig. (4-11b).

The angle between the original and the new in- plane sets of principal directions θ_p may be calculated:

$$\theta_p = \frac{1}{2}.\tan^{-1}\frac{2\tau_{23}}{\sigma_2 - \sigma_3} \qquad \text{….. (4-50)}$$

After the formation of the second crack, the local in-plane constitutive matrix with respect to the new principal directions ($2',3'$) is expressed as:

$$[D_{cr}] = \begin{bmatrix} E_2 & 0 & 0 \\ 0 & E & 0 \\ 0 & 0 & \beta_2 G \end{bmatrix} \qquad \text{….. (4-51)}$$

In the current model, a maximum of three sets of cracks are allowed to form at each sampling point. For triaxial tension states, a third crack may appear when the minor principal stress, (σ_3) exceeds the uniaxial tensile strength f_{tf} in Fig. (4-11c).

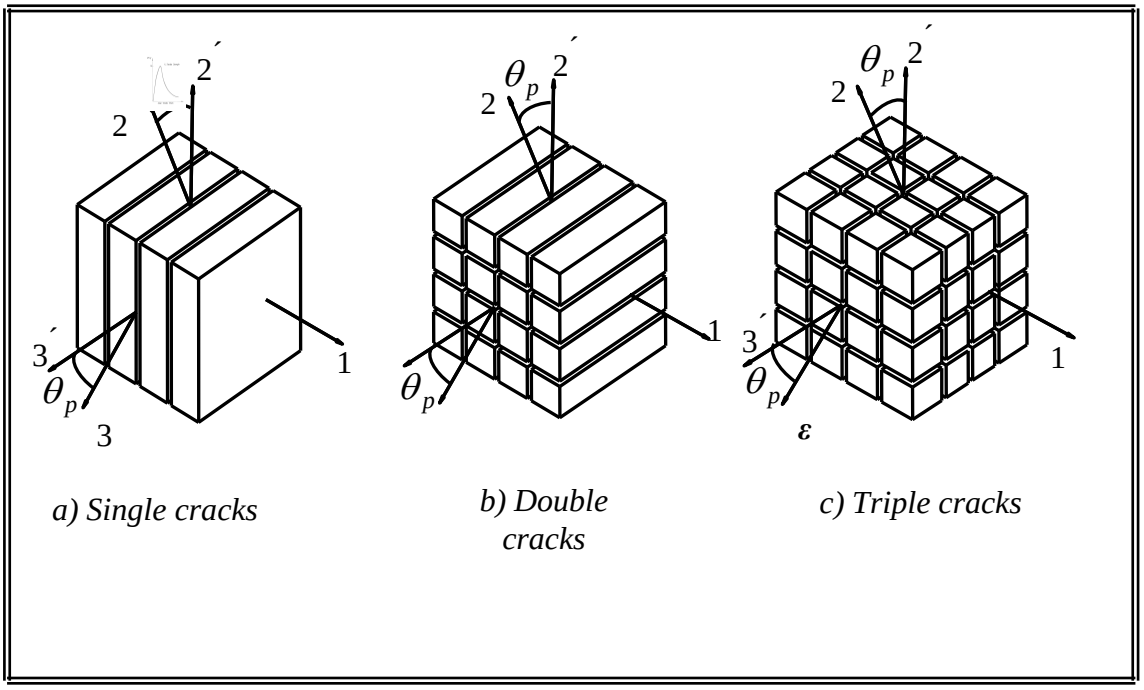

a) Single cracks *b) Double cracks* *c) Triple cracks*

Fig. (4-11): Failure Cracking for Triaxially Loaded Concrete (**Al-Shaarbaf** 1990)

4.4.2 TENSION- STIFFENING MODEL

Since the cracked concrete can still initially carry some tensile stresses in the direction normal to the crack, the tension-stiffening effect is considered. This can be achieved by assuming a gradual release of the concrete stress component normal to the cracked plane Fig. (4-12). in the present work, the normal stress that is carried by cracked concrete can be obtained from the following expression:

a) For $\varepsilon_{cr} \le \varepsilon_n \le \varepsilon_{tf1}$

$$\sigma_n = \alpha_2 . \sigma_{cr} \qquad \text{….. (4-52)}$$

b) For $\varepsilon_{tf1} \le \varepsilon_n \le \alpha_1 \varepsilon_{cr}$

$$\sigma_n = \alpha_2 . \sigma_{cr} \left[\frac{\alpha_1 . \varepsilon_{cr} - \varepsilon_n}{\alpha_1 . \varepsilon_{cr} - \varepsilon_{tf1}} \right] \qquad \text{….. (4-53)}$$

c) For $\varepsilon_n \succ \alpha_1 . \varepsilon_{cr}$

$$\sigma_n = o.o \qquad \text{….. (4-54)}$$

Where:

ε_{cr} Is the cracking strain associated with the cracking stress f_t and α_1 and α_2 are the tension-stiffening parameters. α_1 represents the rate of stress release as the crack widens and α_2 represents the sudden loss of stress at instant of cracking.

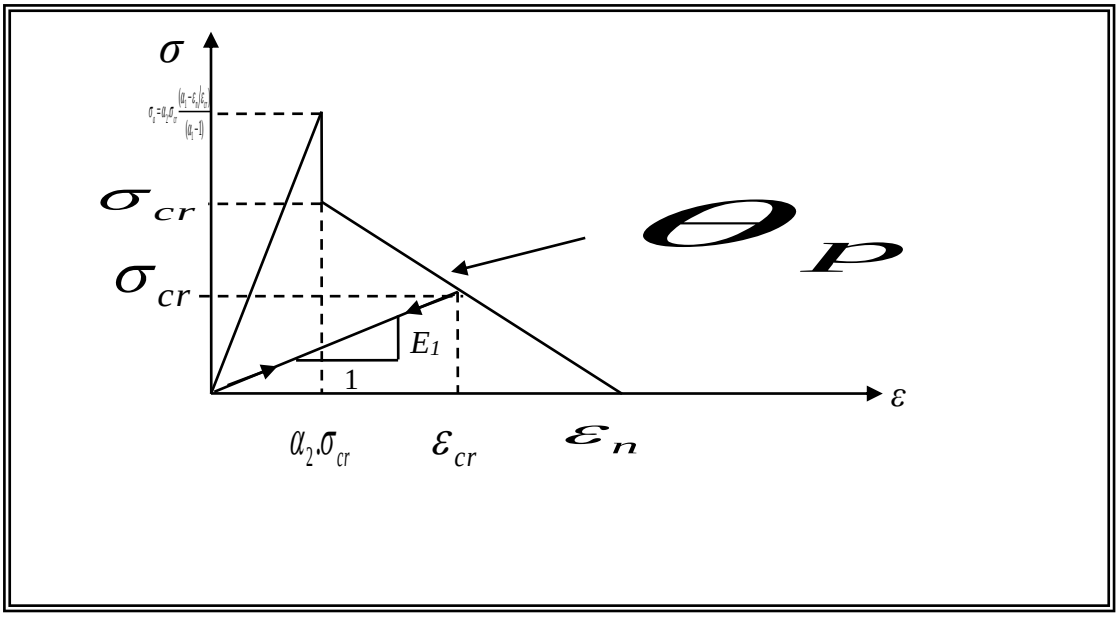

Fig. (4-12): Post-Cracking Model for Concrete in Tension **(Al-Shaarbaf** 1990)

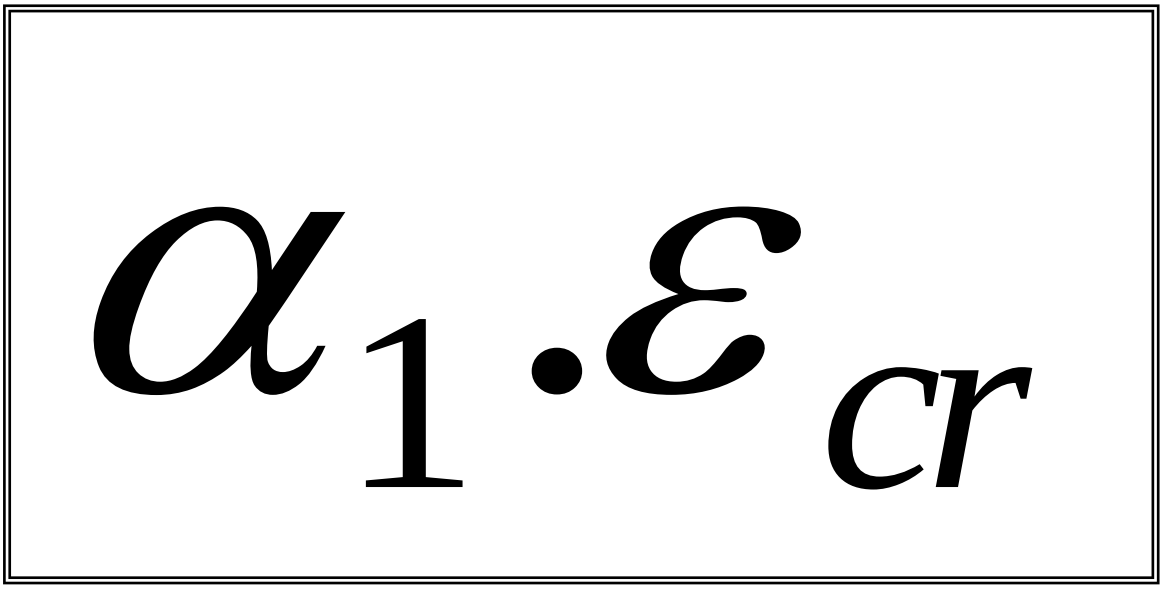

Fig. (4-13): Post-Cracking Model for Steel Fiber in Tension **(Al-Shaarbaf** 1990)

4.4.3 CLOSING AND RE-OPENING OF CRACKS

The unloading and reloading behavior can be obtained by using the secant path shown in Fig. (4-13). the secant modulus E_i can be evaluated from the previously stored maximum strain developed normal to the cracked plane. This secant modulus may be

Used to calculate the retained stress as:

$$\sigma_n = E_i \, \varepsilon_n \qquad \text{….. (4-55)}$$

Where σ_n and ε_n are the stress and strain normal to the cracked plane. When the crack is completely closed, the effects of any residual strain are neglected.

4.4.4 SHEAR RETENTION MODELS

The shear stiffness at a cracked sampling point becomes progressively smaller as the crack widens. The dowel action of the reinforcing steel and aggregate interlocking contributes to produce a considerable residual shear stiffness of cracked concrete. Thus a reduction factor (β) has been used across the cracked planes to reduce the shear stiffness at the cracked sampling point. Before cracking (β) equal (1.0), when the cracks propagate the shear reduction factor (β) is assumed to decrease linearly as shown in Fig. (4-14). When the crack is opened, a constant value of (β) is set to account for the dowel action. The shear retention model can be expressed as **(Al-Shaarbaf** 1990):

a) For $\varepsilon_n < \varepsilon_{cr}$

$$\beta = 1.0 \qquad \text{….. (4-56)}$$

b) For $\varepsilon_{cr} \le \varepsilon_n \le \gamma_1 \varepsilon_{cr}$

$$\beta = \frac{\gamma_2 - \gamma_3}{\gamma_1 - 1}\left[\gamma_1 - \frac{\varepsilon_n}{\varepsilon_{cr}}\right] + \gamma_3 \qquad \text{….. (4-57)}$$

c) For $\varepsilon_n > \gamma_1 \varepsilon_{cr}$

$$\beta = \gamma_3 \qquad \text{….. (4-58)}$$

Where γ_1, γ_2, and γ_3 are the shear retention parameters, γ_1 is the rate of decaying of shear stiffness as the crack widens, γ_2 is the sudden loss in the shear stiffness at the onset of cracking, and γ_3 is the residual shear stiffness due to the dowel action.

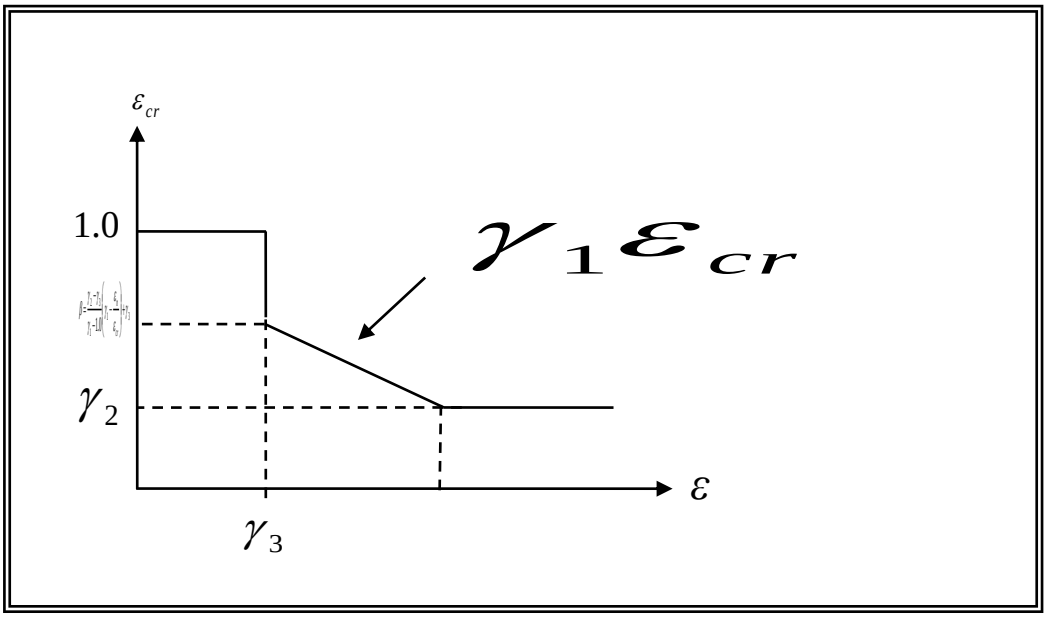

4.4.5 MODELING THE COMPRESSIVE STRENGTH REDUCTION DUE TO ORTHOGONAL CRACKS

In reinforced concrete members, a significant degradation in compressive strength can result due to the presence of transverse tensile strain after cracking.

In plasticity – based model, effects of transverse tensile strain on the yield criterion and the evolution of the subsequent loading surfaces can be simulated by scaling the equivalent uniaxial stress – strain relationships given by equation (b-2) and (4-19) according to the current value of the compressive

strength reduction factor. The model incorporated in the current study is based on the proposals of (**Cervenka** 1985), which illustrates the use of the reduction factor (λ_1) to reduce both the peak stress and corresponding strain, therefore, from equation (b-2, 4-18, 4-19 and 4-20).

The modified stress – strain relationship can be written as **(Al-Shaarbaf** 1990 and **Chen** 1982):

a.) For $\sigma \le \lambda_1 C_p . f'_{cf}$

$$\sigma = E.\varepsilon_{cf} \qquad \text{….. (4-59)}$$

b.) For $\lambda_1 . C_p . f'_{cf} \le \sigma \le \lambda_1 . f'_{cf}$

$$\sigma = \lambda_1 . C_p . f'_{cf} + E\left[\varepsilon_{cf} - \frac{\lambda_1 . C_p . f'_{cf}}{E}\right] - \frac{E}{2\varepsilon'_0}\left[\varepsilon_{cf} - \frac{\lambda_1 . C_p . f'_{cf}}{E}\right]^2 \qquad \text{….. (4-60)}$$

c.) For $\varepsilon_c \ge \varepsilon'_0$

$$\sigma = \lambda_1 . f'_{cf} \qquad \text{….. (4-61)}$$

Where,

$$\varepsilon'_o = \frac{2(1 - C_p).\lambda . f_{cf}}{E} \qquad \text{….. (4-62)}$$

Consequently, the effective stress – plastic strain relation can be modified as:

$$\bar{\sigma} = \lambda_1 . C_p . f'_{cf} - E.\varepsilon_p + \sqrt{2.E.\lambda_1 . \varepsilon'_0 . \varepsilon_p} \qquad \text{….. (4-63)}$$

And hence, the hardening parameter can be expressed as:

$$H' = \frac{d\bar{\sigma}}{d\varepsilon_p} E.\left[\left[\frac{\lambda_1 \varepsilon'_0}{2.\varepsilon_p}\right]^{\frac{1}{2}} - 1.0\right] \qquad \text{….. (4-64)}$$

For a singly cracked sampling point, the compression reduction factor is given by:

$$\lambda_1 = 1.0 - k_1 \frac{\varepsilon}{0.005} \le 1.0 - k_1 \qquad \text{….. (4-65)}$$

Where, ε_1 is the transverse tensile strain in principal direction 1.

For a doubly cracked sampling point the expression can be taken as:

$$\lambda_1 = 1.0 - k_1 \frac{\sqrt{\varepsilon_1^2 + \varepsilon_2^2}}{0.005} \leq 1.0 - k_1 \qquad \text{….. (4-66)}$$

Where ε_2 is the tensile strain normal to the second crack, and k_1 represents a compression reduction parameter. (**Cervenka** 1985) has used values ranging between (0.27 and 0.73) for the parameter k_1.

4.5 MODELING OF REINFORCEMENT

In this study the reinforcing steel is modeled as linear elastic, a homogenous material and can be assumed to have the same strength in tension and compression and behavior and its mechanical properties in comparison to the properties of concrete are well known and well understood. Reinforcing bars are long and slender and therefore can be generally assumed to be capable of transmitting axial forces only.

In current study, an elastic- linear work hardening model as shown in Fig. (4-15) simulates the uniaxial stress-strain behavior of steel bars.

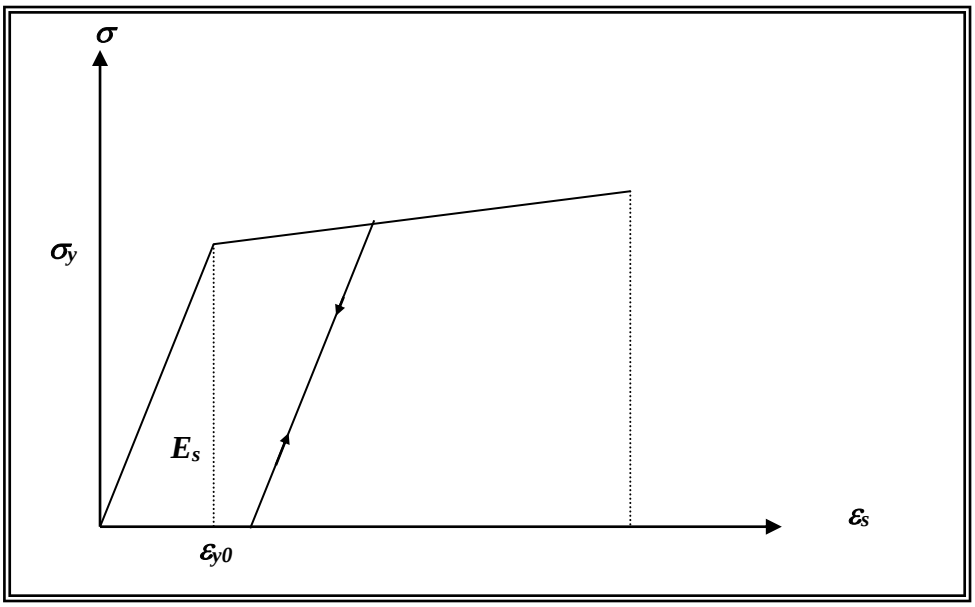

Fig. (4-15): Stress-Strain Relationship of Steel Bars Used in the Present Analysis

Chapter Four

MODELING OF MATERIAL PROPERTIES

4.1 INTRODUCTION

The efficiency and accuracy of the nonlinear finite element approach in the analysis of reinforced concrete structures depends mainly on the suitable modeling of material properties. The modeling implies choosing the suitable element type, simulation of the actual behavior of the material properties, choosing of sufficient number of the sampling points and selection of the proper integration technique (**Diab** 1998).

Cementations materials such as concrete, mortar and cement paste have a weakness in resisting tension, impact and other types of loading. This weakness is due to the material's inability to prevent small cracks, which can originate at flaws or voids, from becoming unstable under small tensile stresses. To overcome this weakness, steel, glass, polymer and other types of fiber have been added as reinforcement, thus producing a composite material. Even though the percentage by volume of the fibers is small, the mechanical behavior of the resulting composite material is substantially different from that of the matrix material. The composite generally possesses higher tensile strength, ductility and fracture toughness. For both design and research purposes, mathematical models have been formulated to predict the mechanical behavior of composite depending on the mechanical properties of the matrix and fibers.

Because non-linear finite element analysis is computationally expensive, simplified models to simulate material behaviour are required. However, these models should adequately predict the overall behaviour of the member. Realistic modeling of material behaviour is also needed to predict the effects caused by static loading at serviceability design load intensities, and to predict ultimate load. This chapter outlines the constitutive models for the fiber reinforced concrete and the reinforcing bars used in the present study.

4.2 BEHAVIOR OF STEEL FIBER REINFORCED CONCRETE

The behavior of steel fiber reinforced concrete material is discussed in the following sections.

4.2.1 UNIAXIAL COMPRESSIVE BEHAVIOR

Fibers do little to enhance the static compressive strength of concrete, with increases in strength ranging from essentially nil to perhaps 25%. Even in members that contain conventional reinforcement in addition to the steel fibers, the fibers have little effect on compressive strength. However, the fibers do substantially increase the post-cracking ductility, or energy absorption of the material.

This is shown graphically in the compressive stress-strain curves of SFRC in Fig. (4-1).The strain at peak compressive stress (ε_{pf}) can be expressed as (**Soroushian** and **Lee** 1989):

$$\varepsilon_{of} = 0.0021+0.0007\left[\frac{V_f . L_f}{D_f}\right] \qquad \text{....(4-1)}$$

where:

V_f The volume fraction of fibers.

L_f The fiber length.

D_f The fiber diameter.

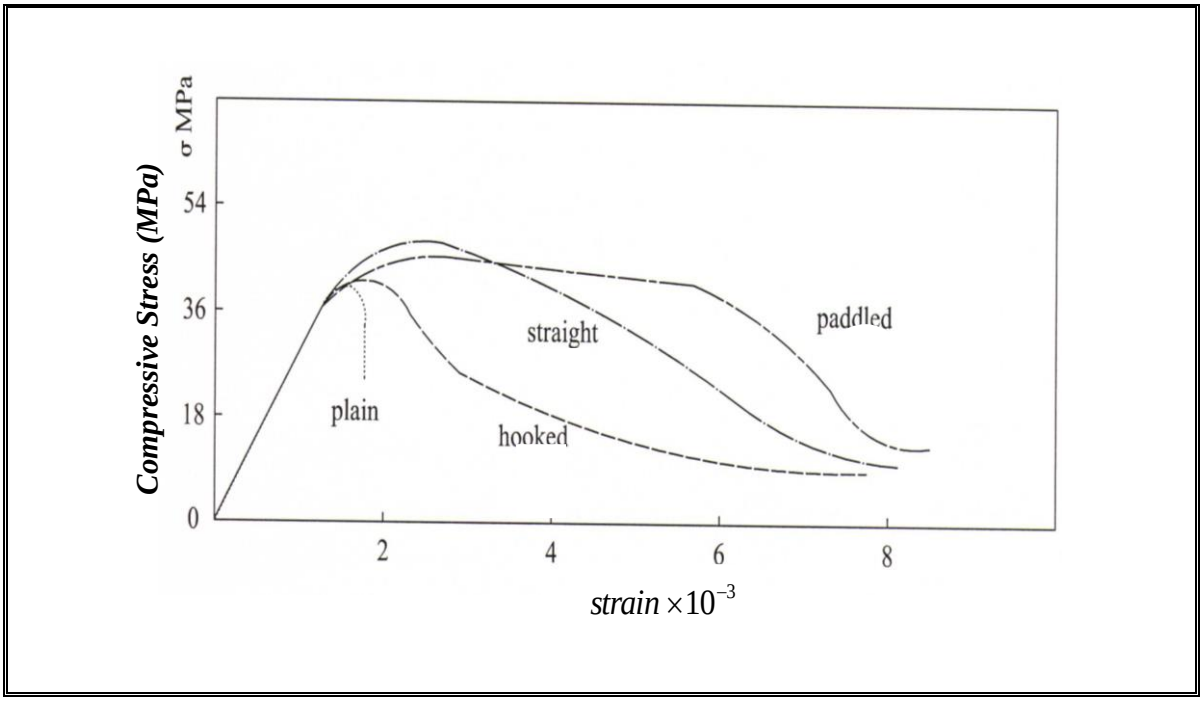

Fig.(4-1) Stress-Strain curves in compression for SFRC

(**Soroushian** and **Lee** 1989)

Also Fig.(4-1), shows that the stress-strain curve has a nearly elastic behavior up to about 30 percent of its maximum compressive strength f'_{cf} (like plain concrete). For stress beyond the level, the curve shows a gradual increase in the curvature up to about 0.8 f'_{cf}, where it bends more sharply and approaches the peak point at f'_{cf}. Beyond peak point, the stress-strain curve has a descending part. The shape of this descending part depends on the fiber parameters. Finally the crushing failure occurs at the ultimate strength ε_{cuf}.

An empirical equation to express the compressive strength of fibrous concrete material suggested by **(Soroushian and Lee** 1989) has been adopted throughout this research work:

$$f'_{cf} = f'_c + 3.6\frac{(Vf.Lf)}{Df} \qquad \text{…..(4-2)}$$

Test results indicate that the compressive strength of fibrous concrete depends on the method of fabrication, fiber geometry and fiber content (**Karij**

and **Pal** 1972). **Chen** and **Carson** (1972**)** concluded that the maximum increase in compressive strength of concrete is observed at volume fraction of fibers equals to 2% by using (0.46 ×13mm) steel fibers. Results of **(Pakotiprapha el.at.** (1974) show that the ultimate strength in axial compressive of the composite is smaller than the ultimate strength of the mortar. However, the presence of the fibers increases the ductility of the composite.

4.2.2 MODULUS OF ELASTICITY AND POISSON'S RATIO

For plain concrete, the modulus of elasticity E_c is highly dependent on the compressive strength f'_c. The modulus of elasticity E_c can be calculated with responsible accuracy from the empirical formula recommended by ACI committee-318 M02 as:

$$E_c = 43.W_c^{1.5}.f'^{0.5}_c.10^{-3} \quad .....(4\text{-}3)$$

Where W_c is concrete unit weight kg/m^3 and both E_c and f'_c are expressed in MPa.

It may be assumed that the steel fibrous concrete material behaves elastically up to the strain value required for crack propagation. During the elastic stage, the load carried by unit area of the composite is divided between the matrix and the fibers. The modulus of elasticity of the steel fiber reinforced material is given by:

$$E_m = E_c.V_m + \eta_\lambda.\eta_o.V_f.E_f \quad .....(4\text{-}4)$$

Where, E_c, is the modulus of elasticity of the matrix given by Eq.(4.3), and E_f, is the modulus of elasticity of the fibers. V_m and V_f are the volume fractions of the matrix and fibers respectively. While, η_o, is the orientation factor of fiber. The value of orientation factor depends on the distribution of fiber. For three-dimensional random orientation, this factor has been found to vary between 0.33 and 0.5. Also, η_λ is the length efficiency factor, to account

for the varying fibers stress at the end portions of fibers. The factor η_λ is defined as the ratio of the average fiber stress to the maximum fiber stress. Hence:

$$\eta_\lambda = \begin{cases} 0.5\dfrac{L_C}{L_f} & for L_f < L_c \\ 1 - L_c / L_f & for L_f > L_c \end{cases} \qquad \text{…..(4-5)}$$

Where, Lf and L_c are the actual and critical lengths of the fiber respectively. The critical length L_c is defined as the length required developing the ultimate fiber stress σ_{fu} when a uniform ultimate bond stress τ_u between the fiber and the matrix is assumed, to occur, therefore,

$L_c = 0.5.\ \sigma_{fu}.\ D_f / \tau_u$ …..(4-6)

Where, σ_{fu} is given by:

$$\sigma_{fu} = \eta_\lambda \eta_o\ V_f\ \frac{L_f}{2r}\ \tau_u \qquad \text{…..(4-7)}$$

And D_f is the diameter of the fiber and r is the ratio of the fiber cross section to its perimeter. The volume fraction of the matrix, V_m is given by:

$V_m = (1 - \eta_o V_f)$ …... (4-8)

Poisson's ratio (υ) for concrete under uniaxial compressive loading ranges from about (0.15 to 0.22). The ratio (υ) remains constant until approximately 80 percent of $f`_c$, at which stress the apparent Poisson's ratio begins to increase (**Chen** 1982).

4.2.3 UNIAXIAL TENSILE BEHAVIOR

In the case of tensile loading, very important change in the stress-strain curve can be achieved by the addition of a suitable amount of fiber reinforcement. A typical tensile stress-strain curve of steel fiber reinforced concrete is shown in Fig. (4-2)

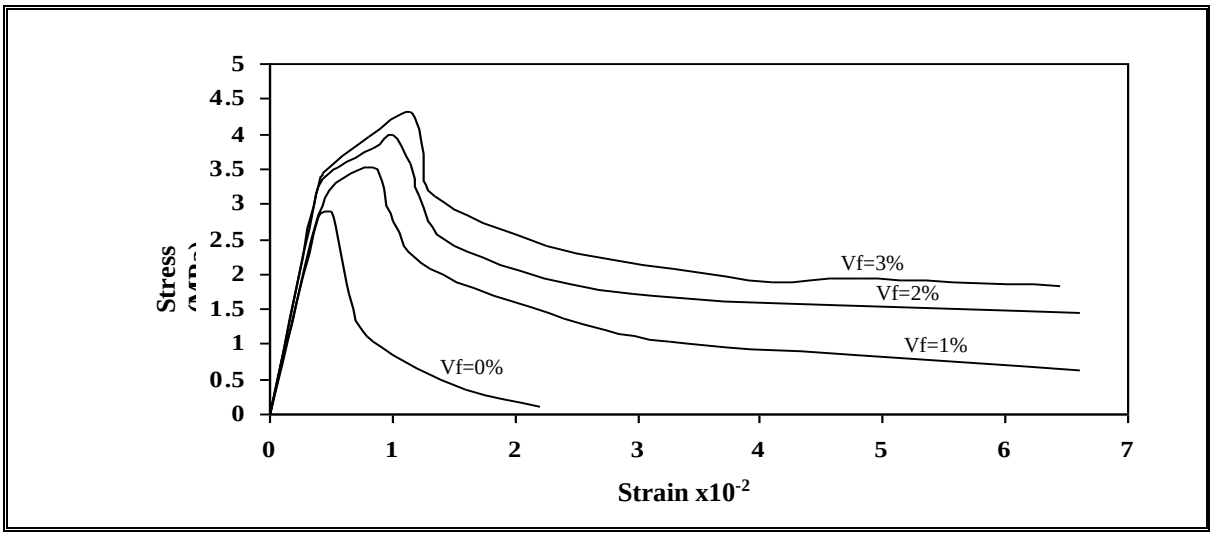

Fig. (4-2) Tensile stress-strain curve of steel fiber reinforced concrete (**Soroushian** and **Bayasi** 1987).

The ascending part of the curve, up to the first cracking, is similar to that of plain concrete, and then it tends to deviate from linearity due to the process of micro crack propagation in matrix prior to the formation of a continuous crack system at peak stress. This is followed by formation of an unstable micro crack system, which grows rapidly under the tensile stress bringing the material to its post-peak region.

The process of micro crack propagation tends to be influenced by the presence of fibers. Micro cracks encountering steel fibers may be shifted or branched out, (spacing concept) Fig. (4-3). Hence, the propagation of micro cracks in steel fiber reinforced concrete involves dissipation of additional energy form the stress-system due to the interaction of micro- cracks with fibers. This explains an important mechanism through which fibers increase the tensile strength of concrete.

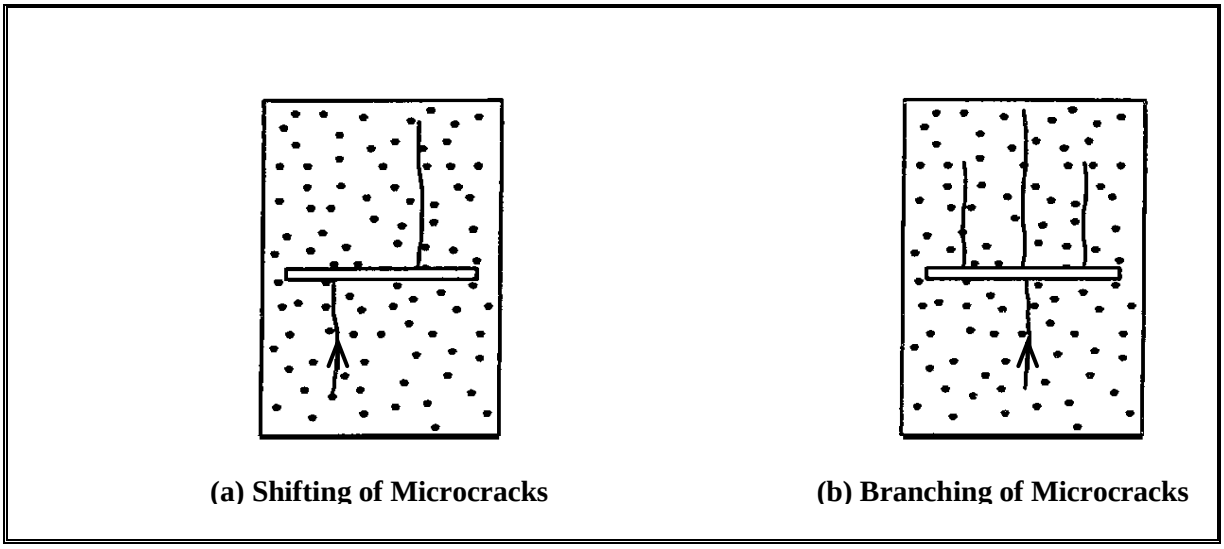

Fig. (4-3) interaction of micro-cracks with steel fibers (**Soroushion and Lee** 1989**)**.

On the other hand, the debonding and pull-out of fibers (composite concept), Fig. (4-4) enhances the tensile behavior of the steel fibrous concrete close to the peak tensile stress and at the post peak region. The pull-out action of the fibers would be mobilized when a crack tends to widen at critical sections, which transfers particularly all tensile stresses to the fibers bridging the crack by fractional forces.

This action starts to occur at peak load and largely provides the post-peak tensile resistance of the fibrous concrete. Therefore, the tensile stress-strain model of steel fiber concrete is divided into two regions, namely the pre-peak and post-peak regions (**Soroushian** and **Bayasi** 1987).

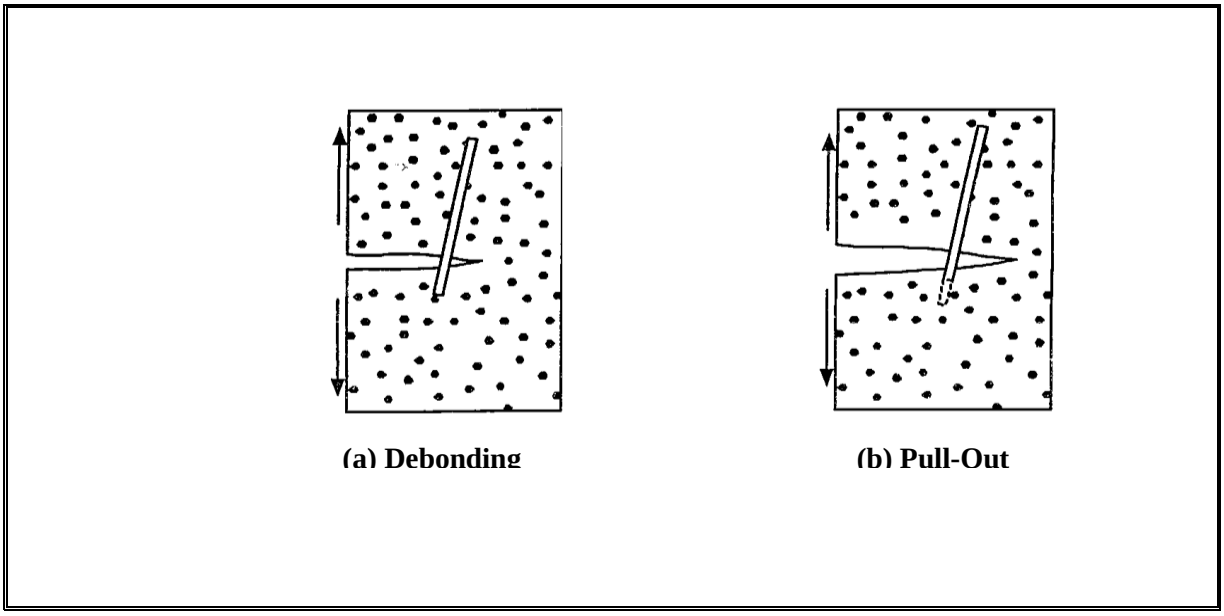

Fig.(4-4) debonding and pull-out of fibers under tension(**Soroushion and Lee** 1989**)**.

Many investigations simulate this region by a linearly elastic model up to its composite tensile strength f_{tf}. Either the "composite material concept", or the "spacing concept" has generally been used to predict the tensile strength of fibers, **(Soroushion** and **Lee** 1989) use the so called "interaction concept", which attributes the increase in tensile strength of fibrous concrete to microcrack-arrest of fibers as well as to the pull-out action of fibers which is only partially mobilized at the peak tensile stress of the material. In their study the following equations have been used to predict the tensile strength f_{tf} of steel fiber reinforced concrete.

$$f_{tf} = ft\left(1 + 0.016Nf^{\frac{1}{3}} + 0.05\pi.df.lf.Nf\right) \qquad \text{…..(4-9)}$$

And the composite tensile strain at peak tensile stress is given by:

$$\varepsilon_{tf} = \varepsilon_t\left(1 + 0.35Nf.df.lf\right) \qquad \text{….. (4-10)}$$

$$\varepsilon_t = \frac{lf.\tau_u}{df.Ef} \qquad \text{….. (4-11)}$$

Where:

Nf The number of fibers per unit cross-section area; given by:

$$Nf = \eta_0 \left[\frac{4vf}{\pi df^2} \right] \quad \text{….. (4-12)}$$

η_0 The orientation factor of fibers; $(\eta_0 = 0.5)$ for random distribution.

τ_u The shear stress between the fiber and the concrete given by:

$$\tau_u = \eta_b (2.26 - 0.0036 Nf) \quad \text{….. (4-13)}$$

η_b The bond efficiency factor ($\eta_b = 1.0$ or 0.75 for hooked or straight fiber respectively).

4.2.4 BIAXIAL BEHAVIOR OF FIBROUS CONCRETE

Michael et. al. (1976) carried out an experimental study for steel fiber reinforced mortar under biaxial compression. They found that the compressive strength was increased by about 72% as compared with the uniaxial compressive strength at a stress ratio (σ_1/σ_2) of 0.6. Fig. (4-5) illustrated a typical biaxial strength envelope for plain concrete subjected to proportional biaxial loading.

(**Abbas** 1989) tested steel fiber reinforced concrete, with different aspect ratios, under biaxial stresses by using sequential loading system. They divided the tested specimens into three groups according to the states of stress (biaxial compression, biaixil compression-tension and biaxial tension states). They concluded from the results that this effect of biaxial stress increased the strength of fibrous concrete under biaxial compression and tension states, whereas it decreased the strength under biaxial tension-compression state.

(**Yin et. al**. 1989) presented an experimental study to investigate the effect of biaxial compression stress on steel fibrous and plain concrete. The compressive stresses were applied through brush – type loading plate to eliminate frictional stresses between the concrete and the plates. The test program covered four principal compression stress ratios ranging from 0.0 to

1. Steel fibers with 25.4 mm diameter and 19 mm length, and volume fraction of 1.0 and 2.0 percent have been used. The test results showed that fiber content possesses higher strength than plain concrete in biaxial compression. The increase was as high as 35% in the case of 25.4 mm fiber length, 2% volume ratio, and a stress ratio of 0.2. Observation of failure modes reveals that splitting type failure occurs in plain concrete but faulting-type failure occurs in the fibrous concrete.

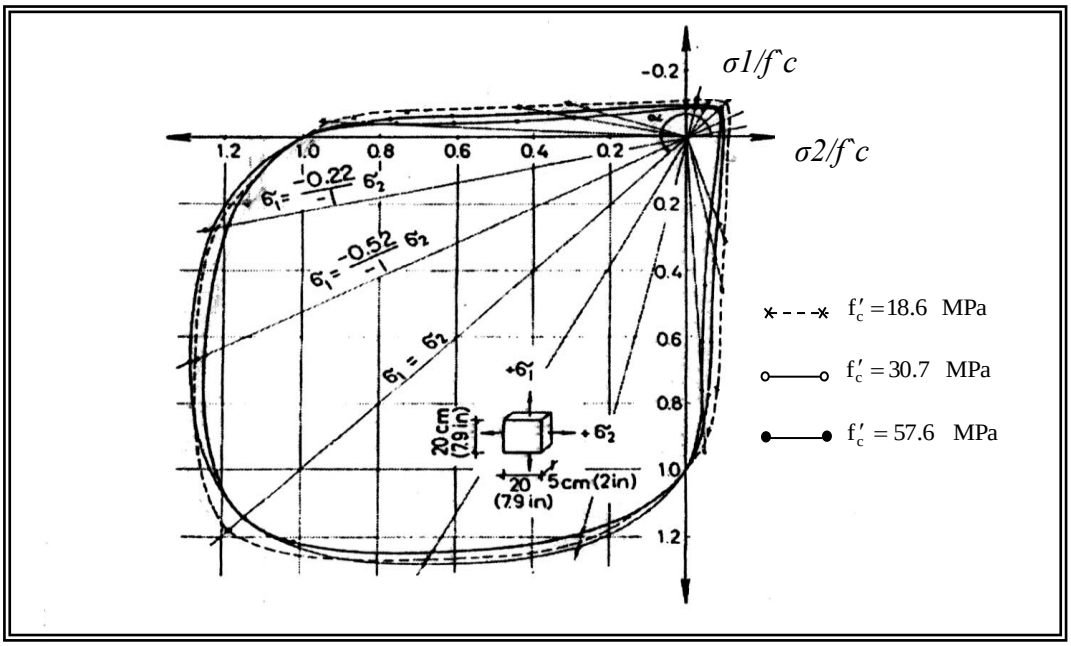

Fig. (4-5): Failure Envelope of Concrete in Biaxial Stress Space (**Chen** 1982)

4.2.5 TRIAXIAL BEHAVIOR OF FIBROUS CONCRETE

Experiments under triaxial loading indicate that the failure surface for concrete is a function of three principal stresses, Fig. (4-6). the deviatoric sections (plains perpendicular to the axial $\sigma_1=\sigma_2=\sigma_3$) of the failure surface are convex and non-circular, but for increasing hydrostatic compression they become more circular. No test of the response of concrete in hydrostatic tension has been reported, most triaxial tests on concrete have been concerned with ultimate failure. Generally, the maximum tensile strength is approximately equal to the tensile strength in the uniaxial tension and the failure mode corresponds to forming a crack plane perpendicular to the largest principal tensile stress direction. Under combination of compression and tension states, it is observed that the compressive strength decreases when the applied tensile stress increases.

Typical stress-strain curves are shown in Fig. (4-7). These curves show that the ultimate axial compressive strength of concrete increases with increasing hydrostatic (confining) stress, and the high stresses resisted by concrete under high confining compression are always accompanied by large deformation or ductility. Much of the deformation under triaxial loading is due to inelastic reduction of volume or a compaction of the concrete under stress. The amount of compaction varies considerably with the quality of concrete (less for high strength concrete). Different modes of failure have been observed for concrete under triaxial compression. The failure modes showed a distinct transion from splitting tension under low confinement, over shear faulting under intermediate confinement, to distribute plastic flow at high confinement.

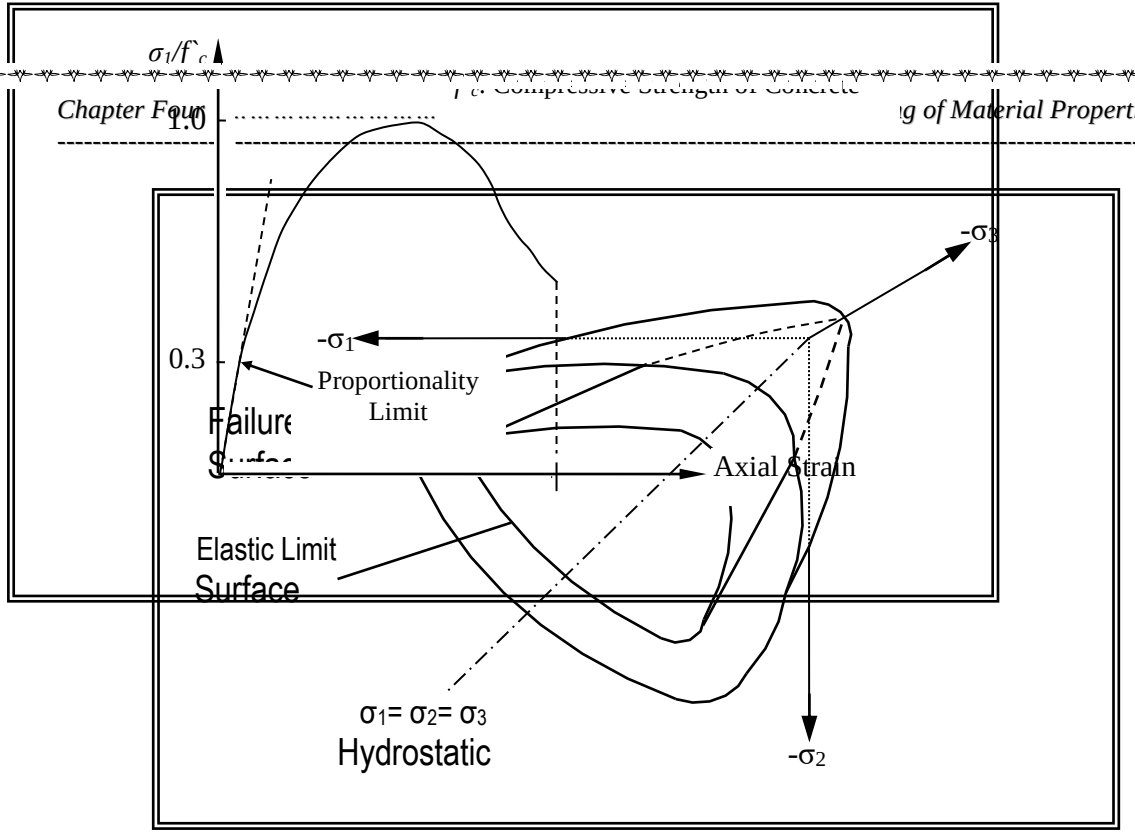

Fig.(4-6): Typical Triaxial Failure Envelope of Concrete (**Chen** 1982)

Fig.(4-7): Typical Unixial Stress-Strain Curve for Concrete in Compression (**Chen** 1982)

4.3 STRESS-STRAIN MODELS FOR CONCRETE IN COMPRESSION

The plasticity – based model has been used to describe the nonlinear behavior of concrete in compression. In this approach, the nonlinear deformations occur when concrete is stressed beyond its limit of elasticity. The total strain may be separated into recoverable and irrecoverable parts. The recoverable part represents the framework of elasticity, while the treatment of the irrecoverable part is based on the theory of plasticity. Under triaxial compression, concrete can flow like a ductile material on the yield or failure surfaces before reaching its crushing strains (**Chen** 1982).

In this study, the behavior of concrete in compression is simulated by an elasto-plastic work hardening model followed by a perfectly plastic response, which is terminated at the onset of crushing. The adopted plasticity model will be illustrated in terms of the following constituents:

a) The yield criterion.
b) The hardening rule.
c) The flow rule.
d) The incremental stress – strain relationship.
e) The crushing condition.

4.3.1 YIELD CRITERION

The meterial is assumed to behave elasticity until it reaches the yeild limit, until a certain function of the stress component reaches a prescribed value, which is known as the yeild surface. For isotropic material, the initial yield criterion should be independent of the orientation of the coordinate system in which the stress state is defined, and therefore, it should be a function of the stress invariants only. The yield criterion used in the present

work has been successfully used by many researchers(**Chen** 1982, **Own** 1980 and **Al-Shaarbaf** 1990) . It can be expressed as:

$$\sigma_o = f(\{\sigma\}) = cI_1 + \left[(cI_1)^2 + 3\beta J_2\right]^{1/2} \quad \text{…..(4-14)}$$

where c and β are material parameters, I_1 is the first stress invariant given by:

$$I_1 = \sigma_x + \sigma_y + \sigma_z \quad \text{…..(4-15)}$$

and J_2 is the second deviatoric stress invariant given by:

$$J_2 = \frac{1}{3}\left\{ \left[\sigma_x^2 + \sigma_y^2 + \sigma_z^2\right] - \left[\sigma_x\sigma_y + \sigma_y\sigma_z + \sigma_z\sigma_x\right] \right\} + \left[\tau_{xy}^2 + \tau_{yz}^2 + \tau_{zx}^2\right] \text{….. (4-16)}$$

And σ_o is the equivalent effective stress at the onset of plastic deformation that can be determined from the uniaxial compression test as:

$$\sigma_o = C_p . f_c' \quad \text{..... (4-17)}$$

Where, C_p is the plasticity coefficient which is used to mark the initiation of the plastic deformation.

The parameters c, andβ, are determined from the uniaxial and biaxial experimental results carried out by (**Kupfer** 1969) for plain concrete as:

$c = 0.17734$ And $\beta = 1.35468$

For steel fiber reinforced concrete, the parameters β and c are determined from the uniaxial and biaxial experimental results given in references ((**Allose** 1995, (**Yin**, **Mansur** and **Thomas** 1989)) taking into account the volume fraction of fibers. The value and procedure for calculation these parameters are given in Table (4-1) and Appendix [B].

Table (4-1) Calculation of parameters β and C for different fiber content.

((**Allose** 1995, (**Yin**, **Mansur**, **Thomas** 1989))

Fiber content V_f (%)	γ	α	β	C
0.0	1.16	0.3546798	1.3546798	0.1773399
0.5	1.39	1.0993042	2.0993042	0.596521
1.0	1.47	1.4900526	2.4900526	0.740263
2.0	1.52	1.760526	2.7960526	0.8980263

4.3.2 THE HARDENING RULE

The hardening rule is required to define the motion of the subsequent loading surfaces during plastic loading. To describe the growth of the subsequent loading surfaces for a strain-hardening material, many hardening rules have been proposed. The isotropic hardening rule is the simplest one to formulate and has been adopted in the present study to simulate concrete behavior. This rule assumes that the yield surface expands uniformly without distortion as plastic deformation occurs **(Al-Shaarbaf** 1990, **Diab** 1998)**)**. Therefore, the subsequent loading surfaces may be written as:

$$\bar{\sigma} = f(\{\sigma\}) = cI_1 + \left[(cI_1)^2 + 3\beta J_2 \right]^{1/2} \qquad \text{….. (4-18)}$$

Where the effective stress or equivalent uniaxial stress $\bar{\sigma}$ represents the stress level at which further plastic deformation will occur.

In the present model, a parabolic stress-strain curve is used for the equivalent uniaxial stress-strain relationship of steel fiber reinforced concrete beyond the limit of elasticity as shown in Fig. (4-8), $C_p f'_{cf}$. This parabolic curve represents the work-hardening stage of behavior. When the peak compressive stress is reached, a perfectly plastic response is assumed to occur **(Al-Shaarbaf** 1990**)**. These relationships are given by:

a) For $\varepsilon_{cf} \leq C_p f'_{cf} \backslash E$

$$\bar{\sigma} = E.\varepsilon_{cf} \qquad \text{…..(4-19)}$$

b) For $C_p f'_{cf} \backslash E \le \varepsilon_{cf} \le f'_{cf} \backslash E$

$$\bar{\sigma} = C_p.f'_{cf} + E\left[\varepsilon_{cp} - \frac{C_p.f'_{cf}}{E}\right] - \frac{E}{2\varepsilon'_o}\left[\varepsilon_{cf} - \frac{C_p.f'_{cf}}{E}\right]^2 \qquad \text{….. (4-20)}$$

c) For $\varepsilon_{cf} \ge (2 - C_p).\frac{f'_{cf}}{E}$

$$\bar{\sigma} = f'_{cf} \qquad \text{…..(4-21)}$$

Where ε'_o is the total strain corresponding to the parabolic part of the curve given by:

$$\varepsilon'_o = 2(1 - C_p)\frac{f'_{cf}}{E} \qquad \text{….. (4-22)}$$

By substituting the value of the total strain component, which is the sum of the elastic and plastic strains into Eq. (4-20), the effective stress-plastic strain relationship can be expressed as:

$$\bar{\sigma} = C_p f'_c - E \cdot \varepsilon_{cp} + (2E^2 \cdot \varepsilon'_o \cdot \varepsilon_p)^{1/2} \qquad \text{….. (4-23)}$$

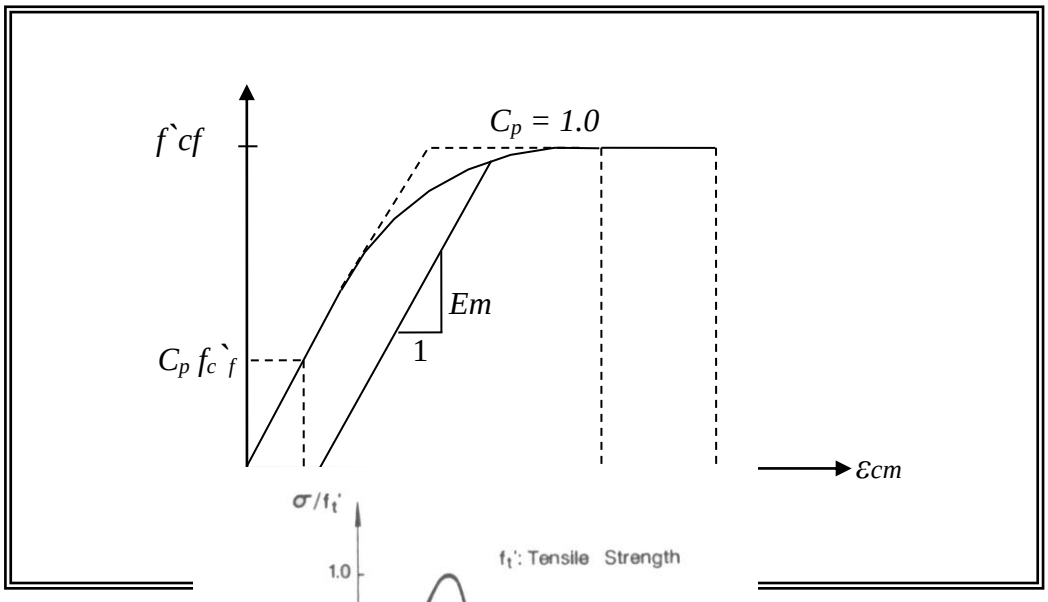

Fig. (4-8): Un e **(Al-Shaarbaf** 1990)

The hardening coefficient H', which is the slope of the effective stress-plastic strain curve, is used in the formulation of the elasto-plastic incremental stress-strain relationship. By differentiation of Eq. (4.23) with respect to the effective plastic strain, the hardening parameter can be expressed as:

$$H' = \frac{d\bar{\sigma}}{d\varepsilon_p} = E\left[\left(\frac{\varepsilon'_o}{2\varepsilon_p}\right)^{1/2} - 1.0\right] \qquad \text{….. (4-24)}$$

4.3.3 THE FLOW RULE

In the plasticity – based theory, when the current yield surface is reached, the material becomes in state of plastic flow upon further loading. The flow rule is usually employed to connect the loading function (*f*) and the stress – strain relation in the plastic range. This rule has been widely used for concrete models because of its simplicity **(Al-Shaarbaf** 1990 and **Chen** 1982).

The plasticity strain vector will be assumed to be normal to the yield surface; the plastic strain increment is given by:

$$d\{\varepsilon_p\} = d\lambda \frac{\partial f(\{\sigma\})}{\partial\{\sigma\}} \qquad \text{….. (4-25)}$$

Where $d\lambda$ is a positive scalar hardening parameter which can vary throughout the staining process. The normal to the current loading surface ($\frac{\partial f(\{\sigma\})}{\partial\{\sigma\}}$) is termed as the flow vector, which can be obtained by the derivatives the yield function with respect to the stress components, and given by:

$$\{a\} = \left[\frac{\partial f}{\partial\sigma_x}, \frac{\partial f}{\partial\sigma_y}, \frac{\partial f}{\partial\sigma_z}, \frac{\partial f}{\partial\tau_{xy}}, \frac{\partial f}{\partial\tau_{yz}}, \frac{\partial f}{\partial\tau_{zx}}\right] \qquad \text{….. (4-26)}$$

These derivatives can be evaluated from equation (b-2) with the use of equations (4-15) and (4-16) as:

$$\left.\begin{aligned}
\frac{\partial f}{\partial \sigma_x} &= C + \left[2(C^2+\beta)\sigma_x + (2C^2-\beta)(\sigma_y+\sigma_z)\right]/Q \\
\frac{\partial f}{\partial \sigma_y} &= C + \left[2(C^2+\beta)\sigma_y + (2C^2-\beta)(\sigma_x+\sigma_z)\right]/Q \\
\frac{\partial f}{\partial \sigma_z} &= C + \left[2(C^2+\beta)\sigma_z + (2C^2-\beta)(\sigma_x+\sigma_y)\right]/Q \\
\frac{\partial f}{\partial \tau_{xy}} &= 6\,\frac{\beta\,\tau_{xy}}{Q} \\
\frac{\partial f}{\partial \tau_{yz}} &= 6\,\frac{\beta\,\tau_{yz}}{Q} \\
\frac{\partial f}{\partial \tau_{zx}} &= 6\,\frac{\beta\,\tau_{zx}}{Q}
\end{aligned}\right\} \quad \text{….. (4-27)}$$

Where (C) and (β) are the material constants given in Table (4-1), and (Q) is given by:

$$Q = 2[(C^2+\beta)(\sigma_x^2+\sigma_y^2+\sigma_z^2) + (2C^2-\beta)(\sigma_x\,\sigma_y + \sigma_y\,\sigma_z + \sigma_z\,\sigma_x) + 3\beta(\tau_{xy}^2+\tau_{yz}^2+\tau_{zx}^2)]^{0.5} \quad \text{….. (4-28)}$$

4.3.4 THE INCREMENTAL STRESS – STRAIN RELATIONSHIP

The total incremental strain is composed of elastic and plastic strain, therefore:

$$d\{\varepsilon\} = d\{\varepsilon_e\} + d\{\varepsilon_p\} \quad \text{….. (4-29)}$$

Substituting equation (4-25) with equation (4-29) yields:

$$d\{\varepsilon\} = d\{\varepsilon_e\} + d\lambda\,\frac{df(\sigma)}{d(\sigma)} \quad \text{….. (4-30)}$$

the elastic strain increment is related to the stress increment by the elastic constitutive relation given by:

$$d\{\sigma\} = [D]\,d\{\varepsilon_e\} \quad \text{….. (4-31)}$$

Hence:

$$d\{\varepsilon_e\} = [D]^{-1}.d\{\sigma\} \qquad \text{….. (4-32)}$$

Where *[D]*, is the elastic constitutive matrix given by:

$$[D] = \frac{E}{(1+\nu)(1-2\nu)}\begin{bmatrix} 1-\nu & \nu & \nu & 0 & 0 & 0 \\ \nu & 1-\nu & \nu & 0 & 0 & 0 \\ \nu & \nu & 1-\nu & 0 & 0 & 0 \\ 0 & 0 & 0 & \frac{1-2\nu}{2} & 0 & 0 \\ 0 & 0 & 0 & 0 & \frac{1-2\nu}{2} & 0 \\ 0 & 0 & 0 & 0 & 0 & \frac{1-2\nu}{2} \end{bmatrix} \qquad \text{….. (4-33)}$$

Substituting equation (4-29) into equation (4-31) yields:

$$d\{\varepsilon\} = [D]^{-1}.d\{\sigma\} + d\lambda.\{a\} \qquad \text{….. (4-34)}$$

Pre-multiplying both sides of equation (4-34) by, *($\{a\}^T.[D]$)* and eliminating *($\{a\}^T.d\{\sigma\}$)*, the following expression for the plastic multiplier, dλ is obtained :

$$d\lambda = \left[\frac{\{a\}^T.[D]}{H' + \{a\}^T.[D].\{a\}}\right].d\{\varepsilon\} \qquad \text{….. (4-35)}$$

By substituting equation (4-35) with equation (4-29) and pre-multiplying both sides by *[D]*, the complete elasto – plastic incremental stress – strain relationship can be expressed as:

$$d\{\sigma\} = \left[[D] - \frac{\{a\}^T.[D]}{H' + \{a\}^T.[D].\{a\}}\right].d\{\varepsilon\} \qquad \text{….. (4-36)}$$

Where the second term in the brackets represents stiffness degradation due to the plastic deformation.

4.3.4 CRUSHING CONDITION

Crushing of concrete indicates the complete rupture and disintegration of the material under compression stress state. After crushing, the current stresses

drop rapidly to zero and the concrete is assumed to lose its resistance completely against further deformation.

In the adopted model, the concrete crushing criterion is obtained when the strain reaches the ultimate strain. The crushing criterion is obtained by simply converting the yield criterion which is written in terms of stresses directly into strains, thus:

$$C.I_1' + \sqrt{(C.I_1')^2 + 3\beta.J_2'} = \varepsilon_{cu} \qquad \text{….. (4-37)}$$

Where ε_{cu} is the ultimate crushing strain of concrete, extrapolated from uniaxial test, I_1' and J_2' are the first strain invariant and the second deviatoric strain invariant that can be obtained by the following equations **(Al-Shaarbaf** 1990**)**:

$$I_1' = \varepsilon_x + \varepsilon_y + \varepsilon_z \qquad \text{….. (4-38)}$$

$$J_2 = \left(\frac{1}{3}\right)\left[\left(\varepsilon_x^2 + \varepsilon_y^2 + \varepsilon_z^2\right) - \left(\varepsilon_x\varepsilon_y + \varepsilon_y\varepsilon_z + \varepsilon_z\varepsilon_x\right)\right] + (\gamma_{xy})^2$$

$$+ (\gamma_{yz})^2 + (\gamma_{zx})^2 \qquad \text{….. (4-39)}$$

4.4 BEHAVIOR OF CONCRETE IN TENSION

The stress – strain curve of concrete in tension is linear up to about stress level of 60 percent of the uniaxial tensile strength f_t. above this level, the bond cracks start to grow and the nonlinearity of the curve starts to increase as the stress level increases until the peak stress. The term cracking indicates a partial collapse of the material across the plane of cracking under tensile stress states (**Chen** 1982).

After cracking, concrete changes from isotropic to orthotropic material. In the finite element analysis of concrete structures, three different approaches have been employed for crack modeling (**Chen** 1982):

1.) Smeared – cracking model.

2.) Discrete – cracking model.

3.) Fracture – mechanics model.

The particular cracking model to be selected depends upon the purpose of the analysis (**Kwak** 1997).

If the overall load – deflection behavior is desired without regard to completely realistic crack patterns and local stresses, the smeared – cracking model is probably the best choice. In this approach the cracked concrete is assumed to remain a continuum, and the concrete becomes orthotropic or transversely isotropic. After the first cracking has occurred, one of the material axes being oriented along the direction of the cracking as shown in Fig. (4-9). For most structural engineering applications, the smeared – cracking modeling is generally used (**Chen** 1982).

The discrete – cracking model represents a continuous smeared – cracking model; this is normally done by disconnecting the displacement at nodal points for adjoining elements as shown in Fig. (4-10). The difficulty in this approach is that the location and orientation of the cracks are not known. This approach is used to obtain details about the local behavior of concrete. While the applicability of fracture – mechanics model to reinforced concrete is still questionable (**Chen** 1982).

In the present study, the behavior of concrete in tension is simulated by linear elastic prior to cracking. The cracking criterion of concrete is expressed in terms of the principal tensile stress or strain. A smeared – cracking model with fixed orthogonal cracks is adopted to represent the fractured concrete.

The adopted model is desired in terms of **(Al-Shaarbaf** 1990**)**:

a.) Cracking criterion.

b.) Tension- stiffening model

c.) Closing and re- opening of cracks.

d.) Shear retention modal.

e.) Compressive strength reduction due to orthogonal crack mod

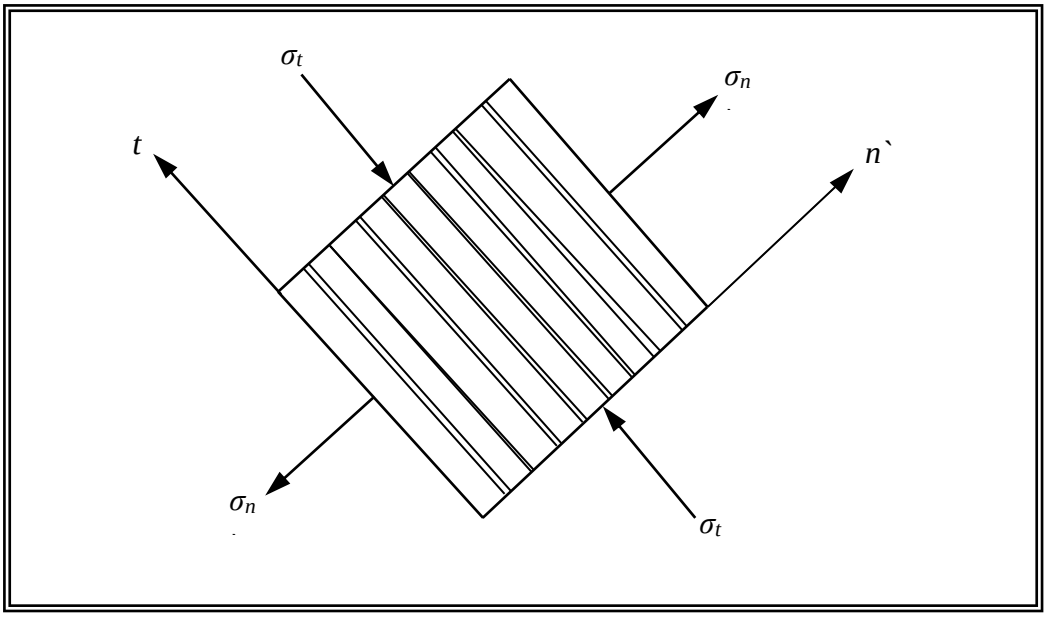

Fig. (4-9): Idealization of a Single Smeared Crack (**Chen** 1982)

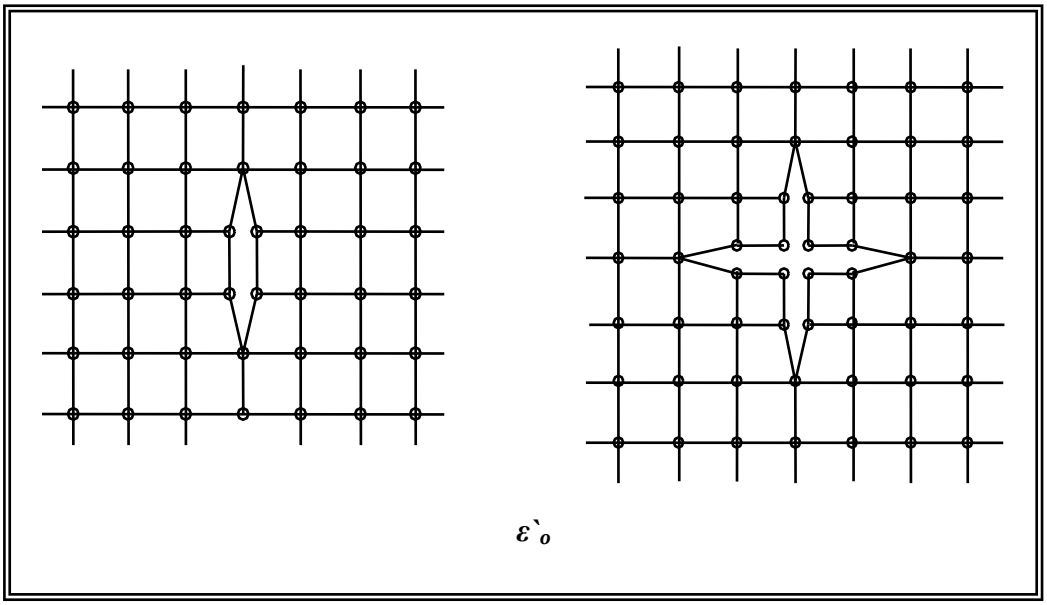

Fig. (4-10): Discrete Crack Model (**Chen** (1982)**)**

4.4.1 THE CRACKING CRITERION

In the present research, the onset of cracking is controlled by a maximum principal stress criterion. According to this criterion, cracking occurs when the principal tensile stress exceeds the limited tensile strength of concrete f_t, the limited tensile stress required to define the onset of cracking can be calculated for states of triaxial tensile stress and for combination of tension and compression principal stresses as **(Al-Shaarbaf** 1990**)**:

a.) For the triaxial tension zone ($\sigma_1 \geq \sigma_2 \geq \sigma_3 \geq 0$)

$$\sigma_i = \sigma_{cri} = f_{tf} \qquad \text{Where } i = 1, 2, 3 \qquad \text{….. (4-40)}$$

b.) For tension – tension – compression zone ($\sigma_1 \geq \sigma_2 > 0, \sigma_3 \leq 0$)

$$\sigma_i = \sigma_{cri} = f_{tf}[1.0 + \frac{0.75\sigma_3}{f'_{cf}}] \qquad i = 1,2 \qquad \text{….. (4-41)}$$

c.) For tension – compression – compression ($\sigma_1 > 0, \sigma_3 \leq \sigma_2 \leq 0$)

$$\sigma_i = \sigma_{cri} = f_t[1.0 + \frac{0.75\sigma_2}{f'_c}].[1.0 + \frac{0.75\sigma_3}{f'_c}] \quad i = 1 \qquad \text{….. (4-42)}$$

Where (σ_{cr}) is the cracking stress and both (ft) and ($f`_c$) are the tensile and compressive strengths of concrete substitute in positive values.

The last two equations (4-41) and (4-42) indicate that the presence of compressive stress in one direction favors the cracking in other directions and thus reduces the tensile capacity of the material.

After cracking, the modulus of elasticity in the direction of the maximum tensile stress (σ_1) is reduced because of the lack of interaction between orthogonal planes caused by cracking, Poisson's ratio (υ), is set to zero and a reduced shear modulus ($\beta_1.G$) is employed to model the shear strength deterioration. Therefore, the incremental stress – strain relationship in local material axes may be expressed as:

$$\begin{Bmatrix}\Delta\sigma_1\\ \Delta\sigma_2\\ \Delta\sigma_3\\ \Delta\tau_{12}\\ \Delta\tau_{23}\\ \Delta\tau_{31}\end{Bmatrix}=\begin{bmatrix}E_1 & 0 & 0 & 0 & 0 & 0\\ 0 & E/1-\nu^2 & \nu E/1-\nu^2 & 0 & 0 & 0\\ 0 & \nu E/1-\nu^2 & E/1-\nu^2 & 0 & 0 & 0\\ 0 & 0 & 0 & \beta_1 G & 0 & 0\\ 0 & 0 & 0 & 0 & G & 0\\ 0 & 0 & 0 & 0 & 0 & \beta_1 G\end{bmatrix}\begin{Bmatrix}\Delta\varepsilon_1\\ \Delta\varepsilon_2\\ \Delta\varepsilon_3\\ \Delta\gamma_{12}\\ \Delta\gamma_{23}\\ \Delta\gamma_{31}\end{Bmatrix} \quad \text{….. (4-43)}$$

Where (E_1) is the reduced modulus of elasticity in the direction of (σ_1) and (G) is the shear modulus of elasticity. Equation (4-43) can be written in a compact form as:

$$\{\Delta\sigma\}=[D_{cr}].\{\Delta\varepsilon\} \quad \text{….. (4-44)}$$

Where $[D_{cr}]$ is the material stiffness in the local axes. The stress increment in the global axes (x, y, and z) may be obtained by using the coordinate transformation matrix such that

$$\{\Delta\sigma\}=[T]^T.[D_{cr}].[T].\{\Delta\varepsilon\} \quad \text{….. (4-45)}$$

Where $[T]$, is the transformation matrix expressed in terms of the direction cosines as:

$$[T]=\begin{bmatrix} l_1^2 & m_1^2 & n_1^2 & l_1 m_1 & m_1 n_1 & n_1 l_1\\ l_2^2 & m_2^2 & n_2^2 & l_2 m_2 & m_2 n_2 & n_2 l_2\\ l_3^2 & m_3^2 & n_3^2 & l_3 m_3 & m_3 n_3 & n_3 l_3\\ 2l_1 l_2 & 2m_1 m_2 & 2n_1 n_2 & (l_1 m_2 + l_2 m_1) & m_1 n_2 + m_2 n_1 & n_1 l_2 + n_2 l_1\\ 2l_2 l_3 & 2m_2 m_3 & 2n_2 n_3 & (l_2 m_3 + l_3 m_2) & m_2 n_3 + m_3 n_2 & n_2 l_3 + n_3 l\\ 2l_3 l_1 & 2m_3 m_1 & 2n_3 n_1 & (l_3 m_1 + l_1 m_3) & m_3 n_1 + m_1 n_3 & n_3 l_1 + n_1 l_3\end{bmatrix} \quad \text{….. (4-46)}$$

Where l_i, m_i, and n_i represent the direction cosines with respect to x,y, and z directions respectively.

For both the tension – tension – compression and the triaxial tension states of stress, the cracking criterion may be violated by the major principal stress (σ_1) and the second principal stress (σ_2) simultaneously. Thus, two sets of orthogonal failure planes develop. These planes are perpendicular to the

principal axes 1 and 2 respectively as in Fig. ((4-11 (a and b)). In this case Poisson's ratio is set to zero in all directions and the constitutive matrix in the local material axis is reduced to the following form:

$$[D_{cr}]=\begin{bmatrix} E_1 & 0 & 0 & 0 & 0 & 0 \\ 0 & E_2 & 0 & 0 & 0 & 0 \\ 0 & 0 & E & 0 & 0 & 0 \\ 0 & 0 & 0 & \beta_1 G & 0 & 0 \\ 0 & 0 & 0 & 0 & \beta_2 G & 0 \\ 0 & 0 & 0 & 0 & 0 & \beta_1 G \end{bmatrix} \qquad \text{….. (4-47)}$$

In a fixed crack model, the rotation of the principal stresses after the formation of the first crack is ignored. However, if the second crack onsets at a subsequent stage of loading, rotation of the principal stresses within the planes perpendicular to direction of, $\sigma 1$ may be taken into account.

Magnitude and directions of the new second and minor principal stresses, $\sigma_1^{/}$ and $\sigma_3^{/}$, may be calculated from the original principal stresses, σ_2 and σ_3, and the shear stresses, τ_{23} accumulated during loading stages beyond the formation of the first crack. Thus:

$$\sigma_1^{/}=\frac{\sigma_2+\sigma_3}{2}\pm\left[\frac{(\sigma_2+\sigma_3)^2}{2}+\tau_{23}^2\right]^{0.5} \qquad \text{i=2, 3} \qquad \text{….. (4-48)}$$

For tension- tension-compression states, the onset of the second crack is expressed in terms of the new principal stresses as:

$$\sigma_2^{/}=\sigma_{cr}=f_{tf}\left[1+\frac{0.75\sigma_3^{/}}{f_{cf}^{/}}\right] \qquad \text{….. (4-49)}$$

Failure planes corresponding to the second crack are assumed to be perpendicular to the direction of the second principal stress, $\sigma_2^{/}$

Fig. (4-11b).

The angle between the original and the new in- plane sets of principal directions θ_p may be calculated:

$$\theta_p = \frac{1}{2}.\tan^{-1}\frac{2\tau_{23}}{\sigma_2 - \sigma_3} \qquad \text{….. (4-50)}$$

After the formation of the second crack, the local in-plane constitutive matrix with respect to the new principal directions ($2',3'$) is expressed as:

$$[D_{cr}] = \begin{bmatrix} E_2 & 0 & 0 \\ 0 & E & 0 \\ 0 & 0 & \beta_2 G \end{bmatrix} \qquad \text{….. (4-51)}$$

In the current model, a maximum of three sets of cracks are allowed to form at each sampling point. For triaxial tension states, a third crack may appear when the minor principal stress, (σ_3) exceeds the uniaxial tensile strength f_{tf} in Fig. (4-11c).

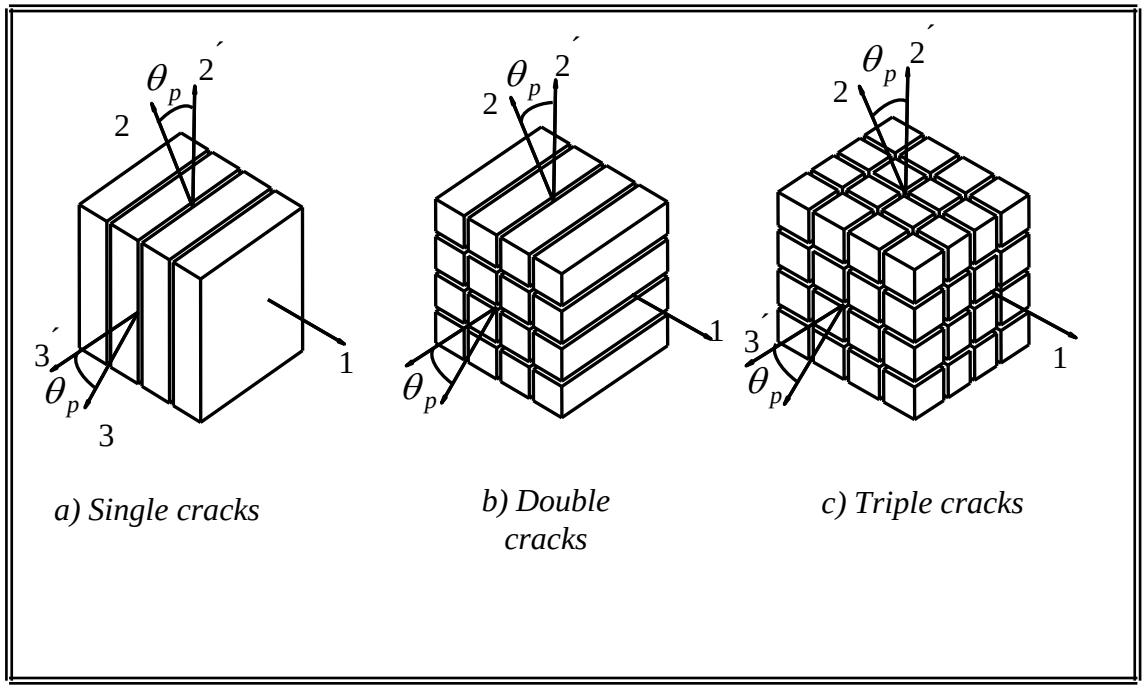

a) Single cracks *b) Double cracks* *c) Triple cracks*

Fig. (4-11): Failure Cracking for Triaxially Loaded Concrete (**Al-Shaarbaf** 1990)

4.4.2 TENSION- STIFFENING MODEL

Since the cracked concrete can still initially carry some tensile stresses in the direction normal to the crack, the tension-stiffening effect is considered. This can be achieved by assuming a gradual release of the concrete stress component normal to the cracked plane Fig. (4-12). in the present work, the normal stress that is carried by cracked concrete can be obtained from the following expression:

a) For $\varepsilon_{cr} \le \varepsilon_n \le \varepsilon_{tf1}$

$$\sigma_n = \alpha_2 . \sigma_{cr} \qquad \text{….. (4-52)}$$

b) For $\varepsilon_{tf1} \le \varepsilon_n \le \alpha_1 \varepsilon_{cr}$

$$\sigma_n = \alpha_2 . \sigma_{cr} \left[\frac{\alpha_1 . \varepsilon_{cr} - \varepsilon_n}{\alpha_1 . \varepsilon_{cr} - \varepsilon_{tf1}} \right] \qquad \text{….. (4-53)}$$

c) For $\varepsilon_n \succ \alpha_1 . \varepsilon_{cr}$

$$\sigma_n = o.o \qquad \text{….. (4-54)}$$

Where:

ε_{cr} Is the cracking strain associated with the cracking stress f_t and α_1 and α_2 are the tension-stiffening parameters. α_1 represents the rate of stress release as the crack widens and α_2 represents the sudden loss of stress at instant of cracking.

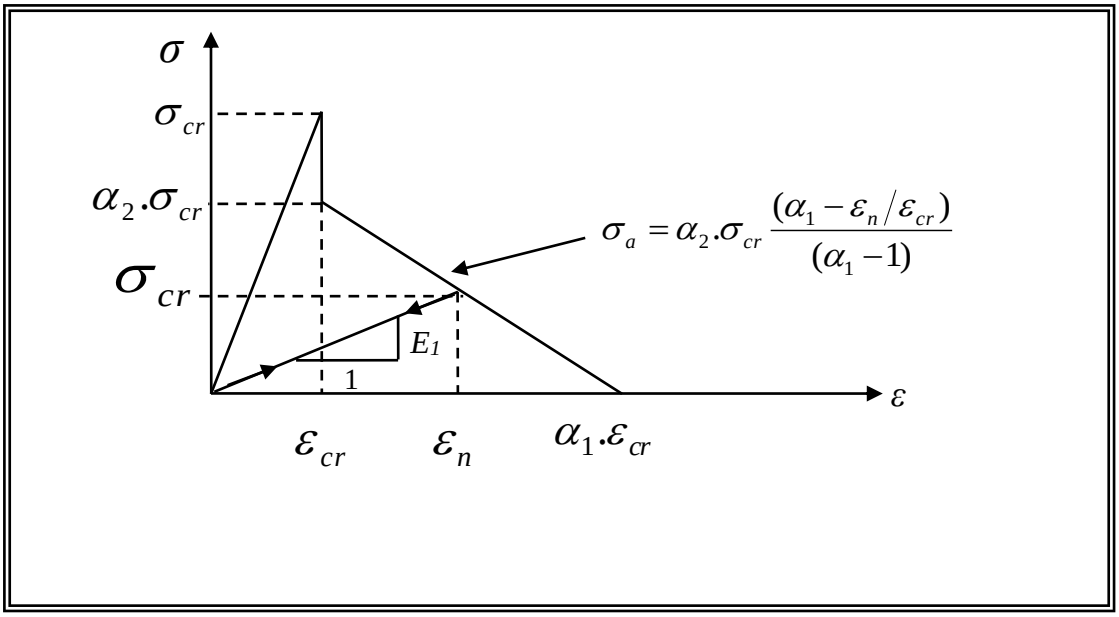

Fig. (4-12): Post-Cracking Model for Concrete in Tension **(Al-Shaarbaf** 1990)

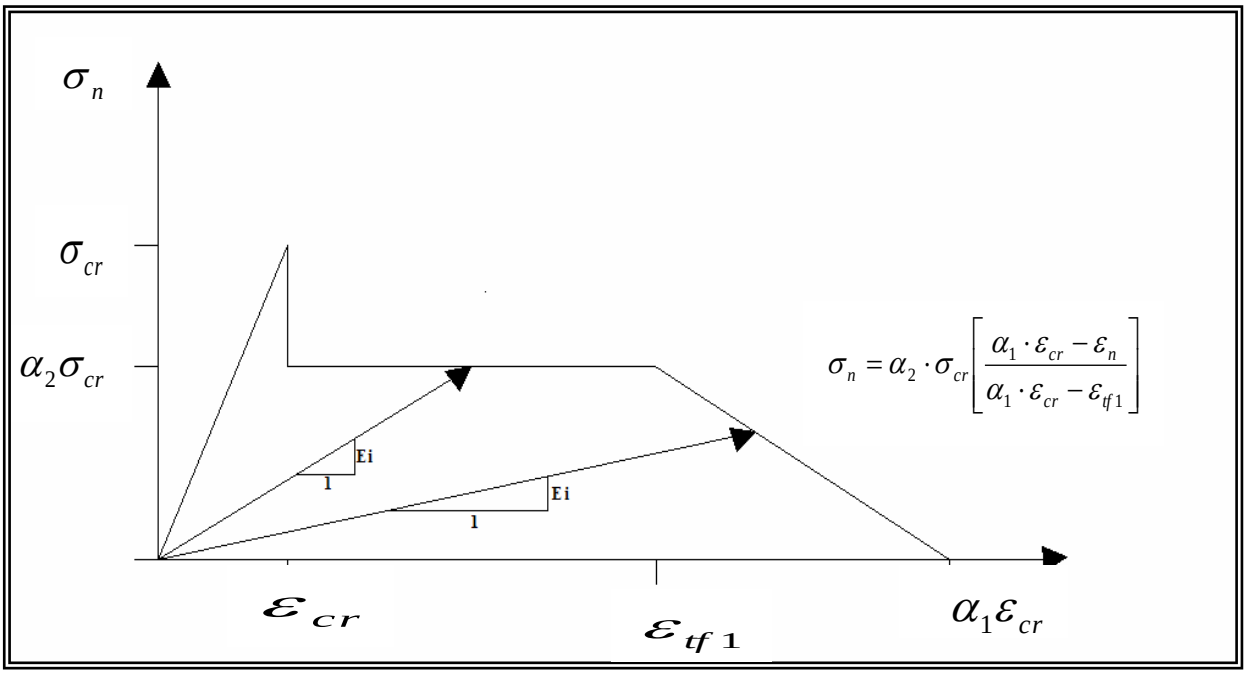

Fig. (4-13): Post-Cracking Model for Steel Fiber in Tension (**Al-Shaarbaf** 1990)

4.4.3 CLOSING AND RE-OPENING OF CRACKS

The unloading and reloading behavior can be obtained by using the secant path shown in Fig. (4-13). the secant modulus E_i can be evaluated from the previously stored maximum strain developed normal to the cracked plane. This secant modulus may be

Used to calculate the retained stress as:

$$\sigma_n = E_i \, \varepsilon_n \qquad \text{….. (4-55)}$$

Where σ_n and ε_n are the stress and strain normal to the cracked plane. When the crack is completely closed, the effects of any residual strain are neglected.

4.4.4 SHEAR RETENTION MODELS

The shear stiffness at a cracked sampling point becomes progressively smaller as the crack widens. The dowel action of the reinforcing steel and aggregate interlocking contributes to produce a considerable residual shear stiffness of cracked concrete. Thus a reduction factor (β) has been used across the cracked planes to reduce the shear stiffness at the cracked sampling point. Before cracking (β) equal (1.0), when the cracks propagate the shear reduction factor (β) is assumed to decrease linearly as shown in Fig. (4-14). When the crack is opened, a constant value of (β) is set to account for the dowel action. The shear retention model can be expressed as **(Al-Shaarbaf** 1990):

a) For $\varepsilon_n < \varepsilon_{cr}$

$$\beta = 1.0 \qquad \text{….. (4-56)}$$

b) For $\varepsilon_{cr} \le \varepsilon_n \le \gamma_1 \varepsilon_{cr}$

$$\beta = \frac{\gamma_2 - \gamma_3}{\gamma_1 - 1}\left[\gamma_1 - \frac{\varepsilon_n}{\varepsilon_{cr}}\right] + \gamma_3 \qquad \text{….. (4-57)}$$

c) For $\varepsilon_n > \gamma_1 \varepsilon_{cr}$

$$\beta = \gamma_3 \qquad \text{….. (4-58)}$$

Where γ_1, γ_2, and γ_3 are the shear retention parameters, γ_1 is the rate of decaying of shear stiffness as the crack widens, γ_2 is the sudden loss in the shear stiffness at the onset of cracking, and γ_3 is the residual shear stiffness due to the dowel action.

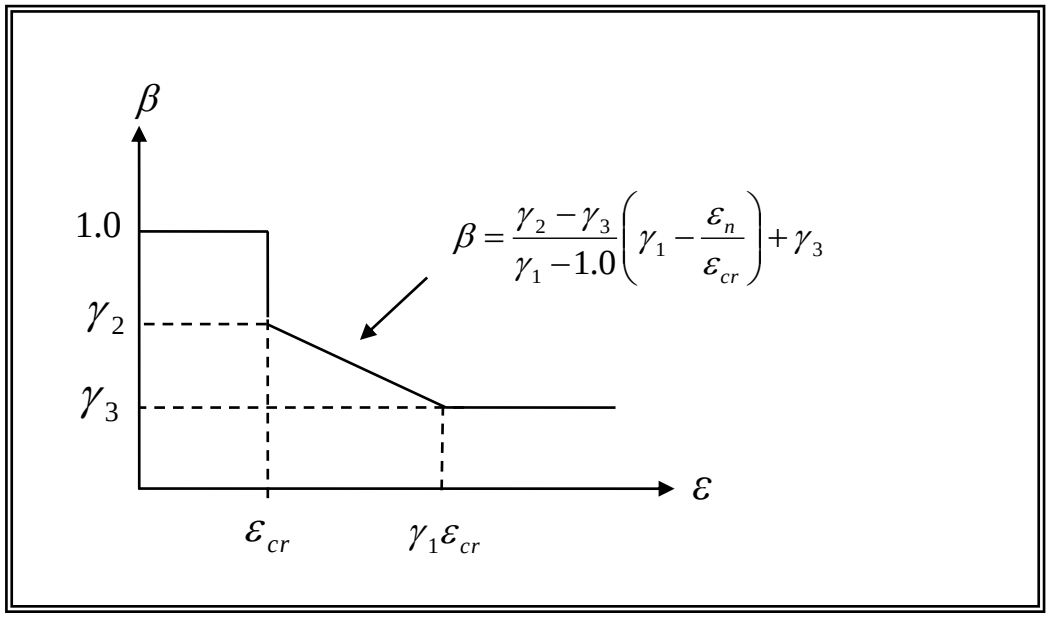

Fig. (4-14): Shear Retention Model for Concrete**(Al-Shaarbaf** 1990)

4.4.5 MODELING THE COMPRESSIVE STRENGTH REDUCTION DUE TO ORTHOGONAL CRACKS

In reinforced concrete members, a significant degradation in compressive strength can result due to the presence of transverse tensile strain after cracking.

In plasticity – based model, effects of transverse tensile strain on the yield criterion and the evolution of the subsequent loading surfaces can be simulated by scaling the equivalent uniaxial stress – strain relationships given by equation (b-2) and (4-19) according to the current value of the compressive strength reduction factor. The model incorporated in the current study is based on the proposals of (**Cervenka** 1985), which illustrates the use of the

reduction factor (λ_1) to reduce both the peak stress and corresponding strain, therefore, from equation (b-2, 4-18, 4-19 and 4-20).

The modified stress – strain relationship can be written as **(Al-Shaarbaf** 1990 and **Chen** 1982):

a.) For $\sigma \le \lambda_1 C_p . f'_{cf}$

$$\sigma = E.\varepsilon_{cf} \qquad \text{….. (4-59)}$$

b.) For $\lambda_1 . C_p . f'_{cf} \le \sigma \le \lambda_1 . f'_{cf}$

$$\sigma = \lambda_1 . C_p . f'_{cf} + E\left[\varepsilon_{cf} - \frac{\lambda_1 . C_p . f'_{cf}}{E}\right] - \frac{E}{2\varepsilon'_0}\left[\varepsilon_{cf} - \frac{\lambda_1 . C_p . f'_{cf}}{E}\right]^2 \qquad \text{….. (4-60)}$$

c.) For $\varepsilon_c \ge \varepsilon'_0$

$$\sigma = \lambda_1 . f'_{cf} \qquad \text{….. (4-61)}$$

Where,

$$\varepsilon'_o = \frac{2(1 - C_p).\lambda . f_{cf}}{E} \qquad \text{….. (4-62)}$$

Consequently, the effective stress – plastic strain relation can be modified as:

$$\bar{\sigma} = \lambda_1 . C_p . f'_{cf} - E.\varepsilon_p + \sqrt{2.E.\lambda_1 . \varepsilon'_0 . \varepsilon_p} \qquad \text{….. (4-63)}$$

And hence, the hardening parameter can be expressed as:

$$H' = \frac{d\bar{\sigma}}{d\varepsilon_p} E.\left[\left[\frac{\lambda_1 \varepsilon'_0}{2.\varepsilon_p}\right]^{\frac{1}{2}} - 1.0\right] \qquad \text{….. (4-64)}$$

For a singly cracked sampling point, the compression reduction factor is given by:

$$\lambda_1 = 1.0 - k_1 \frac{\varepsilon}{0.005} \le 1.0 - k_1 \qquad \text{….. (4-65)}$$

Where, ε_1 is the transverse tensile strain in principal direction 1.

For a doubly cracked sampling point the expression can be taken as:

$$\lambda_1 = 1.0 - k_1 \frac{\sqrt{\varepsilon_1^2 + \varepsilon_2^2}}{0.005} \le 1.0 - k_1 \qquad \text{….. (4-66)}$$

Where ε_2 is the tensile strain normal to the second crack, and k_1 represents a compression reduction parameter. (**Cervenka** 1985) has used values ranging between (0.27 and 0.73) for the parameter k_1.

4.5 MODELING OF REINFORCEMENT

In this study the reinforcing steel is modeled as linear elastic, a homogenous material and can be assumed to have the same strength in tension and compression and behavior and its mechanical properties in comparison to the properties of concrete are well known and well understood. Reinforcing bars are long and slender and therefore can be generally assumed to be capable of transmitting axial forces only.

In current study, an elastic- linear work hardening model as shown in Fig. (4-15) simulates the uniaxial stress-strain behavior of steel bars.

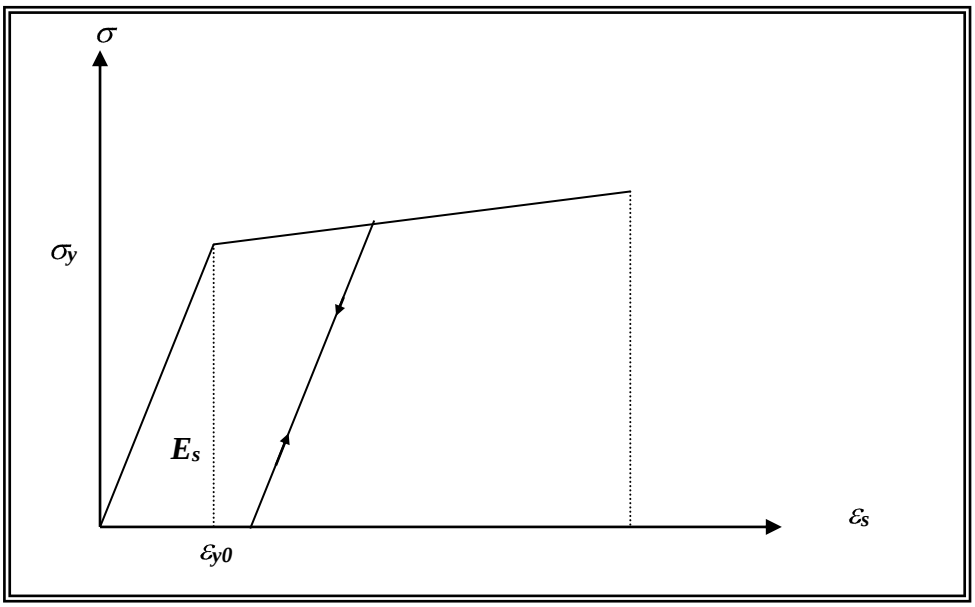

Fig. (4-15): Stress-Strain Relationship of Steel Bars
Used in the Present Analysis

Chapter Three

FINITE ELEMENT METHOD AND NONLINEAR SOLUTION TECHNIQUE

3.1 INTRODUCTION

The finite element method is one of the well-known numerical methods in engineering practice. It is now a very powerful tool for solving problems in reinforced concrete member. In the finite element method, a given continuum is divided into a number of discrete (or separate) pieces called elements. These elements are assumed to be connected together at selected points called nodes (**Diab** 1998). The displacement fields within the element are expressed as polynomial with coefficients related to the unknown nodal values. Material properties are determined from the actual behavior and are specified in terms of deformation modullies. These modullies remain constant for linear materials and depend on the state of stresses for non-linear materials.

The element stiffness relating the nodal force to the nodal displacements can be computed by using the principle of the virtual work. Then the element stiffness matrix is assembled to form the stiffness matrix for the whole assemblage. Equivalent nodal forces are used to represent the external forces. The boundary conditions are applied to the assembled nodal displacement matrix and the resulting simultaneous equilibrium equations are solved to obtain the unknown nodal

displacement. Strains and stresses in each element are computed by back substituting the computed displacement and using specific relationships.

3.2 FINITE ELEMENT FORMULATION

The governing equations of static equilibrium can be established by using the principle of virtual displacement. Consider a three –dimensional body subjected to external forces. These forces cause a displacement having components *u, v,* and *w* in the *x, y,* and *z* directions respectively. The displacement vector at any point within the element $\{u\}^e$ can be expressed as:

$$\{u\}^e = [N] \ . \ \{a\}^e \qquad \text{---------- (3-1)}$$

Where *[N]* is a matrix containing the interpolation functions which relate the displacement $\{u\}^e$, to the nodal displacements, $\{a\}^e$, where $\{u\}^e$ is given by:

$$\{u\}^e = [u \quad v \quad w]^e \qquad \text{---------- (3-2)}$$

The corresponding strains $\{\varepsilon\}^e$ are obtained by differentiation of the displacements:

$$\{\varepsilon\}^e = [A] \ \{u\}^e \qquad \text{---------- (3-3)}$$

Where *[A]* is a matrix which contains the differential operators.

Substitution of equation (3-1) into equation (3-3) yields:

$$\{\varepsilon\}^e = [B] \ \{a\}^e \qquad \text{---------- (3-4)}$$

Where *[B]* is the strain-displacement matrix given by:

$$[B] = [A][N] \qquad \text{---------- (3-5)}$$

The stress-strain relationship is usually given by:

$$\{\sigma\}^e = [D]\{\varepsilon\}^e \qquad \text{---------- (3-6)}$$

Where *[D]*, is the constitutive matrix, $\{\sigma\}^e$ is the stress vector and given by:

$$\{\sigma\}_e^{\mathrm{T}} = \begin{bmatrix}\sigma_x & \sigma_y & \sigma_z & \tau_{xy} & \tau_{yz} & \tau_{zx}\end{bmatrix} \qquad \text{---------- (3-7)}$$

And the $\{\varepsilon\}^e$ is the strains vector given by:

$$\{\varepsilon\}^e = \begin{Bmatrix}\varepsilon_x \\ \varepsilon_y \\ \varepsilon_z \\ \gamma_{xy} \\ \gamma_{yz} \\ \gamma_{zx}\end{Bmatrix} = \begin{Bmatrix}\partial u/\partial x \\ \partial v/\partial y \\ \partial w/\partial z \\ \dfrac{\partial u}{\partial y} + \dfrac{\partial v}{\partial x} \\ \dfrac{\partial v}{\partial z} + \dfrac{\partial w}{\partial y} \\ \dfrac{\partial u}{\partial z} + \dfrac{\partial w}{\partial x}\end{Bmatrix} \qquad \text{---------- (3-8)}$$

Substitution of equation (3-4) into equation (3-6) yields the stress-displacement relationship,

$$\{\sigma\}^e = [D][B]\{a\}^e \qquad \text{---------- (3-9)}$$

The principle of virtual displacements which has been used in the study states that , ***a deformable body is in equilibrium if the total work done by all external forces minus the total work done by all internal forces during any kinematically admissible virtual displacement is zero*** (**Dawe** 1984) . By considering the external work, W_{ext}, and the internal work, W_{int}, the principle can be written as:

$$\delta W_{int} - \delta W_{ext} = 0 \qquad \text{---------- (3-10)}$$

Where δW_{int} is the internal work and δW_{ext} is the external work.

By considering a system of volume (*V*) and surface area (*S*) subjected to body forces $\{b\}$ and surface forces $\{t\}$, the external work is expressed as:

$$\delta W_{ext} = \int_V \partial\{u\}^T \{b\}\, dV + \int_S \partial\{u\}^T \{t\}\, dS \qquad \text{---------- (3-11)}$$

The internal work can be expressed as:

$$\delta W_{\text{int}} = \int_V \partial\{\varepsilon\}^T \{\sigma\} dV \qquad \text{---------- (3-12)}$$

Substituting of equation (3-6) into equation (3-12) yields:

$$\delta W_{\text{int}} = \int_V \partial\{\varepsilon\}^T [D]\{\varepsilon\} dV \qquad \text{---------- (3-13)}$$

By substituting equation (3-11) and (3-13) into equation (3-10) yields:

$$\int_V \partial\{\varepsilon\}^T [D]\{\varepsilon\} dV - \int_V \partial\{u\}^T \{b\} dV - \int_S \partial\{u\}^T \{t\} dS = \{0\} \qquad \text{---------- (3-14)}$$

This expression represents the equation of static equilibrium for a general body.

Substituting equation (3-1) and (3-4) in equation (3-14) yields:

$$\partial\{a\}^T \left[\sum_n \int_{V^e} [B]^T [D]\ [B] dV^e \{a\}^e - \sum_n \int_{V^e} [N]^T \{b\}^e dV^e - \sum_n \int_{S^e} [N]^T \{t\}^e dS^e \right] = \{0\} \quad (3.15)$$

Where (*n*) is the total number of elements of discrete system.

Since, $\partial\{\mathrm{a}\}^{\mathrm{T}}$ is arbitrary, thus it may be canceled from both two sides of equation (3-15) and yields the following expression:

$$\{\mathrm{f}\} = [\mathrm{K}]\ \{\mathrm{a}\} \qquad \text{---------- (3-16)}$$

Where, *[K]* is the stiffness matrix of the element assemblage which is formed by systematic addition of the element stiffness matrices, and is given by:

$$[K] = \sum_n \int_{V^e} [B]^T [D]\ [B] dV^e \qquad \text{---------- (3-17)}$$

{a} is the corresponding element assemblage nodal displacement vector, and *{f}* is the element assemblage of external nodal force vector. The body force vector and the surface traction vector are calculated by direct addition of element body forces vector and the element surface traction vectors as shown in the following expression (**Al-Shaarbaf** 1990).

$$\{f\} = \sum_{n} \int_{V^e} [N]^T \{b\}^e dV^e + \sum_{n} \int_{S^e} [N]^T \{t\}^e dS^e \qquad \text{---------- (3-18)}$$

3.3 STRUCTURAL IDEALIZATION OF REINFORCED CONCRETE

Several works have been done in treating reinforced concrete members as a general three- dimensional solid. This is because of the computational effort involved and the lack of knowledge of the behaviour of concrete under three-dimensional stress states. However such treatment is necessary for reinforced concrete members under torsion plus bending.

In this study, concrete is simulated by hexahedral brick elements and the reinforcement bars are modeled as one dimensional elements embedded into the three- dimensional concrete elements.

3.3.1 CONCRETE IDEALIZATION

In this study concrete is modeled by using 20-noded isoperimetric brick element as shown in Fig. (3-1a); the major advantage of using 20-noded brick element is that the warping displacement of the beam cross section can be adequately approximated with fewer elements. The element sides are defined in the local coordinate system by ($\xi=\pm1$, $\zeta=\pm1$, and $\eta=\pm1$) and the origin of the local coordinate system is the center of the element as shown in Fig. (3-1b) (**Al-Shaarbaf** 1990).

Each nodal point has three degrees of freedom of movement (*u*, *v*, and *w*) along the Cartesian coordinates (*x*, *y*, and *z*), respectively. The element coordinate and displacement field within the element are defined in terms of the shape functions and displacement values at the nodes.

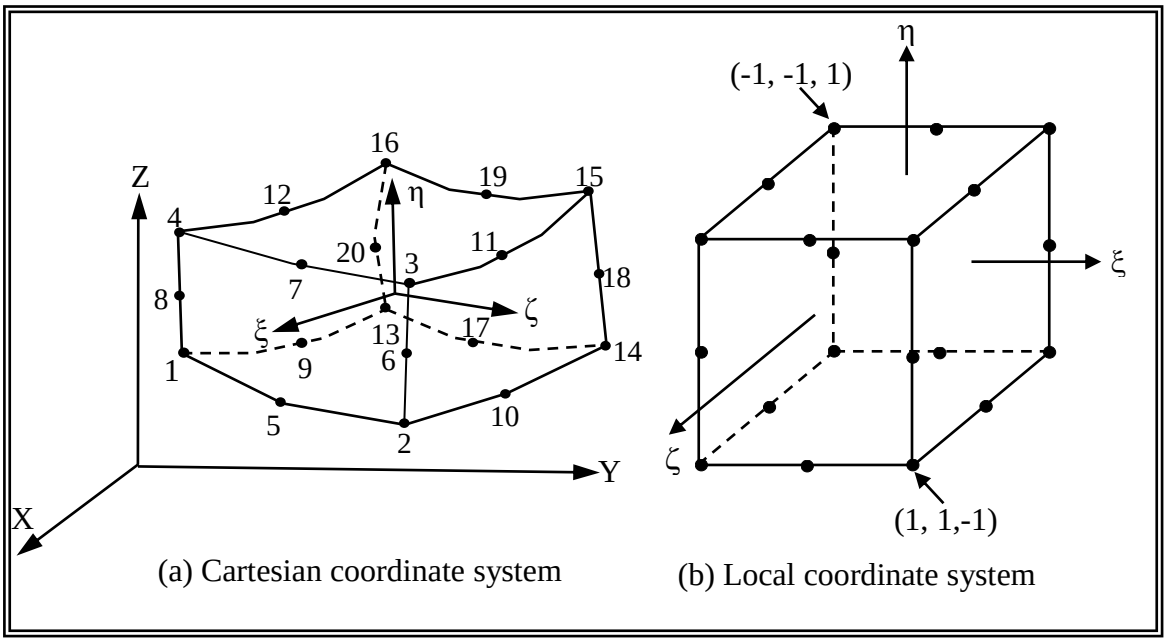

Fig. (3-1): The 20-Noded Isoparametric Brick Element (**Al-Shaarbaf 1990**)

The displacement field is given by:

$$\left.\begin{aligned} u(\xi,\eta,\zeta) &= \sum_{i=1}^{20} N_i(\xi,\eta,\zeta).u_i \\ v(\xi,\eta,\zeta) &= \sum_{i=1}^{20} N_i(\xi,\eta,\zeta).v_i \\ w(\xi,\eta,\zeta) &= \sum_{i=1}^{20} N_i(\xi,\eta,\zeta).w_i \end{aligned}\right\} \quad \text{---------- (3-19)}$$

Where *Ni (ξ, η, ζ)* represents the shape function in the local coordinates *ξ*, *η*, and *ζ* at the node (*i*) at which the nodal displacements at (*x*, *y*, and *z*) coordinates are u_s, v_i and w_i respectively. The value of (*i*) range from one

to twenty. The shape functions of the 20-noded brick element are given in Table (3-1).

The global coordinates in terms of the natural coordinates are given by:

$$\left.\begin{aligned} x(\xi,\eta,\zeta) &= \sum_{i=1}^{20} N_i(\xi,\eta,\zeta).x_i \\ y(\xi,\eta,\zeta) &= \sum_{i=1}^{20} N_i(\xi,\eta,\zeta).y_i \\ z(\xi,\eta,\zeta) &= \sum_{i=1}^{20} N_i(\xi,\eta,\zeta).z_i \end{aligned}\right\} \qquad \text{---------- (3-20)}$$

Where x_i, y_i and z_i are the nodal coordinates.

By substituting equation (3-19) into equation (3-8), the strain fields' vector $\{\varepsilon\}$ can be expressed by the following expression:

$$\begin{Bmatrix} \varepsilon_x \\ \varepsilon_y \\ \varepsilon_z \\ \gamma_{xy} \\ \gamma_{yz} \\ \gamma_{zx} \end{Bmatrix} = \sum_{i=1}^{20} \begin{bmatrix} \frac{\partial N_i}{\partial x} & 0 & 0 \\ 0 & \frac{\partial N_i}{\partial y} & 0 \\ 0 & 0 & \frac{\partial N_i}{\partial z} \\ \frac{\partial N_i}{\partial y} & \frac{\partial N_i}{\partial x} & 0 \\ 0 & \frac{\partial N_i}{\partial z} & \frac{\partial N_i}{\partial y} \\ \frac{\partial N_i}{\partial z} & 0 & \frac{\partial N_i}{\partial x} \end{bmatrix} \begin{Bmatrix} u_i \\ v_i \\ w_i \end{Bmatrix} \qquad \text{---------- (3-21)}$$

The shape functions, (N_i) can be expressed in either local or global coordinate systems. The derivatives of the brick shape functions can be given by the usual chain rule:

$$\begin{bmatrix} \frac{\partial N_i}{\partial \xi} \\ \frac{\partial N_i}{\partial \eta} \\ \frac{\partial N_i}{\partial \zeta} \end{bmatrix} = \begin{bmatrix} \frac{\partial x}{\partial \xi} & \frac{\partial y}{\partial \xi} & \frac{\partial z}{\partial \xi} \\ \frac{\partial x}{\partial \eta} & \frac{\partial y}{\partial \eta} & \frac{\partial z}{\partial \eta} \\ \frac{\partial x}{\partial \zeta} & \frac{\partial y}{\partial \zeta} & \frac{\partial z}{\partial \zeta} \end{bmatrix} \cdot \begin{bmatrix} \frac{\partial N_i}{\partial x} \\ \frac{\partial N_i}{\partial y} \\ \frac{\partial N_i}{\partial z} \end{bmatrix} \qquad \text{---------- (3-22)}$$

$$\begin{bmatrix} \frac{\partial N_i}{\partial \xi} \\ \frac{\partial N_i}{\partial \eta} \\ \frac{\partial N_i}{\partial \zeta} \end{bmatrix} = [J] \cdot \begin{bmatrix} \frac{\partial N_i}{\partial x} \\ \frac{\partial N_i}{\partial y} \\ \frac{\partial N_i}{\partial z} \end{bmatrix} \qquad \text{---------- (3-23)}$$

Where *[J]* is known as the Jacobean matrix.

Then, the shape function derivatives with respect to (*x*, *y*, and *z*) can be obtained by:

$$\begin{Bmatrix} \partial N_i/\partial x \\ \partial N_i/\partial y \\ \partial N_i/\partial z \end{Bmatrix} = [J]^{-1} \begin{Bmatrix} \partial N_i/\partial \xi \\ \partial N_i/\partial \eta \\ \partial N_i/\partial \zeta \end{Bmatrix} \qquad \text{---------- (3-24)}$$

Hence the element stiffness matrix in terms of local coordinates can be written as:

$$[k]^e = \int_{-1}^{1}\int_{-1}^{1}\int_{-1}^{1} [B]^T.[D].[B].|J|.d\xi.d\eta.d\zeta \qquad \text{---------- (3-25)}$$

The element stiffness matrix $[K]^e$ can be evaluated numerically by the numerical integration.

Table (3-1) Shape Functions for the 20-Nodded Brick Element (**Al-Shaarbaf** 1990 and **Diab** 1998).

Nodes	***Shape function*** $N_i(\xi,\eta,\zeta)$
Corner nodes $\xi_i = \pm 1, \eta_i = \pm 1, \zeta_i = \pm 1$	$\frac{1}{8}(1+\xi\xi_i)(1+\eta\eta_i)(1+\zeta\zeta_i)(\xi\xi_i+\eta\eta_i+\zeta\zeta_i-2)$
Mid side nodes $\xi_i = 0, \eta_i = \pm 1, \zeta_i = \pm 1$	$\frac{1}{4}(1-\xi^2)(1+\eta\eta_i)(1+\zeta\zeta_i)$
Mid side nodes $\xi_i = \pm 1, \eta_i = 0, \zeta_i = \pm 1$	$\frac{1}{4}(1+\xi\xi_i)(1-\eta^2)(1+\zeta\zeta_i)$
Mid side nodes $\xi_i = \pm 1, \eta_i = \pm 1, \zeta_i = 0$	$\frac{1}{4}(1+\xi\xi_i)(1+\eta\eta_i)(1-\zeta^2)$

ξ_i, η_i, ζ_i denote the coordinates of i-th node

3.3.2 REINFORCEMENT IDEALIZATION

In developing a finite element model of a reinforced concrete member, three alternative representations for steel bars have been usually used:

1. Discrete representation.
2. Distributed representation.
3. Embedded representation.

In discrete representation the steel bars are replaced by a truss element that is connected to the concrete elements at the nodes. This approach allows to slip bar within the parent element and can use linkage element with this representation to account for the slip. However, this increases the number of degrees of freedom per element (**Chen** 1982).

In distributed representation the bars are assumed as a two-dimensional membrane layer of equivalent thickness. The bars are assumed to resist

axial force only in the bar direction and assumed a perfect bond between steel and concrete. This representation is suitable for homogenous distributed reinforcement.

The current study adopts the embedded representation in which the bar element is assumed to be built in the parent brick element so that the displacement of two types of element (concrete and steel) are to be consistent, the steel bars are capable to transmitting axial force only with assumed perfect bond between concrete and reinforcement. The major advantage of this representation is that the steel bars can be placed in their correct positions without imposing any restrictions on mesh choice, and hence the finite element analysis can be carried out with a smaller number of elements, as compared to the discrete representation. The three types of reinforcement representation are shown in Fig. (3-2).

Assuming a bar element is embedded in the brick element, as shown in Fig. (3-2c), parallel to ξ and has a position $\eta = \eta_i$ and $\zeta = \zeta_i$, the shape function of the brick element can be used to represent the displacement of the bar element as follows (**Al-Shaarbaf** 1990):

$$\left.\begin{aligned} u &= \sum_{i=1}^{20} N_i(\xi) u_1 \\ v &= \sum_{i=1}^{20} N_i(\xi) v_1 \\ w &= \sum_{i=1}^{20} N_i(\xi) w_1 \end{aligned}\right\} \quad \text{---------- (3-26)}$$

Where (i) is equal to 1 and 2 in the embedded steel representation. Since, the bar is capable of transmitting axial forces only; one component of strain contributes to the strain energy (**Belarbi** 1995). The strain-displacement relationship is given by (**Al-Shaarbaf** 1990 and **Belarbi** 1995):

$$\{\varepsilon\} = \sum_{i=1}^{20}\left[\frac{1}{h^2}\begin{bmatrix} c_1 & c_2 & c_3 \\ c_2 & c_4 & c_5 \\ c_3 & c_5 & c_6 \end{bmatrix}\cdot\begin{bmatrix} \frac{\partial N_i}{\partial x} \\ \frac{\partial N_i}{\partial y} \\ \frac{\partial N_i}{\partial z} \end{bmatrix}\right]\cdot\begin{bmatrix} u_i \\ v_i \\ w_i \end{bmatrix} \qquad \text{---------- (3-27)}$$

Where:

$$C_1 = (\partial x/\partial\xi)^2, C_2 = (\partial x/\partial\xi)(\partial y/\partial\xi),$$
$$C3 = (\partial x/\partial\xi)(\partial z/\partial\xi), C_4 = (\partial y/\partial\xi)^2, \qquad \text{---------- (3-28)}$$
$$C_5 = (\partial y/\partial\xi)(\partial z/\partial\xi), C_6 = (\partial z/\partial\xi)^2$$

$$h = \sqrt{C_1^2 + C_4^2 + C_6^2}$$

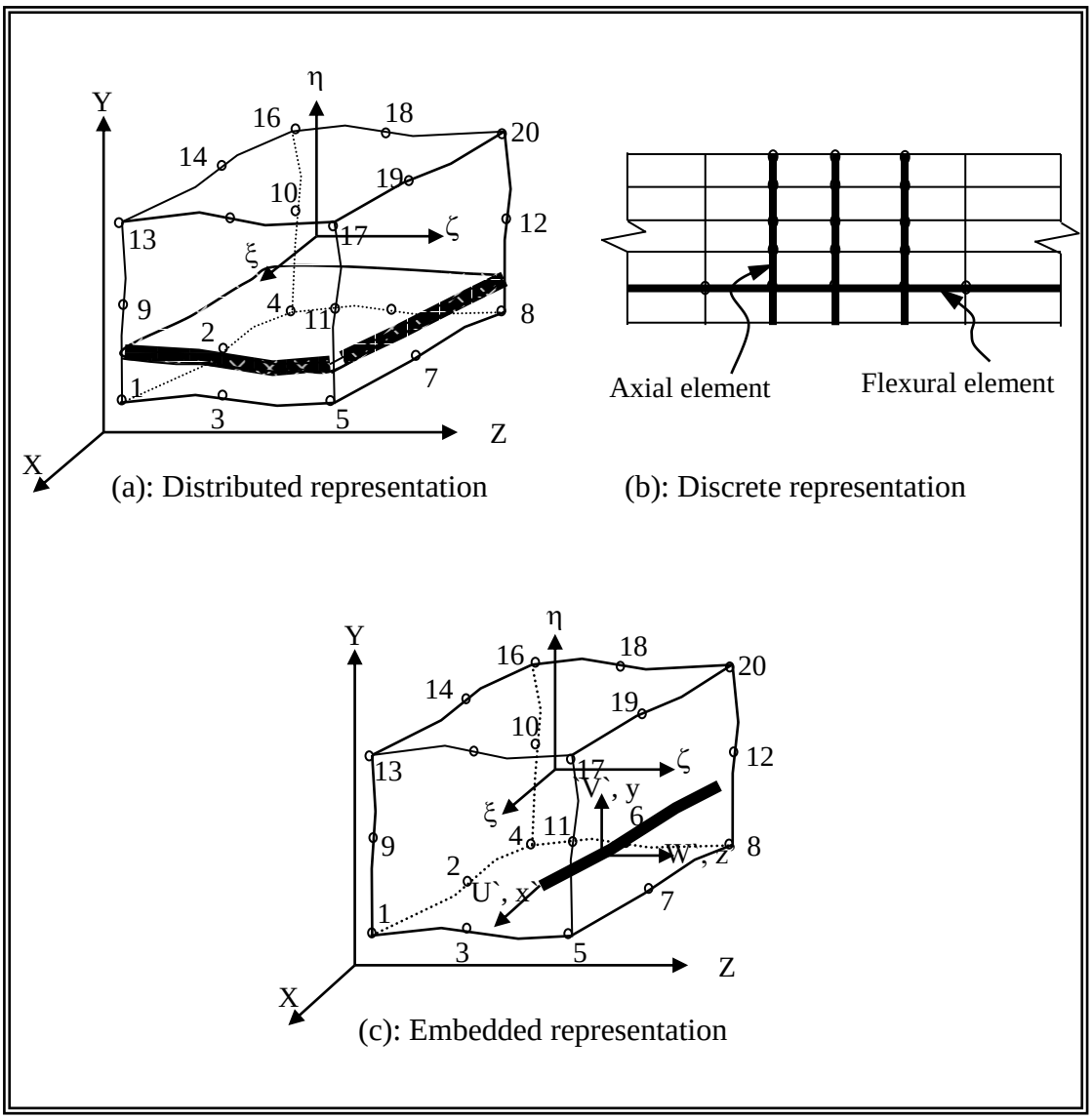

Fig. (3-2): Representation of Steel Reinforcement (**Hinton** 1988)

Finally, equation (3-27) may be rewritten in form:

$\{\varepsilon'\} = [B'].\{a\}^e$ ---------- (3-29)

The stiffness matrix of an axially loaded bar element may be expressed as

$$[K'] = \int_{V^e} [B']^T . [D'] . [B'] . dV \qquad \text{---------- (3-30)}$$

Where the constitutive matrix *[D`]* represents the modulus of elasticity of the steel bar.

$dV^e = A_s \,.\, dx = A_s \,.\, h \,.\, d\xi$ ---------- (3-31)

Where (A_s) represents the area of the steel bar.

Substituting equation (3-31) in equation (3-30), the stiffness matrix of the embedded bar can be expressed as:

$$[k'] = As\int_{-1}^{1}[B']^{T}.[D'][B'].h.d\xi$$ ---------- (3.32

A similar derivation can be used for bar parallel to the η and ζ axes.

3.4 NUMERICAL INTEGRATION

The evaluation of the element stiffness matrix of concrete brick element and embedded reinforcement element may be very difficult or even impossible. Therefore, an alternative arrangement of numerical integration is used. Usually the Gauss-Legendre scheme is used to perform the integration required to set up the stiffness matrix.

For the isoperimetric concrete brick element, the required integration of equation (3-25) can be expressed by **(Al-Shaarbaf** 1990):

$$I = \int_{-1}^{1}\int_{-1}^{1}\int_{-1}^{1} F(\xi,\eta,\zeta)\,d\xi d\eta d\zeta$$ ---------- (3-33)

This can be calculated numerically as:

$$I = \sum_{i=1}^{ni}\sum_{j=1}^{nj}\sum_{k=1}^{nk} W_i.W_j.W_k \;\; F(\xi_i,\eta_j,\zeta_k)$$ ---------- (3-34)

Where *ni, nj,* and *nk* represent the number of Gaussian points in the ξ, η, and ζ direction respectively, and *wi, wj,* and *wk* are the weight factor of *ith, jth,* and *kth* integration point. The function *F (ξi, ηj, ζk)* represents the matrix multiplication $[[B]^T.[D][B]|J|]$ in equation (3-25).

Generally the numbers of integration points are taken equal in the three directions. In a similar manner the integration of the stiffness matrix of the embedded reinforcement can be written as:

$$I = \int_{-1}^{1} F(\xi).d\xi \cong \sum_{i=1}^{ni} Wi.F(\xi i) \qquad \text{---------- (3-35)}$$

In which, $F(\xi i)$ represents the matrix multiplication $[[B']^T.[D'][B']]$ in equation (3.32). It is necessary to choose a suitable integration rule that minimizes the computation time with sufficient accuracy. The 27 (3x3x3) and 15-point Gauss-Quadrature integration rule has been used in this investigation. While for steel bars the one dimensional 2-points Gauss integration rule has been used. Fig. (3-3) shows the distribution of the sampling points and the corresponding weights and locations are tabulated in Table (3-2).

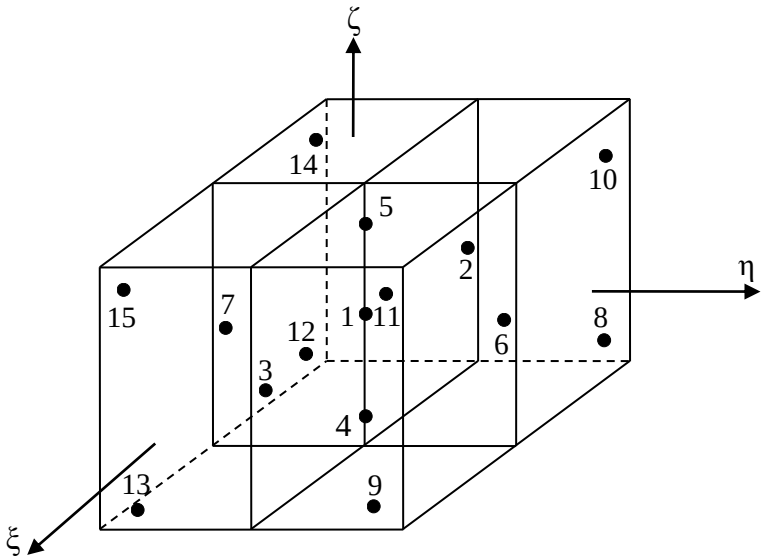

(a): 15-Point Rule

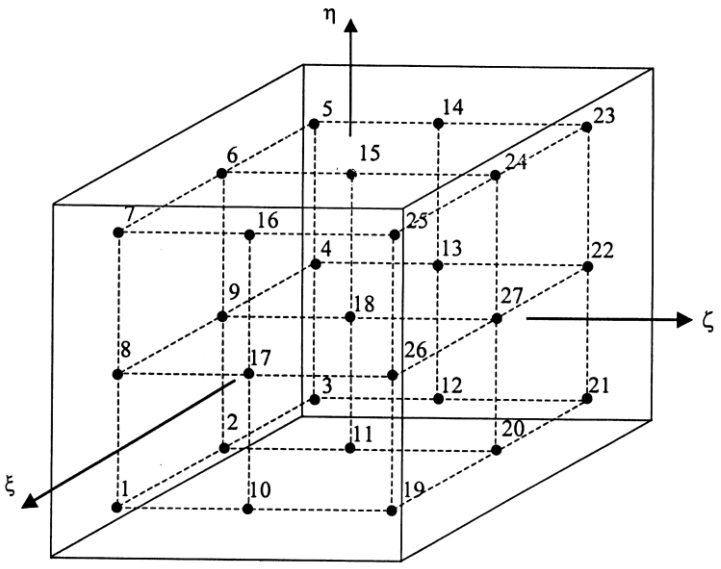

(b): 27-Point Integration Rule

Fig. (3-3): Distribution of Sampling Points over the Element in 15 and 27- Gaussian point integration Rules (Diab 1998).

Table (3-2) Weights and Locations of Sampling Points for the 15 and 27 – Point Integration Rules (Diab 1998).

Integration rule	***Sampling Point***	***Load Coordinates***			***Weight***
		ξ	η	ζ	
15a	1	0	0	0	1.56444
	2,3	±1	0	0	0.35555
	4,5	0	0	±1	0.35555
	6,7	0	±1	0	0.35555
	8 to 15	±0.6714	±0.6714	±0.6714	0.53777
15b	1	0	0	0	0.71213
	2,3	±0.848418	0	0	0.68622
	4,5	0	0	±0.848418	0.68622
	6,7	0	±0.848418	0	0.68622
	8 to 15	±0.727662	±0.727662	±0.727662	0.39631
27	1,3,5,7,19,21,23,25	±0.57735	±0.57735	±0.57735	0.17146
	2,4,6,8,10,12,14,16,20,22,26	±0.7746	±0.7746	±0.7746	0.27434
	9,11,13,15,17,27	±0.7746	±0.7746	±0.7746	0.43895
	18	0	0	0	0.70233

3.5 NONLINEAR SOLUTION TECHNIQUES

The nonlinear behavior of concrete structures may be due to the material or geometrical nonlinearities. The material nonlinear behavior results from cracking and crushing of concrete, yielding of reinforcement and plastic deformation of concrete and reinforcement. The geometrical nonlinearity is related to the large deformations and, in many cases, this nonlinearity is neglected as a result of early onset of the material nonlinearity in reinforced concrete structures **(Al-Shaarbaf** 1990). Thus, the material nonlinearity only is considered in the present study.

The general form of the set of algebraic equations which describes the nonlinearity of the system is given by **(Al-Shaarbaf** 1990):

$$\{r(a)\} = \{p(a)\} - \{f\} \qquad \text{---------- (3-36)}$$

Where *{r (a)}*, is the out of balance residual force vector, *{a}* is the vector of the nodal displacements, *{f}* is the vector of external loads and {p(a)} is the internal nodal loads vector which is given by :

$$\{p(a)\} = \int_V [B]^T . \{\sigma\} . dV \qquad \text{---------- (3-37)}$$

Where *{σ}* is the stress vector. The solution of the set of equilibrium equations (3-36) is based on obtaining a balance between the external and the internal load vectors such that residual forces approach zero. The solution of nonlinear problems is usually performed by three basic techniques; these techniques are the incremental technique, iterative technique, and the incremental-iterative technique.

In the incremental approach Fig. (3-4a), the external load is applied as sequence of small increments. Because the purely incremental technique does not account for the redistribution of forces during the application of loading increments; this technique suffers from continuous drift from the true equilibrium path. While, in the iterative technique Fig. (3-4b), the load is applied in a single increment. An initial estimate of the vector of unknown nodal displacement is obtained. Then, for each estimation, the internal forces are calculated, and after that the out of balance forces are obtained to check the convergence. The purely iterative technique unable to trace out the overall behavior throughout the entire range of loading.

The incremental-iterative technique, Fig. (3-4c), implies the subdivision of the total external load into smaller increments, within each increment of loading, iterative cycles are performed in order to obtain a converged solution corresponding to the stage of loading under

consideration. The progress of the iterative procedure is monitored with reference to specified convergence criterion **(Al-Shaarbaf** 1990).

The main approaches of incremental-iterative technique are (**Diab** 1998):

1.) The Standard Newton – Raphson Method :

In this method, the tangential stiffness matrix is updated and a new system of equations is solved for each iteration. This method is an expensive computational procedure as shown in figure (3-4d).

2.) The Modified Newton – Raphson Method [KT1]:

In this method, the tangential stiffness matrix is updated at the first iteration of each increment of loading as shown in Fig. (3-4e).

3.) The Modified Newton – Raphson Method [KT2]:

In this method, the tangential stiffness matrix is updated at the second iteration of each increment of loading.

4.) The Modified Newton – Raphson Method [KT1a]:

In this method, the tangential stiffness matrix is updated at the 1st, 6^{th}, 11^{th}… Iteration of each increment of loading, Fig. (3-4f).

5.) The Modified Newton – Raphson Method [KT2a]:

In this method, the tangential stiffness matrix is updated at the 2^{nd}, 12^{th}, 22^{th}… Iteration of each increment of loading. This method adopted by researchers (**Al-Radi** 2002, **Al-Mousely** 1998 and **Diab**

1998) who tested beams under torsion and under flexural load, this method has been used in the analysis.

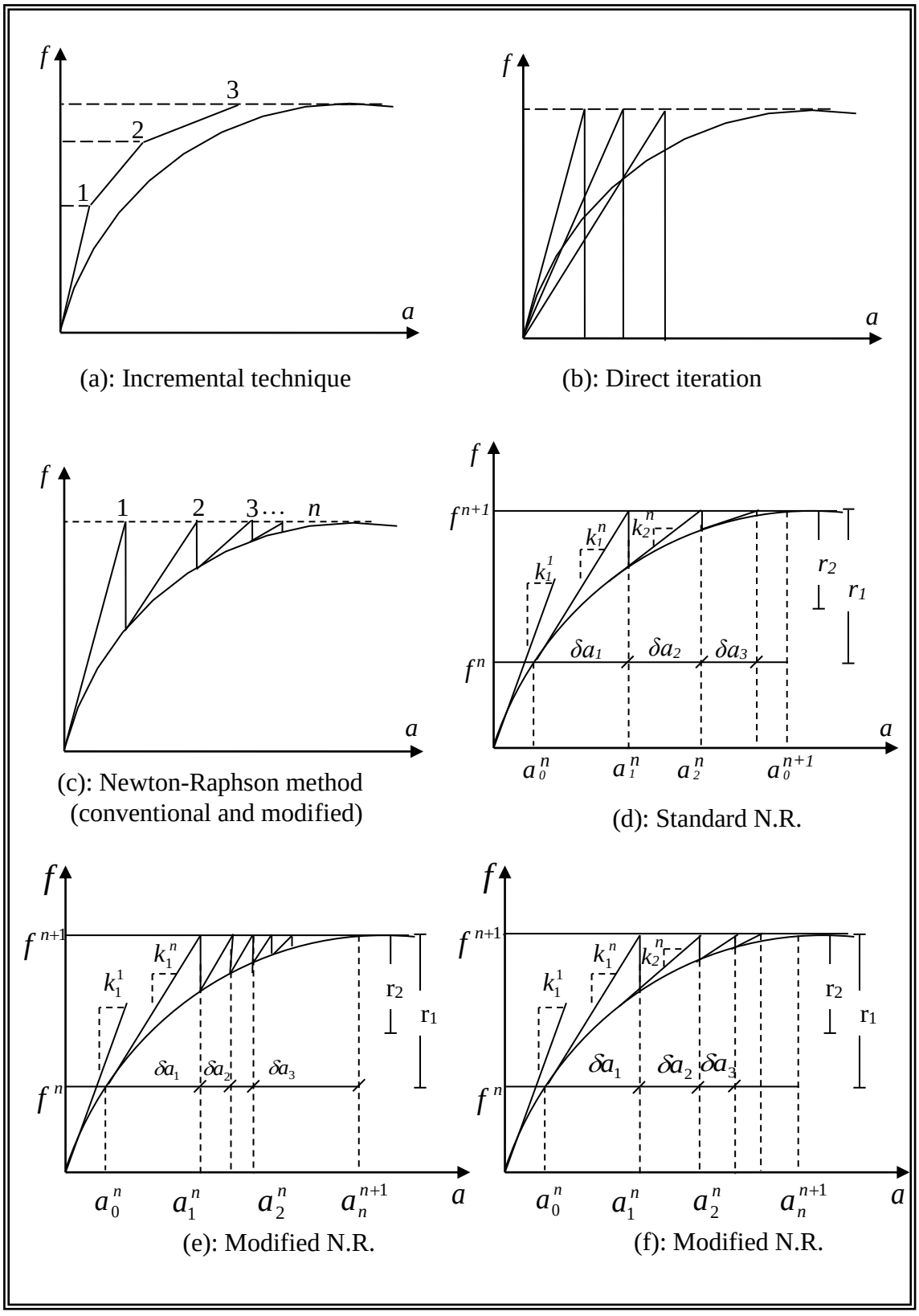

Fig. (3-4): Non-Linear Solution Techniques (**Diab** 1998).

3.6 CONVERGENCE CRITERIA

When the difference between the external and internal forces becomes negligibly small, the convergence is assumed to occur and then the iterative process is terminated. The accuracy of the approximate solution is usually specified by selection of a suitable convergence tolerance.

In general, the main types of convergence criteria for nonlinear structural analysis are the force, displacement and internal work convergence criteria. The force convergence criterion has been considered in the present work, which is based on out of balance forces and can be expressed in the form **(Al-Shaarbaf** 1990):

$$\frac{\sqrt{\{r(a)\}^T.\{r(a)\}}}{\sqrt{\{f\}^T.\{f\}}} \leq \text{Convergence tolerance} \qquad \text{---------- (3-38)}$$

Where *r {a}* represents the residual forces and *{f}* is the applied loads for each increment.

3.7 EQUIVALENT NODAL FORCES

Generally, in the finite element analysis, any external loads must be represented by an equivalent set of forces applied at the nodes. In the case of applying an external torque these forces should be distributed amongst the nodes of the free end to provide the same configuration of shear stresses as those induced by the original torque. When applying the nodal loads in proportions other than the correct one, this will lead to an incorrect distribution of stresses especially in the region adjacent to the loaded section.

An iterative scheme can be used to determine the proper distribution of nodal loads corresponding to elastic pure torque. This approach which is proposed by **(Al-Shaarbaf** 1990) is based on the fact that the reaction forces at the nodes of the restrained ends represent better estimate of the correct loads than obtained from the corresponding nodal forces applied

at the free end. In this iterative scheme, a set of nodal loads is applied at the free end such that they produce a torque moment equivalent to the external applied torque. The reactions corresponding to the applied nodal loads at the fixed end are found using the finite element analysis within the elastic stage. Then, the obtained reactions are assumed to be a new set of nodal loads at the free end. This procedure is repeated until the difference between the applied forces and the reactions is negligible. The nodal forces represent the equivalent forces that are applied at the ends of the beams under torsion.

Chapter Five

APPLICATION AND DISCUSSION

5.1 INTRODUCTION

In this chapter, various examples have been analyzed to prove the validity of the proposed models, and to show the accuracy and efficiency of the computational method. Also the torque – twist curves of the tested beams that obtained from the finite element analysis are compared with the available experimental torque – twist curves.

Parametric studies have been carried out in this chapter to investigate the effects of some important material parameters, and geometrical parameters on the numerical results as obtained for the considered cases.

5.2 CASE ONE: REINFORCED CONCRETE BEAMS WITH STEEL FIBER UNDER PURE TORSION

5.2.1 WAFA BEAMS (B) AND (B1)

(**Wafa** 1992) tested a series of rectangular reinforced concrete beams with steel fiber under torsion with various properties and detail of reinforcement. Among these tested beams, three dimensional nonlinear finite element analyses are considered in the present study.

5.2.2 DESCRIPTION AND MATERIAL PROPERTIES (WAFA 1992) BEAMS (B) AND (B1)

Beams [B, B1] was cantilever reinforced concrete beam over (2190 mm) span and has a supported length of (1850 mm), with (100 x 250) mm rectangular cross sectional dimensions. Fig. (5-1) shows the dimension details of beams [B, B1] and the finite element mesh of opening beam. The material properties of concrete and the additional material parameters of the tested beam are listed in Table (5-1).

Table (5-1): Material Properties and Material Parameters For (Wafa 1992**) Beams [B- B1]**

Concrete		***B***	***B1***
E_c	Young's modulus (N/mm^2)	29000	29000
$f`_c$	Compressive strength (N/mm^2)	37.93	35.1
f_t	Tensile strength (N/mm^2)	3.14	4.05
υ	Poisson's ratio*	0.2	0.2
k_1	Compression reduction parameter*	0.6	0.6
α_1	Tension stiffening parameters*	10	10
α_2		0.5	0.5
γ_1	Shear - Retention parameters*	10	10
γ_2		0.5	0.5
γ_3		0.1	0.1
Vf%	Volumes fraction of fibers	0.0	0.5
Lf/df	Aspect ratio	0	100
steel			
E_s	Young's modulus (N/mm^2)	200000	200000
H'	Hardening parameter	0	0
f_y	Yield stress (N/mm^2)	342	342

** Assumed values: selected to obtain the best results in comparing with the experimental results.*

5.2.3 FINITE ELEMENT, BOUNDARY CONDITIONS AND EQUIVALENT NODAL FORCES OF (WAFA 1992) BEAMS [B] AND [B1]

Since all the tested beams have the same length and cross sectional dimensions, the same finite element mesh will be used for all beams. Each tested beam was simulated by (36) isoperimetric 20-noded brick elements. The external torque was modeled as a set of equivalent nodal forces were applied at the end of the beam as described Fig. (5 -2).

The angle of twist was calculated at the free end of the beams (at z = 1850 mm). The imposed boundary conditions maintain the stability of the beams and allow to post cracking extension of the beams in z-direction to occur. An opening is provided at mid span of beams (B and B1), area of the opening is equal to (4%) of the side view area of the beam as shown in Fig. (5-1).

The finite element mesh, boundary conditions, and the equivalent nodal forces of beams [B] and [B1] are shown in Fig. (5-2).

The present finite element analysis has been carried out using 27-Gauss point integration rule, with a convergence tolerance (5%). The modified Newton – Raphson (KT2a) method has been adopted as a nonlinear solution algorithm.

5.2.4 RESULTS OF ANALYSIS OF (WAFA 1992) BEAM [B] AND [B1]

For beam [B], Fig. (5-3) shows the experimental by **(Wafa** 1992) and present numerical torque – twist curve with or without opening. This figure shows a good agreement between the numerical results and the experimental results throughout the entire range of loading. The numerical ultimate torque was (2.191, 2.7) kN.m with and without openings respectively, while the experimental ultimate torque was (2.68) kN.m thus the difference between these results are (0.7%) for beam without opening and (18.4%) for beam with opening. Fig. (5-4) shows the experimental by (**Wafa** 1992) and presents numerical torque – twist curves of beam [B1] with or without opening. This figure shows an acceptable agreement between the experimental and the present finite element analysis results. The present numerical ultimate torque of beam [B1] was (2.64, 3.3) kN.m with and without opening respectively, while the experimental ultimate torque was (2.99) kN.m and the difference between them is equal to (10%) for beam without opening and (11.7%) for beam with opening. The results for the two beams ([B] and [B1]) explain that when increasing the amount of steel fiber the ultimate, cracking torque and ductility will increase as shown in Fig. (5-5).

Where the present numerical cracking torque of beams [B] and [B1] was (2.1, 2.55) kN.m respectively, while the experimental cracking torque was (1.9, 2.77) kN.m for beams (B, B1) and the difference between them is equal to (10.5%) for beam (B) and (8%) for beam (B1).The ultimate and cracking torque which is obtained from the present finite element analysis and the experimental ultimate torque and cracking torque by (**Wafa** 1992) for beams [B] and [B1] are presented in Table (5-2).

Table (5-2): Comparison between the Experimental and Predicted Ultimate and cracking Torque of (Wafa 1992) Beams [B-B1]

Beam	T_{exp} (kN.m)	T_U (kN.m)	$\frac{T_U - T_{exp}}{T_{exp}}$	$\frac{T_U}{T_{exp}}$	Tcr_{exp} (kN.m)	T_{cr} (kN.m)	$\frac{Tcr_U - T_{exp}}{T_{exp}}$
[B]	2.68	2.7	0.7 %	1.007	1.9	2.1	10.5%
[B1]	2.99	3.3	10 %	1.1	2.77	2.55	8%

Where:
T_{exp}: The ultimate experimental torque (by Wafa).
T_u : The ultimate torque obtained from the prese
Tcr_{exp} :The ultimate experimental cracking torque (by Wafa).
T_{cr} :The ultimate cracking torque obtained from the prese

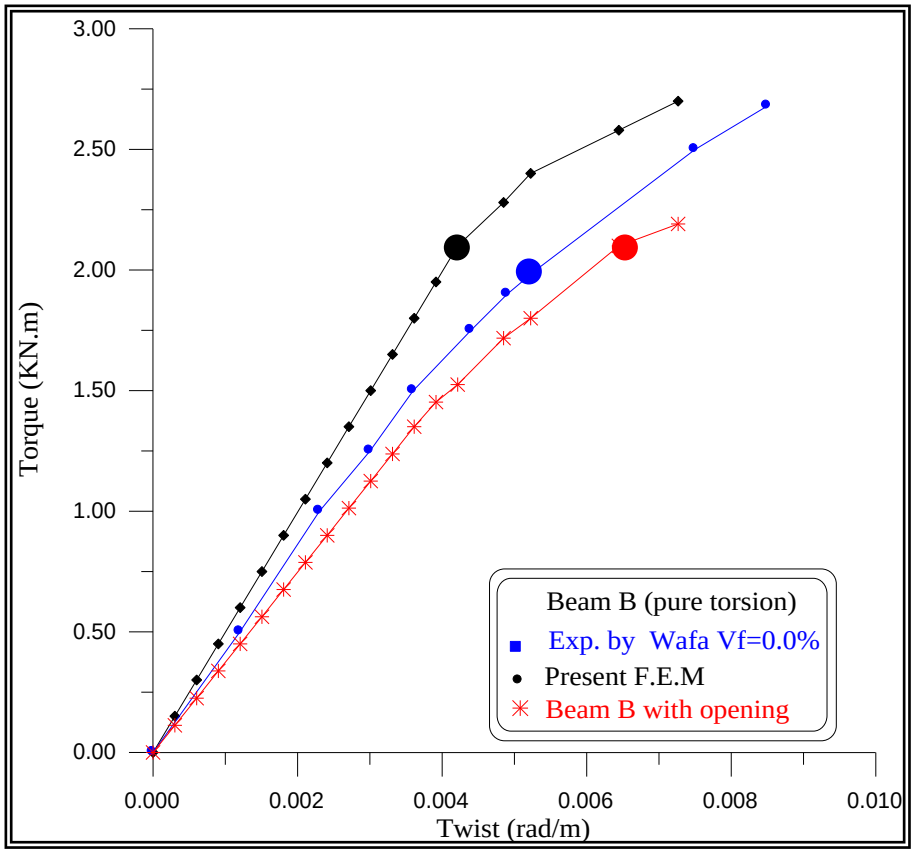

Fig. (5-3): Torque- Twist Curve for Beam B (Case One)

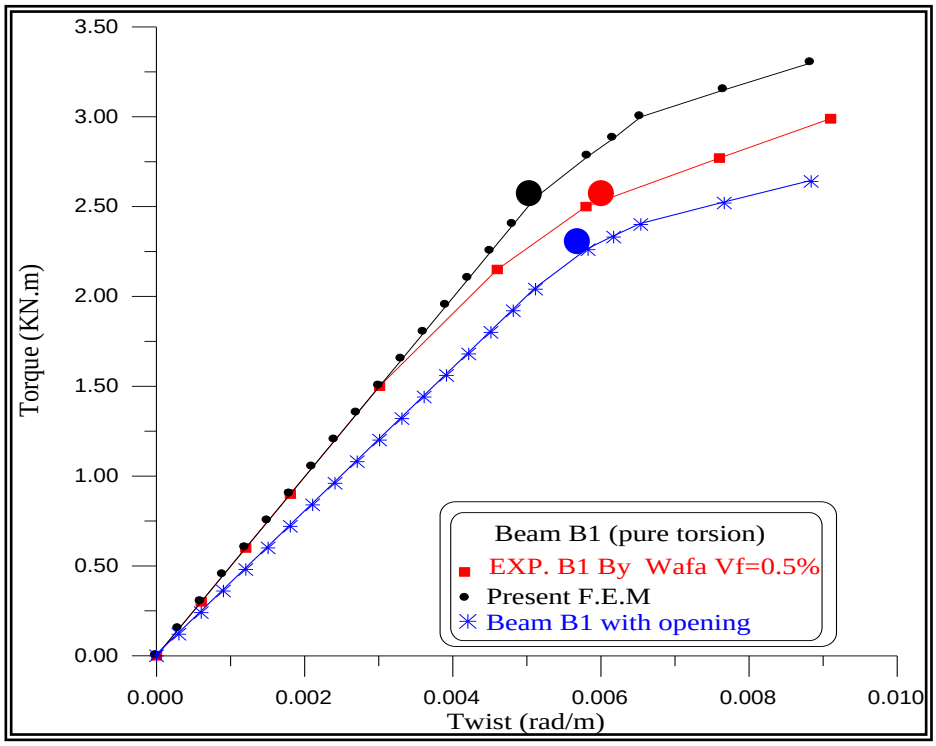

Fig. (5-4): Torque- Twist Curve for Beam B1

(Case One)

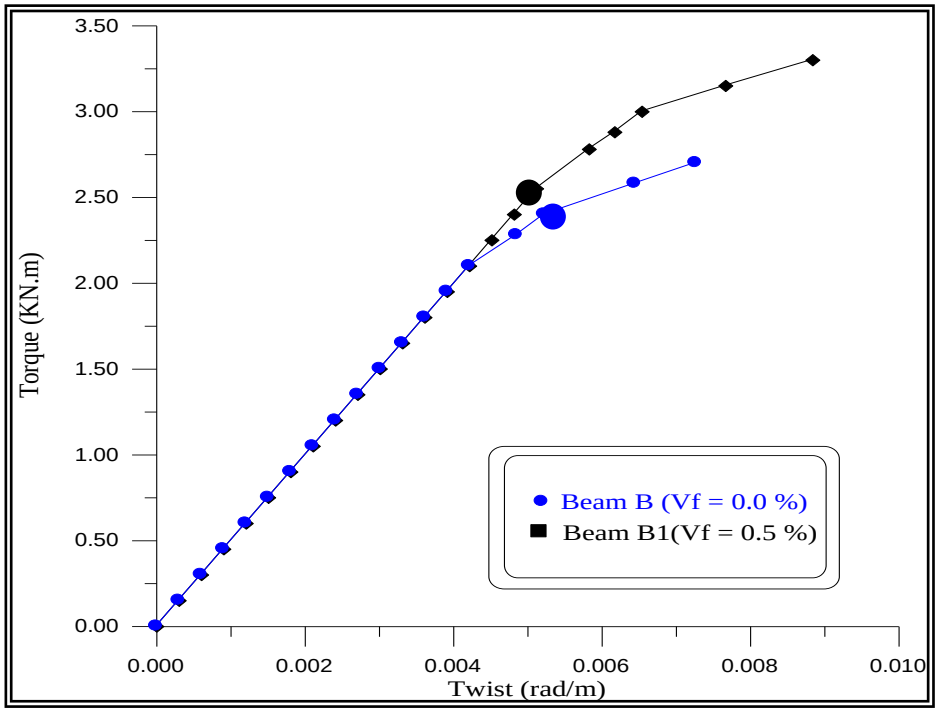

Fig. (5-5): Torque- Twist Curve for Beams (B and B1)

(Case One)

5.3 CASE TWO: REINFORCED CONCRETE BEAMS WITH STEEL FIBER UNDER COMBINED SHEAR, BENDING AND TORSION

5.3.1 MANSUR BEAMS H AND F

In the present study, groups (**H and F**) have been considered which tested by (**Mansur** 1982), each group consisted of (**3**) concrete beams were tested under combined bending and torsion. In these groups the amount of torsion to moment was varied.

5.3.2 DESCRIPTION AND MATERIAL PROPERTIES OF GROUPS (H) AND (F) BEAMS

Groups (H) and (F) have the same dimensions. All beams of groups (H) and (F) have (2000 mm) overall length, and (1800 mm) supported length with (100 x 150) mm cross sectional dimensions. Fig. (5-6) shows the dimensions details of beams [F, H]. Within each groups the beams were tested with different torsion to bending moment ratio (T/M). The material parameters and material properties of the tested beams are listed in Table (5-3).

Table (5-3): Material Properties and Material Parameters For (**Mansur** 1982) **Beams [H] and [F]**

Concrete		***[H] or[F]***
E_c	Young's modulus (N/mm^2)	25000
$f`_c$	Compressive strength (N/mm^2)	25.7
f_t	Tensile strength (N/mm^2)	3.87
υ	Poisson's ratio*	0.2
k_1	Compression reduction parameter*	0.6
Vf%	Volume fraction of fiber	0.75
Lf/df	Aspect ratio	75
α_1	Tension stiffening parameters*	10
α_2		0.5
γ_1	Shear - Retention parameters*	10
γ_2		0.5
γ_3		0.1
steel		
E_s	Young's modulus (N/mm^2)	200000
f_y	Yield stress (N/mm^2)	342
H'	Hardening parameter	0

** Assumed values: selected to obtain the best results in comparing with the experimental results.*

5.3.3 FINITE ELEMENT, BOUNDARY CONDITIONS, AND EQUIVALENT NODAL FORCES OF THE TESTED BEAMS F AND H

Since all the tested beams have the same length and cross sectional dimensions, the same finite element mesh will be used for all beams. Each tested beam was simulated by (36) isoperimetric 20-noded brick elements, and the reinforcement modeled as one dimensional element embedded within the 20-noded brick element. The concentrated load (P) was modeled as a line load uniformly distributed across the width of the beam, while the external torque was modeled as a set of equivalent nodal forces applied at the end of the beam (at z = 1800), as described in the Fig. (5-7).

The imposed boundary conditions maintain the stability and allow to post cracking extension of the beam in z – direction to occur, the angle of twist was calculated at (z = 1800 mm). Fig. (5-7) shows the finite element mesh, boundary conditions, and the equivalent nodal forces of the tested beams.

The numerical analysis was carried out using the modified Newton Raphson method (KT2a). Many numerical tests have been considered to study the suitable convergence tolerance and proper integration rule. The results of these tests show that a convergence tolerance (2%) and the 27 – Gauss point integration rule give closer results to the experimental results.

5.3.4 RESULTS OF ANALYSIS OF THE TESTED BEAMS F AND H

For beams of groups (H and F) the results of the present finite element analysis show a good agreement with the experiment by **(Mansur** 1982) results, with a different range (8.9 % - 7.9 %) for ultimate torque and a different range (13.6 % - 11 %) for ultimate cracking torque . A comparison between the experiment by **(Mansur** 1982) and the present finite element analysis torque-twist curve of beams of groups F (T/M = 1.21) and H (T/M = 0.44) are shown in Fig. (5-8) and (5-9) respectively. The results of the present finite element analysis, the experimental results by **(Mansur** 1982), and the comparison between the experimental and numerical results are tabulated in Table (5-4).

Table (5-4): Comparison between the Experimental and Predicted Ultimate and cracking Torque of Groups (H) and (F) Beams

Beam	T/M	T_{exp} (KN.m).	T_u (KN.m)	$\frac{T_u}{T_{exp.}}$ (KN.m)	$\frac{T_u - T_{exp.}}{T_{exp.}}$ (KN.m)	Tcr_{exp} (KN.m)	T_{cr} (KN.m)	$\frac{T_{cr} - T_{crexp.}}{T_{crexp.}}$ (KN.m)
H	0.44	0.662	0.721	1.089	8.9 %	0.63	0.7	11 %
F	1.21	1.343	1.450	1.079	7.9 %	1.1	1.25	13.6%

Where:

T_{exp} : The ultimate experimental torque (kN.m) (by Mansur).

T_u: The ultimate torque obtained from the present F.E.A. (kN.m) for reinforced beams.

Tcr_{exp}:The ultimate experimental cracking torque (kN.m) (by Mansur)

T_{cr}:The ultimate cracking torque (kN.m) obtained from the present F.E.A. for reinforced beams.

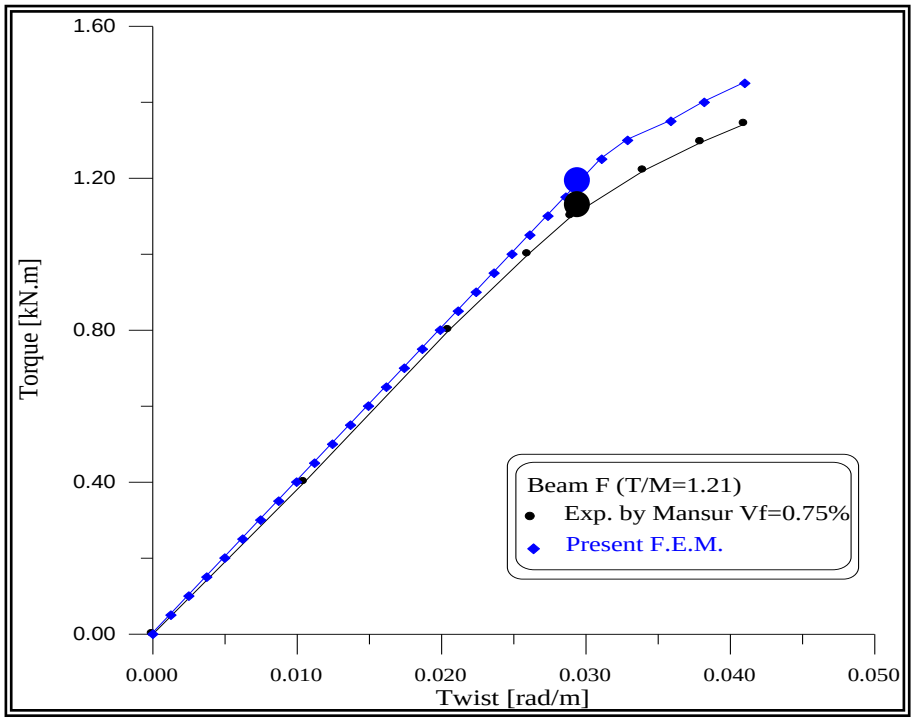

Fig. (5-8): Torque – Twist Curve of Beam (F) (Case Two)

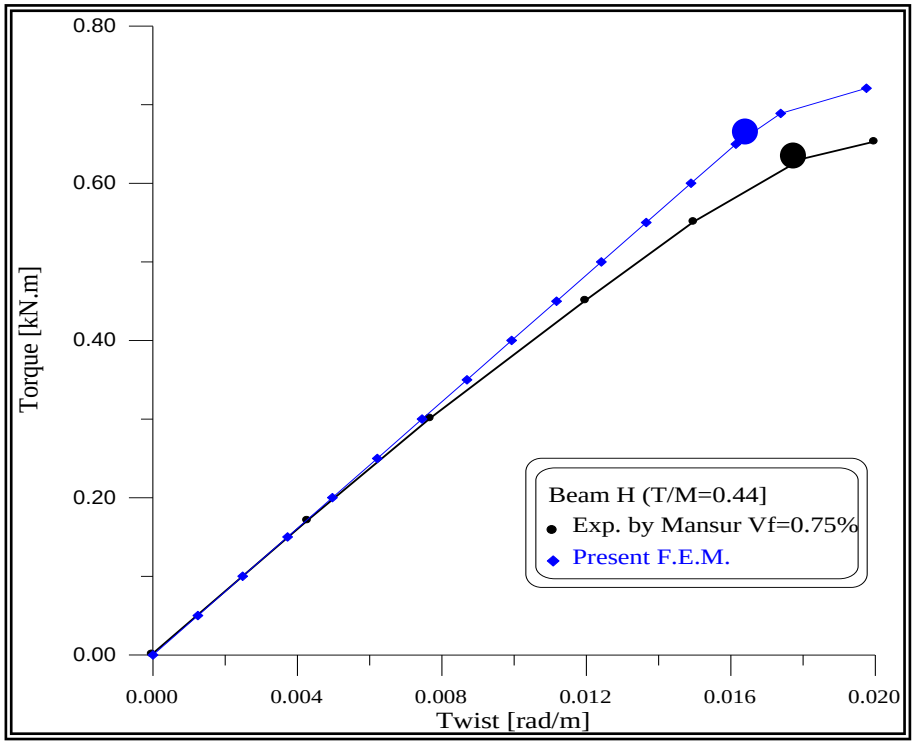

Fig. (5-9): Torque – Twist Curve of Beam (H) (Case Two)

5.4 PARAMETRIC STUDY

openings are provided in beam F with position and size indicated by symbols, which are ranging from F to A7 as explained in Fig.(5-10) and Tabel (5-5). Two openings are provided in each beam symmetrically about the mid-span except beam F that is solid without opening.

The beams is analyzed as shown in Fig.(5-11), thirty six 20- node brick elements were used for F, sixteen 20- node brick elements for A1, A2, A3,A4, A5, A6 and A7.

A Parametric study is presented including the influence of both beam and opening proportions in many items:

1. Effect of openings location through the depth of the beam.
2. Effect of openings shape.
3. Effect of openings size.
4. Effect of steel fiber ratio on the beams with openings.
5. Effect of (T/P) ratio on the ultimate capacity.

The effect of tension stiffening parameters, shear retention parameters, Effect of Integration Rule and Poison's ratio have been studied on beam (H) (T/M = 0.44) which was subjected to combined shear, bending and torsion.

Among different material parameters in these numerical tests one parameter was selected to be varying and all the other parameters were kept constant.

Table (5-5): Opening Notation

Beam No.	Size		Position	
	a_1	a_2	k_1	k_2
F	-	-	-	-
A1	0.6	0.2	0.2	0.1
A2	0.3	0.1	0.533	0.1
A3	0.3	0.1	0.35	0.1
A4	0.3	0.1	0.2	0.1
A5	0.666	0.045	0.166	0.1
A6	0.3	0.05	0.35	0.1
A7	0.6	0.1	0.2	0.1

5.4.1 EFFECT OF OPENING LOCATION THROUGH THE DEPTH OF THE BEAM.

To explain the effect of openings on the behavior of reinforced concrete beam, the openings are provided along beam span and through the beam depth as shown in Fig. (5-10), Fig. (5-11) and Fig. (5-12). Fig. (5-13) show the influence of opening position on the ultimate torque. Presence of openings in the different zone of a beam leads to reduce considerably the ultimate torque as shown in Fig.(5.13). The ultimate torque in beams A2, A3, and A4 is about (1.4, 1.1, and 1.05) KN.m respectively, where the ultimate torque in beam F is (1.45KN.m).

The best position of the openings through the beam depth was in beam A2, when the openings at tension zone. Where the ultimate torque of the beams (A2, A3, and A4 was about (3.4%, 24.14% and 27.586) less than that case of no opening of a similar solid one F respectively, as shown in Table (5-6).

Table (5-6): Comparison between the Ultimate Torque for Beam F and Ultimate Torque of (A2, A3, and A4) Beams

	Tult (KN.m)	(TF- TA)/TF%
F	1.45	–
A2	1.4	3.4
A3	1.1	24.14
A4	1.05	27.58

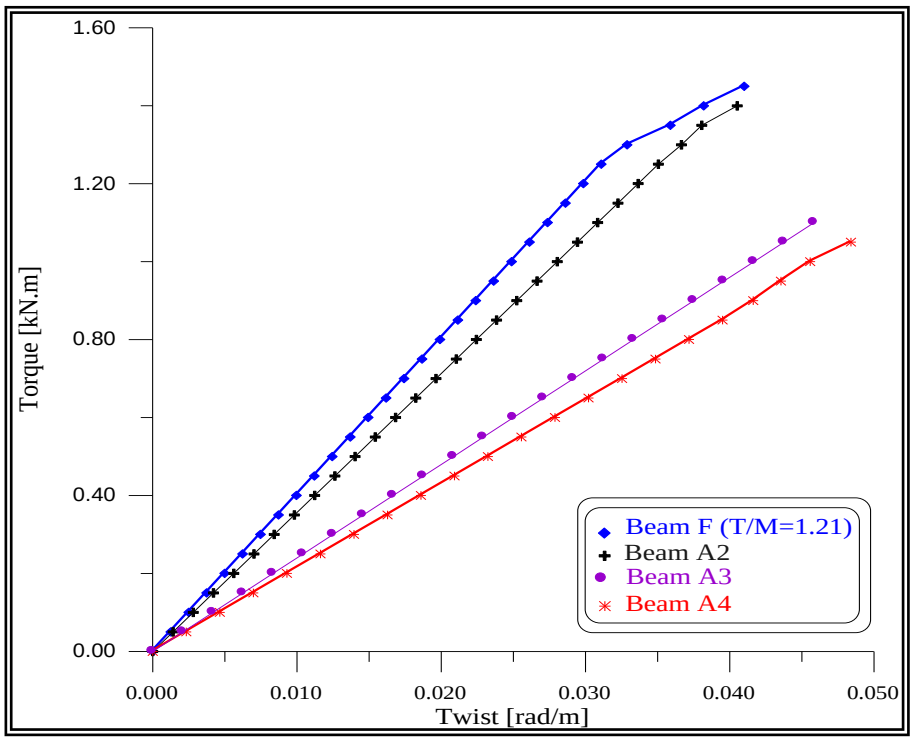

Fig. (5-13): Effect of Positions for Openings through the Beam Depth on the Torque – Twist Behavior

5.4.2 EFFECT OF OPENING SHAPE.

Reinforced concrete beams (A1, A3, and A5) are considered. All information is shown in Fig. (5-10) and Table (5-5). Fig. (5-14) illustrates the influence of 0penings shape on the ultimate torque. The curve indicates that the ultimate torque for beams A1, A3 and A5 is decrease about (24.137%, 24.125%, and 27.586) less than that case of no opening of a similar solid one F respectively, as shown in the table (5-7), where the openings have different shape for the same area as shown in Fig. (5-10) and Table (5-5).

Table (5-7): Comparison between the Ultimate Torque for Beam F and Ultimate Torque of (A1, A3, and A5) Beams

	Tult (KN.m)	(TF- TA)/TF%
F	1.45	_
A1	1.11	24.137
A3	1.1	24.125
A5	1.05	27.586

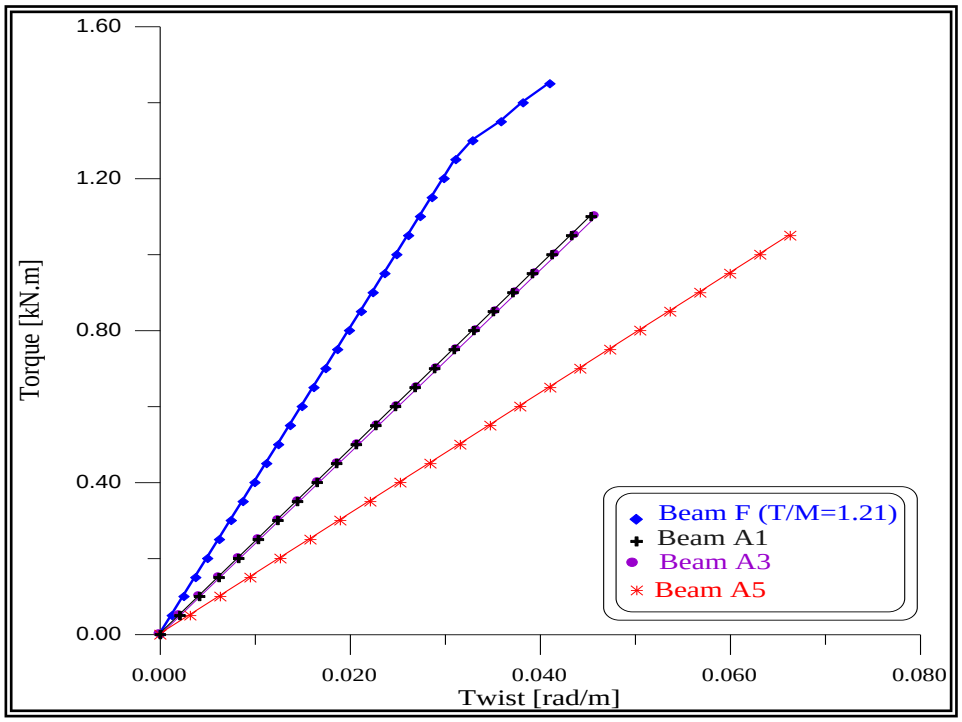

Fig. (5-14): Effect of Shape for Openings On the Torque – Twist Behavior

5.4.3 EFFECT OF OPENING SIZE.

To show the effect of opening size, reinforced concrete beams A5 and A6 are considered. Fig. (5-15) shows the effect of opening size on the ultimate torque of reinforced beam. As may be seen from the figure, the ultimate torque for opening size 4% and 2% are about (27.586% and 24.137) less than that case of no opening of a similar solid one F respectively, as shown in Table (5-8).

Table (5-8): Comparison between the Ultimate Torque for Beam F and Ultimate Torque of (A5, and A6) Beams

	Tult (KN.m)	(TF- TA)/TF%
F	1.45	_
A5	1.05	27.586
A6	1.1	24.137

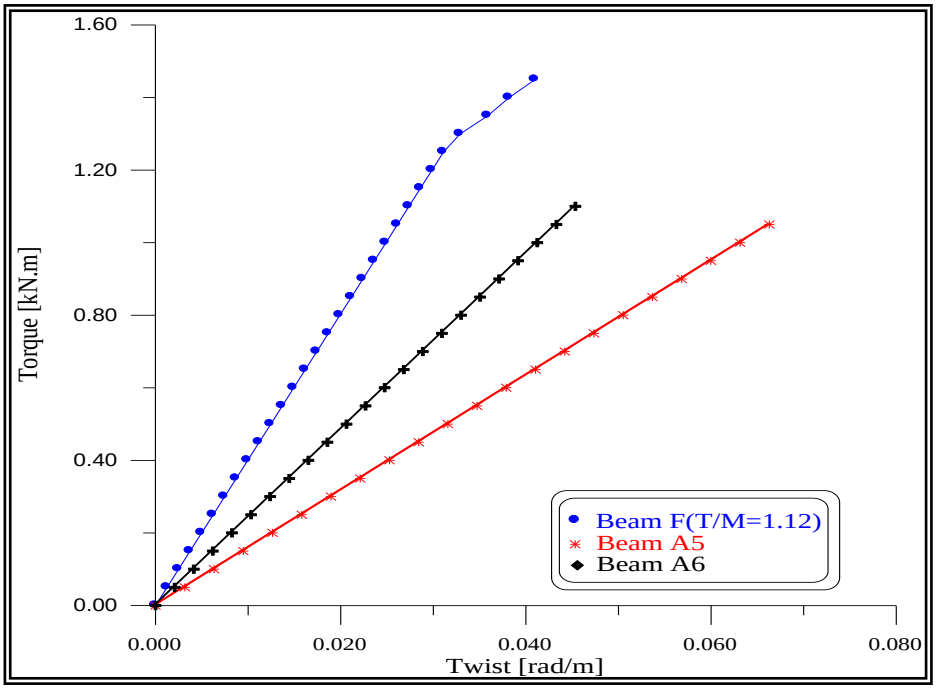

Fig. (5-15): Effect of Openings Size On the Torque – Twist Behavior

5.4.4 EFFECT OF FIBER RATIO

To investigate the effect of fiber ratio, reinforced concrete beams F and A1 are considered. All information is shown in Fig. (5-11) and table (5-5).

From Fig. (5-16) and Fig. (5-17), it can be noticed that the ultimate torque increases with increasing of fiber ratio by about (34.96% and 39.54%) for F and A1, respectively.

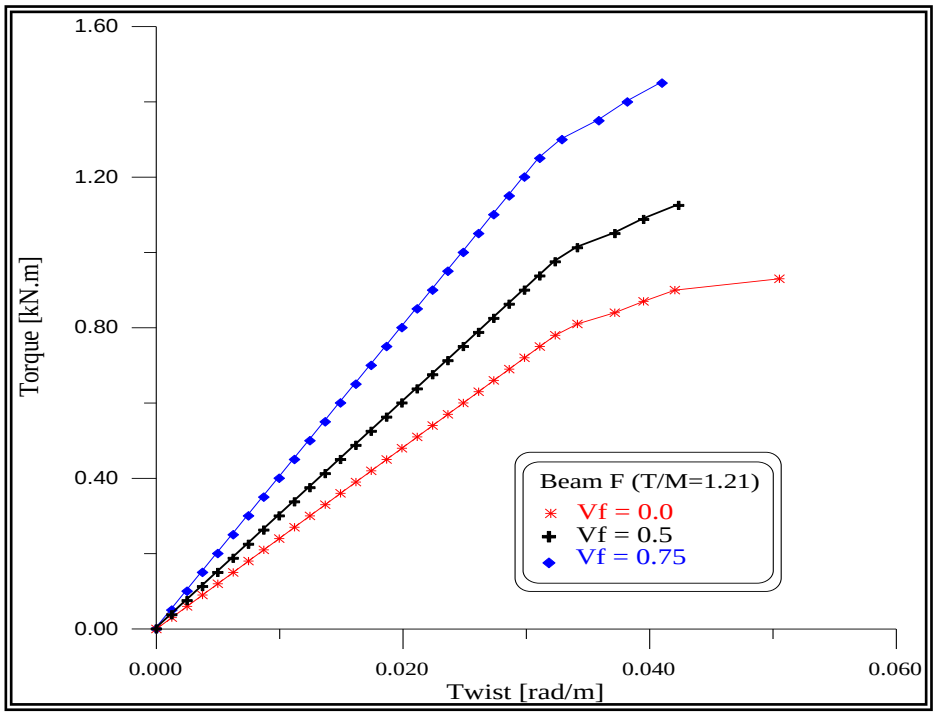

Fig. (5-16): Effect of Fiber Ratio
On the Torque – Twist Behavior for Beam (F)

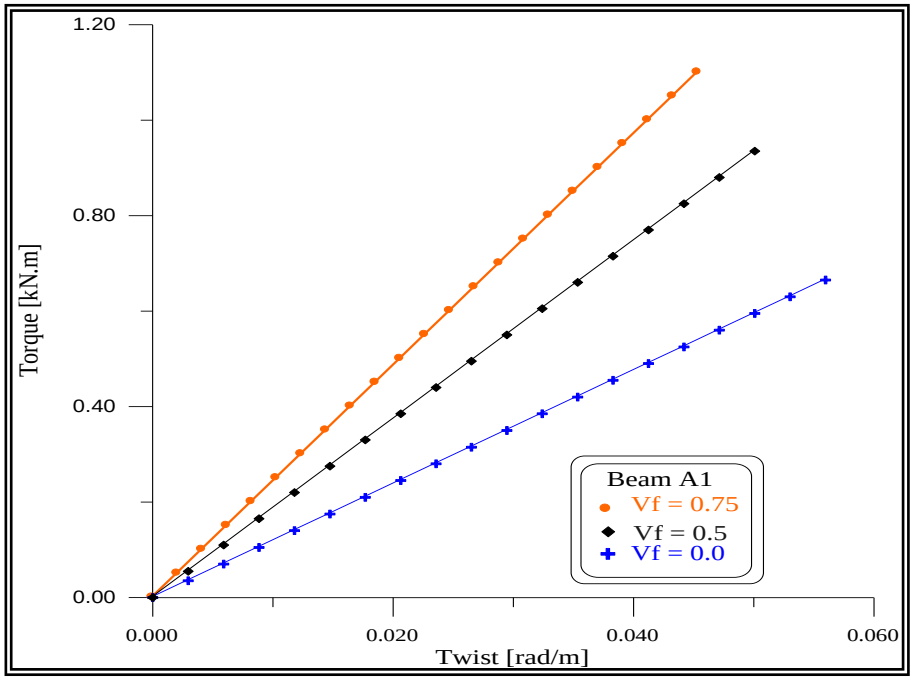

Fig. (5-17): Effect of Fiber Ratio

On the Torque – Twist Behavior for Beam (A1)

5.4.5 EFFECT OF TENSION STIFFENING PARAMETERS (α_1 AND α_2):

To study the effect of tension stiffening parameters (α_1 and α_2) on the behavior and ultimate capacity of beams subjected to combined shear, bending and torsion loads, beam (H) has been analyzed with different values of (α_1) and (α_2).

Numerical tests of beam H with values of (α_1) equal to (5, 10, 15 and 30) have been carried out, in these tests (α_2) was set to (0.5) for beam H. Throughout the numerical tests of beam H the tension stiffening parameter (α_1), which represents the rate of stress release as the crack widens, has a strongly effect on the post cracking behavior of the tested beam. Fig. (5-18) show that the effect of (α_1) is largely influence on the post cracking response and the ultimate capacity of the beam. The higher

value of (α_1 = 30) causes slightly stiffer response while the lower value (α_1 = 5) shows a softer response. The best fit to the experimental results of beam H was obtained when (α_1) set is equal to (10).

To study the effect of the tension stiffening parameter (α_2), which represents the sudden loss in the tensile stress at instant of cracking, numerical tests on beam (H) with values of (α_2) equal to (0.3, 0.5and 0.6) have been carried out, in these tests (α_1) was set equal to (10) during the analysis. The parameter (α_2) has a significant effect on the post cracking torque-twist response and a small effect on the ultimate capacity of the tested beam as shown in Fig. (5-19). the best fit to the experimental results was obtained when (α_2) is equal to (0.5). Similar analysis has been carried out on beams of series (H) and (F) to choose the best values of tension stiffening parameters as listed in Table (5-3).

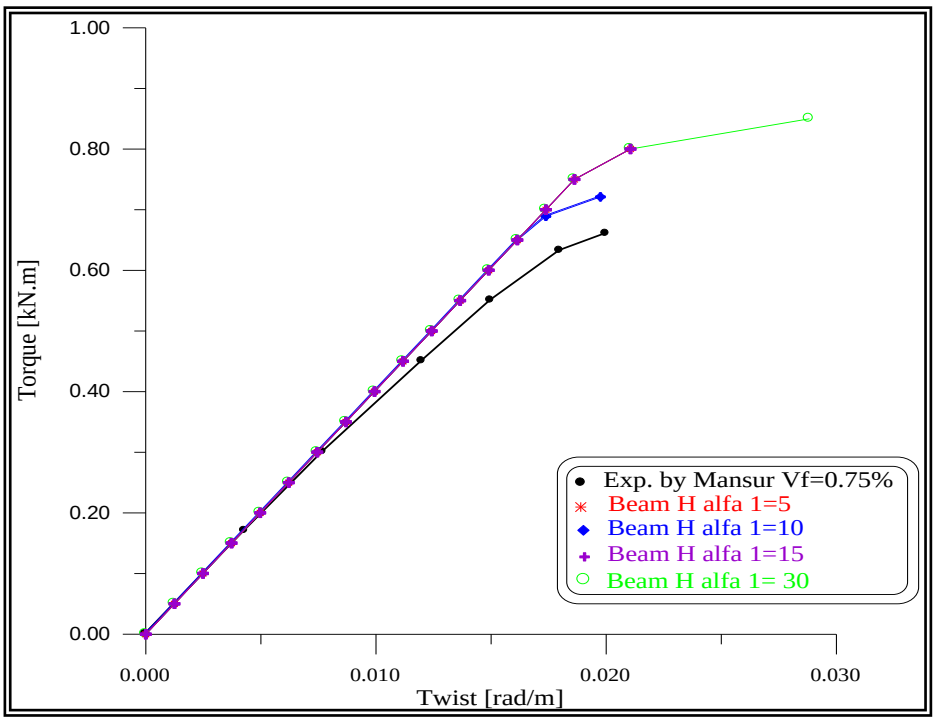

Fig. (5-18): Effect of Tension Stiffening Parameter (α_1) On the Torque – Twist Behavior of Beam (H) (Case Two)

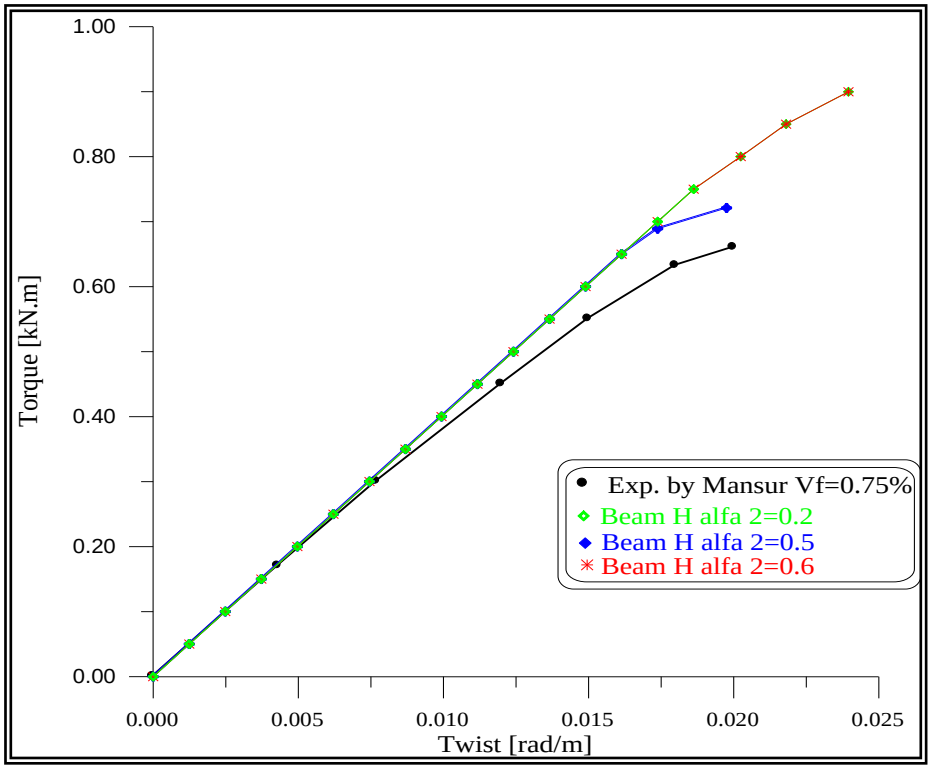

Fig. (5-19): Effect of Tension Stiffening Parameter (α_2) On the Torque – Twist Behavior of Beam (H) (Case Two)

5.4.6 EFFECT OF SHEAR RETENTION PARAMETER (γ_1, γ_2 AND γ_3)

Different values of shear retention parameters (γ_1, γ_2, and γ_3) have been used in a numerical test of beam (H) to study the effect of shear retention parameters on the torque – twist response and ultimate capacity of the tested beam. Numerical tests with values of (γ_1) which represents the rate of decay of the shear stiffness as the crack widens equal to (5, 10, 15 and 30) and (γ_2) equals to (0.5) and (γ_3) equals to (0.1) were carried out. A slightly stiff response was obtained for (γ_1) equal to (30), as shown in Fig. (5-20). the best fit to the experimental results of the tested beams is obtained when (γ_1) is equal to (10). Three numerical tests on beams (H) with (γ_2) equal to (0.2, 0.5, and 0.7), the parameters (γ_1) and (γ_2) were set equal to (10) and (0.1) respectively in all tests have been considered to

study the effect of shear retention parameter (γ_2) which represents the sudden loss in shear stiffness at instant of cracking. The results of these tests show that no significant effect of (γ_2) on the torque-twist curve of the tested beam as shown in Fig. (5-21). The best value of (γ_2) for the tested beams was set equal to (0.5). The effect of shear retention parameter (γ_3) which represents the residual shear stiffness due to dowel action is examined by four numerical tests of beams (H) with (γ_3) equals to (0.05, 0.1 and 0.3). Fig. (5-22) show that (γ_3) has a small effect on the behavior and slightly effect on the ultimate capacity of the tested beam, the best value of the parameter (γ_3) has been taken equal to (0.1). From the results of the above testes of parameters (γ_1, γ_2 and γ_3) it is clear that a small effect of these parameters on the behavior and ultimate capacity of the tested beam. Thus, for beams of series (H) and (F) can use values (10, 0.5, and 0.1) for parameters (γ_1, γ_2 and γ_3) respectively.

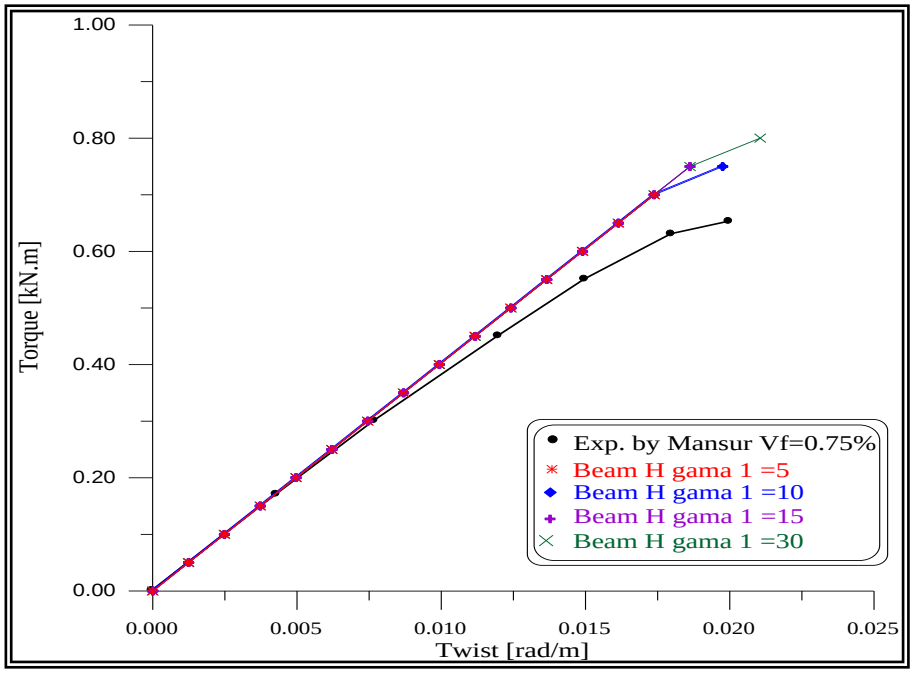

Fig. (5-20): Effect of Shear Retention Parameter (γ_1)
On the Torque – Twist Behavior of Beam (H) (Case Two)

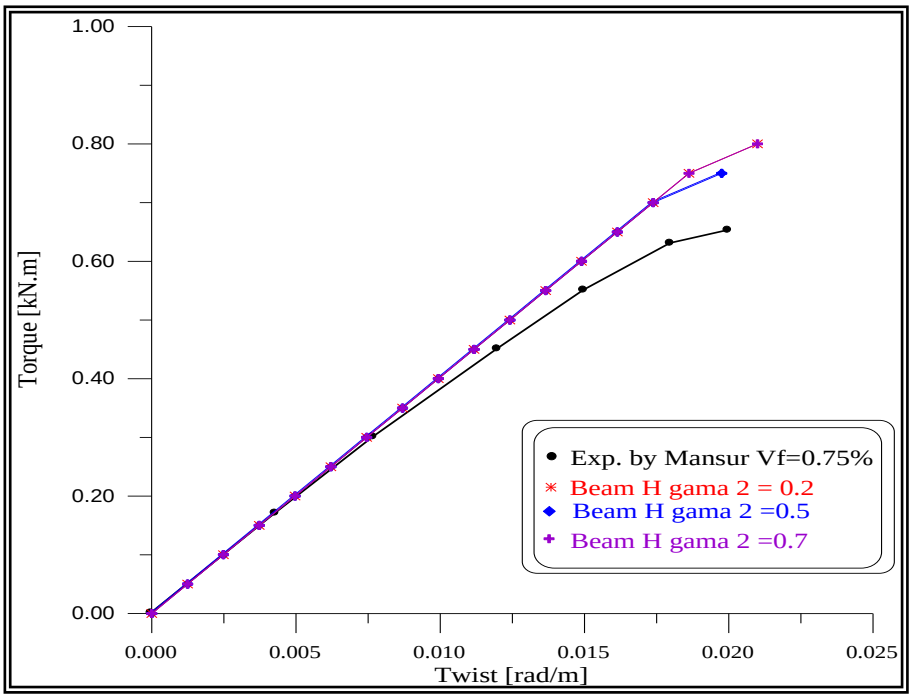

Fig. (5-21): Effect of Shear Retention Parameter (γ_2)

On the Torque – Twist Behavior of Beam (H) (Case Two)

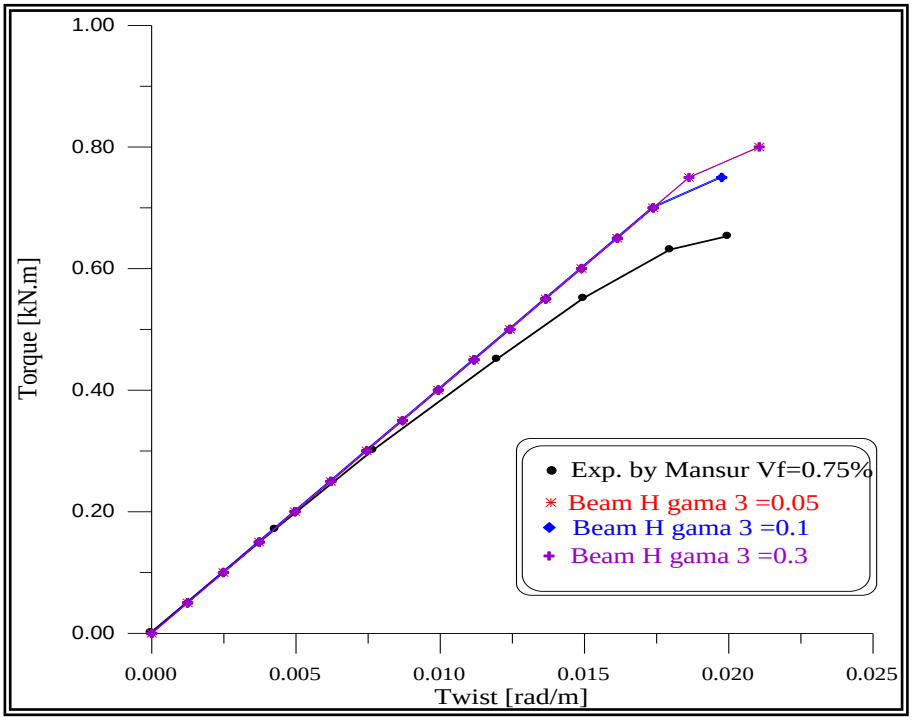

Fig. (5-22): Effect of Shear Retention Parameter (γ_3)

On the Torque – Twist Behavior of Beam (H) (Case Two)

5.4.7 EFFECT OF POISSON'S RATIO (υ)

The beam (H) was analyzed using three different values of Poisson's ratio. These values are (0.15, 0.2, and 0.3). Fig. (5-23) shows that no considerable difference is noticed in torque-twist response and ultimate capacity of the tested beam for Poisson's ratio equal to (0.15 and 0.2) but the value (0.3) gives decreasing ultimate capacity of the tested beam. The best value of Poisson's ratio was set equal to (0.2) for beams of series (H) and (F).

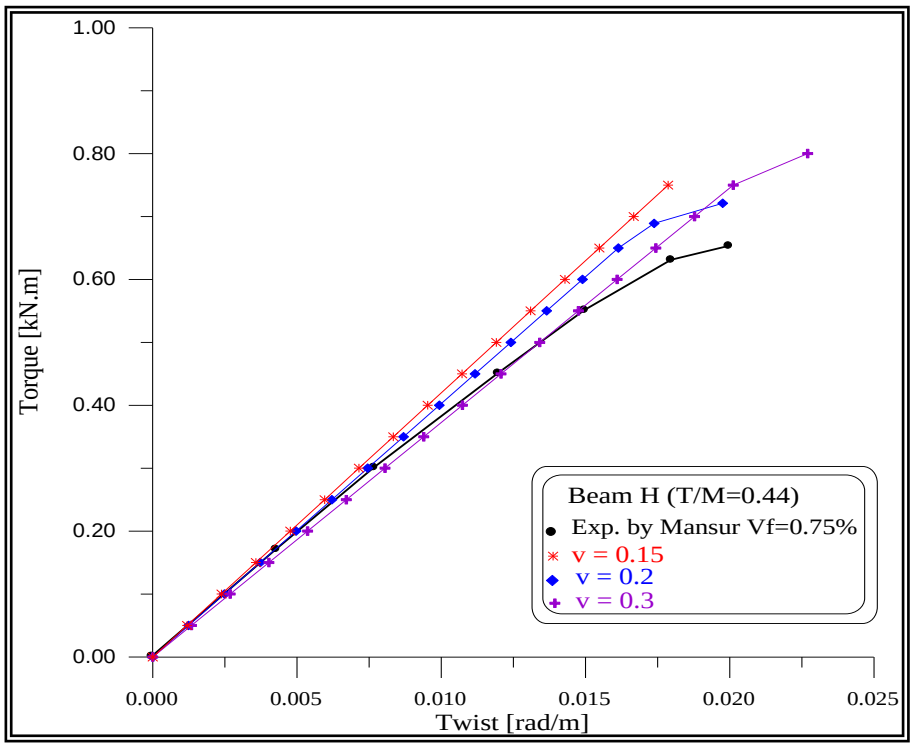

Fig. (5-23): Effect of Poisson's Ratio (υ) on the Torque – Twist Behavior of Beam (H) (Case Two)

5.4.8 EFFECT OF INTEGRATION RULE

In order to study the accuracy and efficiency of the integration rule, beam (F) tested using two different rules. These are 15b and 27-point integration rule. The effect of integration rule on the torque – twist response is illustrated in Fig. (5-24). In general, this figure shows that significant difference is obtained between the effects of type of integration rule on the overall behavior of the tested beams. The 15b and 27-Gauss point rules give a different effect but 27 point rule is more close to the experimental results.

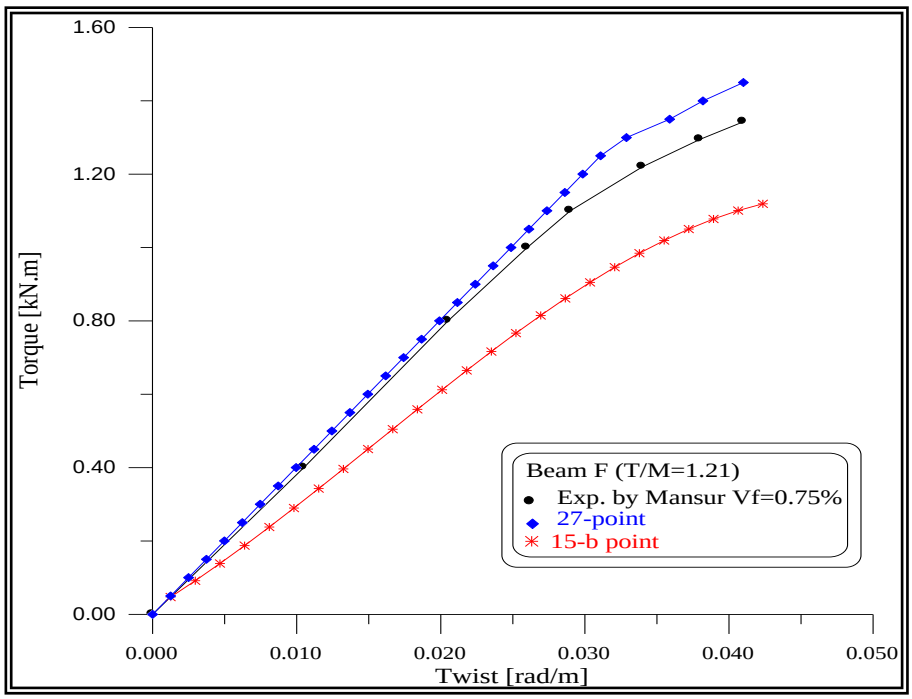

Fig. (5-24): Effect of Integration Rule on the Torque- Twist Behavior of Beam (F) (Case Two)

5.4.9 EFFECT OF (T/P) RATIO ON THE ULTIMATE CAPACITY

In order to study the effect of torque to transverse load (T/P) ratio on the ultimate capacity of concentrically beam (A2) which was subjected to combined shear, bending and torsion, many values of the ratio (T/P) have been considered. The results of the analysis are tabulated in Table (5-9), from the results it is clear that the ultimate torque is increase in the case of pure torsion and the ultimate load is increase in the case of pure shear compared with the combined loading.

Table (5-9): Ultimate Torque and Ultimate Load for Different Values of (T/P) Ratio of Beam (A2)

T/P [kN.m/kN]	T [kN.m]	P[kN]
1/1.84	1.4	2.576
1/0	1.8	0.0
0/1.84	0.0	5.152

5.5 OUTLINE OF THE COMPUTER PROGRAM

In the present study, the computer program **P3DNFEA** (Program of 3-Dimensional Nonlinear Finite Element Analysis) which is originally developed by **(Al-Shaarbaf** 1990), has been used. This program was coded in **FORTRAN-77** Language to analyze ordinary reinforced concrete

members under general three – dimensional state of loading up to failure.A special emphasis is given to the analysis of beams under torsion.

In the present study, new subroutines have been added to the main program, in order to improve the simulation of the post- cracking behavior of the steel fiber reinforced concrete**.** The flow chart of this program is given in appendix (A) to outline the main steps in the program.

Chapter Two

REVIEW OF LITERATURE

2.1 INTRODUCTION

This chapter reviews the previous experimental works of steel fiber concrete beams subjected to flexure, torsion, and combined shear, bending and torsion. The theories of torsion used to predict the torsion strength of concrete beams are presented in this chapter.

The nonlinear finite element analysis of steel fiber reinforced concrete beams subjected to flexure and torsion are also reviewed.

Concrete is the most frequently used construction material in the world. However, it has low tensile strength, low ductility, and low energy absorption. An intrinsic cause of the poor tensile behavior of concrete is its low toughness and the presence of defects. Therefore, improving concrete toughness and reducing the size and amount of defects in concrete would lead to better concrete performance. An effective way to improve the toughness of concrete is by adding a small fraction (usually 0.5 – 2 % by volume) of short steel fibers to the concrete mix during mixing (**Hartmann** 1999).

2.2 EXPERIMENTAL WORKS

A number of researchers have been interested with testing beams under combined torsion and bending such as (**Narayanan and Toorani** 1979). They have studied the influence of the steel fibers on the torsional and flexural rigidity of the concrete beams. They have found that the fiber reinforced concrete beams have a considerable post ultimate reseve and pronounced ductility. A satisfactory prediction of ultimate torque is obtained by using sand-heap analogy and a reduced value of tensile strength of concrete is assumed.

(**Mansur and Paramavisam** 1985) tested 33 steel fiber reinforced concrete beams under different combinations of torsion, bending and shear. Based on the skew bending theory, they derived two equations to predict the ultimate torsion moments .

$$Tu_2 = \frac{b^2 h}{3}(0.71 fr) \qquad \text{---------- (2-1)}$$

for mode (2)

$$Tu_1 = \frac{b^2 h}{3}\, fr\left[1 + 0.29\frac{(1-R)}{(1+R)}\right]\left[\sqrt{\left(\frac{1}{Q^2}+1\right)} - \frac{1}{Q}\right] \qquad \text{---------- (2-2)}$$

for mode (1)

where:

$$Q = \frac{T}{M}$$

$$R = \sqrt{1 + \left(\frac{Q}{3K}\right)^2}$$

k A numerical factor depending on h/b ratio

b The beam width

h The beam height

fr The modulus of rupture for the composite

$Tu1$ The ultimate torsional moment strength for mode one

$Tu2$ The ultimate torsional moment for mode two

T The applied torque

M The applied moment %.

This theoretical model gives good predictions of the ultimate torque of failure mode and interaction behavior of torsion, bending and shear.

Batson, et al. tested fiber reinforced concrete beams subjected to combined bending and torsion with different T\M ratios. The beams were reinforced with longitudinal steel bars only. The volume fractions of fibers in this experimental work were 0.0, 0.5, 1.0 and 1.5 percent.

Mindess (1980) investigated torsion tests of steel fiber reinforced concrete beams. Fiber contents ranged from 0 to 2.0 % by volume and two different fiber lengths. It was shown that the fiber reinforced specimens did not break completely into two pieces at the maximum load, while the unreinforced specimens did tend to hold the two halves together, thus providing certain a mount of post-cracking ductility. Most of the specimens' failure was due to the diagonal tensile stresses occurring at about 45º to the axis of the specimen and few specimens failed in shear. This probably due to the occurrence of localized regions of low fiber content in these specimens

Mansur (1982) made an experimental investigation on steel-reinforced concrete beams under combined bending and torsion. Ten groups of beams has used, each consisting of three specimens. On the basis of the observed skew-bending mechanism of torsional failure, equations were derived for ultimate torque. The main conclusions drawn from the work were:

1. Uncracked torsion stiffness of a beam was dependent on torsion to moment ratio.

2. Failure of a fiber-reinforced concrete beam in tension or in combined bending and torsion occurred by bending about a skew axis.
3. The increase in torsion strength with increasing beam depth was approximately linear.
4. A small increase in bending moment significantly reduces the torsion capacity.

Chern, et al., (1992**)** studied experimentally the strength and deformation behavior of steel fiber reinforced concrete subjected to multiaxial stresses. The tested results showed that steel fiber reinforced concrete performed better than plain concrete, particularly when tensile stresses were involved. Adding steel fibers to cementations materials improved many engineering properties by providing a different deformation and failure mechanism than that of a plain cementations matrix, the fibers could provide a crack arrest mechanism and thus greatly improved the toughness of concrete. The effect of fiber was more obvious under tensile loading than compressive loading.

Noghabai (2000**)** investigated shear and bending on beams of fibrous concrete. The tests were conducted on 32 beams with four different depths: 250, 300, 500, and 700 mm. Various types of fibers (metallic and nonmetallic) were added to the concrete matrix. Contrast to the nonmetallic fibers, steel fibers were more able to redistribute the strains among the arisen cracks. It was found that the failure may also occur in the tension zone as a bond failure, which manifests in longitudinal splitting cracks.

2.3 THEORETICAL AND ANALYTICAL STUDIES

2.3.1 TORSION THEORIES

2.3.1.1 SKEW BENDING THEORY

This theory which was initially proposed by (**Lessig** 1959), has been widely used to compute the torsion capacity of reinforced concrete members. The basic characteristic of this approach is the formation of the skew failure surface which was initiated by a helical crack along three faces of the member. The ends of the helical crack were connected by a compression zone near the fourth face. The skew failure surface intersects both the closed stirrups and the longitudinal steel.

The assumptions of this theory were, both stirrups and longitudinal steel yield at failure, the tensile strength of concrete was neglected, the spacing of the stirrups was constant within the failure zone, no external loads were presented within the failure zone, the effect of steel near the compression zone was neglected, and the shape of shear-compression zone was rectangular. Based on these assumptions the torsion strength can be determined by taking equilibrium of the free body about the axis of twist (internal torque equal to the external torque). The components of the internal torsion moment were the axial forces of the stirrups, the shear-compression face of concrete and the dowel forces of the longitudinal bars as shown in Fig. (2-1) (**Diab** 1998).

The theory was extended and modified by (**Hsu et.al.** 1968), **Hsu** made a major contribution experimentally to the development of the skew bending theory as it stand in the **ACI 318m-02 code**. **Hsu** proposed the following expression to calculate the ultimate torque for the rectangular section:

$$T_n = T_c + \alpha_t \frac{x_1.y_1}{s} A_t.f_{sy} \quad \text{---------- (2-3)}$$

$$\alpha_t = \frac{1}{3}\left(2 + \frac{y_1}{x1}\right) \leq 1.5 \quad \text{---------- (2-4)}$$

Where:

T_c: Torque resisted by concrete.

a_t: Coefficient accounts for crack geometry.

x1: Shortest length of the stirrups.

y1: Longest length of the stirrups.

A_t: Area of transverse steel.

Fsy : Yield stress of one leg of the stirrups.

s: Spacing of stirrups.

(T_c) was taken equal to (*0.4*) of cracking torque (T_{cr}) (**Pognani** 1992) hence:

$$T_c = 0.4\frac{x^2.y}{3}(0.85)f_r \quad \text{---------- (2-5)}$$

Where:

fr: Modulus of rupture of concrete.

x, y: The cross sectional dimensions of concrete members.

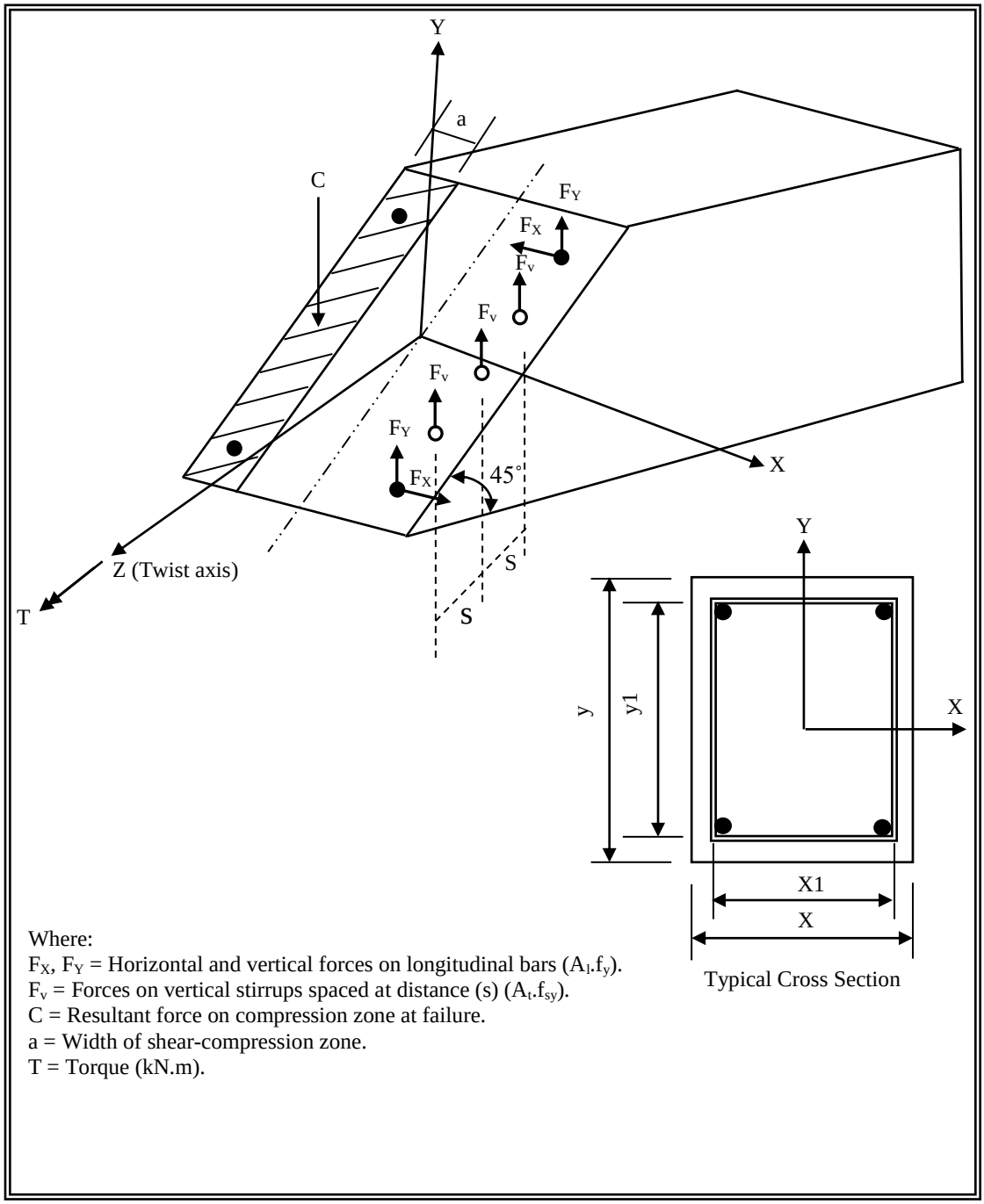

Where:
F_X, F_Y = Horizontal and vertical forces on longitudinal bars ($A_l.f_y$).
F_v = Forces on vertical stirrups spaced at distance (s) ($A_t.f_{sy}$).
C = Resultant force on compression zone at failure.
a = Width of shear-compression zone.
T = Torque (kN.m).

Fig. (2-1): Skew Bending Failure and Forces Acting on a Skew Plane at Failure of Reinforced Concrete Beam (**Diab** 1998)

2.3.1.2 SPACE TRUSS ANALOGY

This theory, which was originally developed by (**Rausch** 1929), assumed that a member with arbitrary solid cross-section was assumed to act like a tube, so that the external torsion moment was resisted by circulatory shear flow in the wall of the tube. Each wall segment of the tube was assumed to act like a plane truss where the longitudinal bars served as a chord member while the stirrups and the concrete within the segment served as the web members. After cracking, the concrete is separated by 45-degrees cracks into a series of helical members. These helical concrete members were assumed to interact with the longitudinal and hoop steel bars to form a space truss as shown in figure (2-2). This figure illustrates that the torsion is resisted by the tangential component of the diagonal compression which produced a shear flow (q), around the perimeter. This shear flow (q) was related to the applied torque (T) by the equilibrium equation:

$$T = 2A_o.q \qquad \text{---------- (2-6)}$$

Where (A_o) is the area enclosed by the shear flow path (q).

The longitudinal component of the diagonal compression is balanced by tension in the longitudinal bars.

Lampert and **Thurlimann** (1968) proposed two modifications to the **Rauschs** approach. The first modification was that the crack inclination (θ) which was assumed equal to 45-degrees by **Rausch** was assumed to be variable; hence the model is called the variable – angle truss model. Secondly, assumed that the perimeter connecting the centeriod of the corner longitudinal bars represent the centerline of the shear flow.

Collins and **Mitchell** (1980) suggested thin-walled tube approach which represents an extension to the space truss analogy. This approach

assumes that the concrete cover outside the centerline of the stirrups provides the resistance of torsion by the outer skin of the cross section roughly centered on the closed stirrups as shown in figure (2-3). The **ACI 318M-02 code** adopted the thin walled tube space truss analogy.

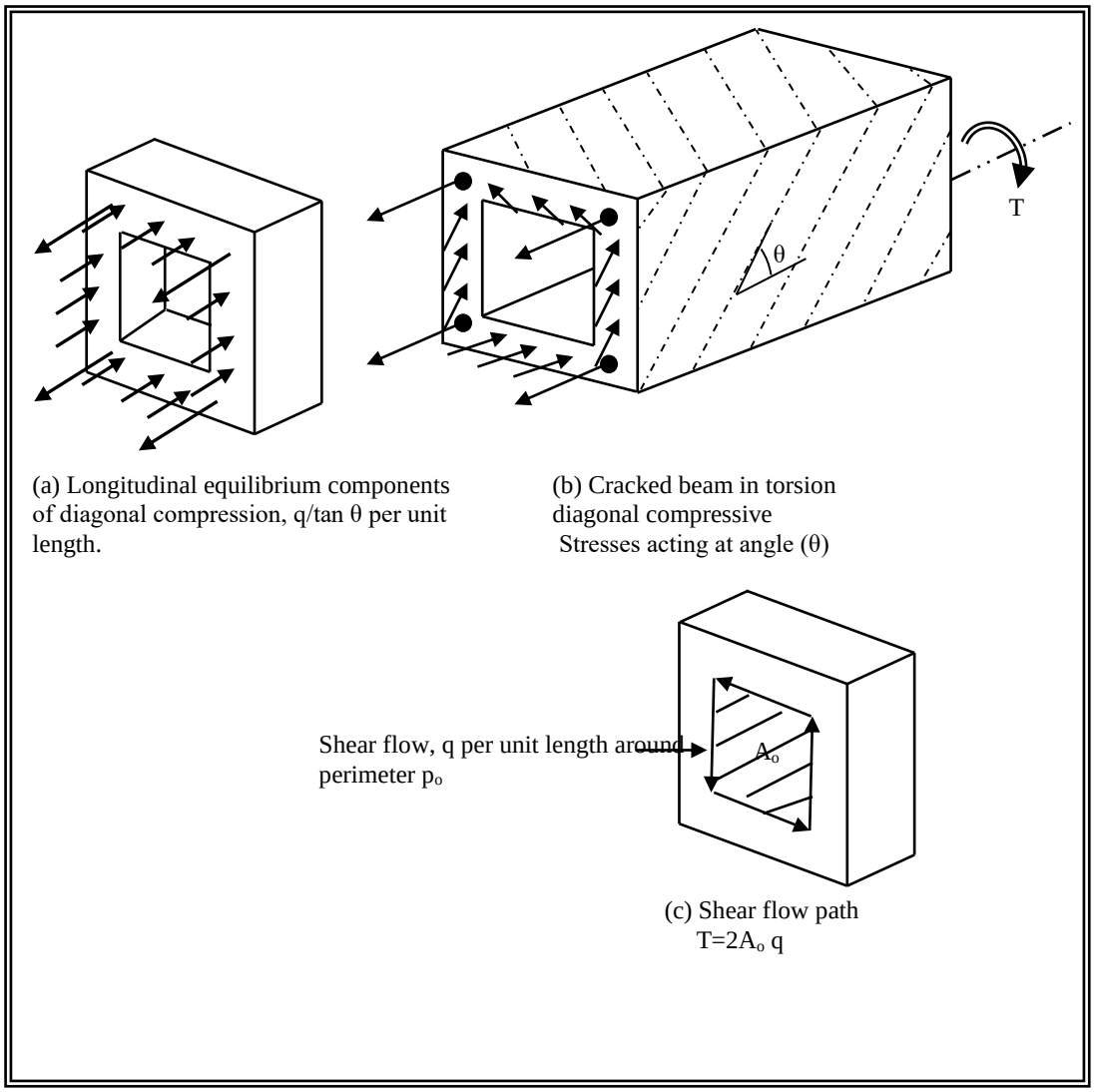

Fig. (2-2): Space Truss Model for Hollow Rectangular Reinforced Concrete Beam (**Collins** and **Mitchell** 1980)

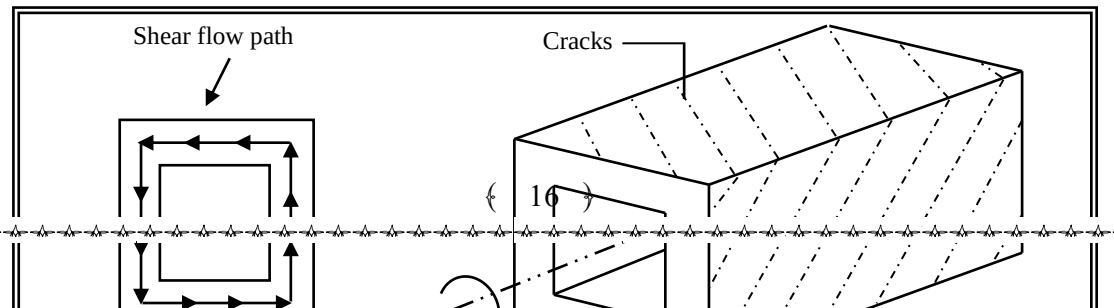

2.3.2 ANALYTICAL STUDIES

It is found that the 20-noded brick element is very efficient when used in the non-linear analysis of beams subjected to torsion and torsion plus bending so it will be adopted throughout this work.

Swamy, et al. (1974) predicted the first crack and ultimate flexural strength of randomly oriented steel fibrous concrete, using equations developed by crack control-composite mechanics approach. The various factors which influence the fiber reinforcement of cement matrices were briefly discussed. The equations showed an excellent correlation with available test result from various studies.

These equations are:

(a) First crack composite strength;

$$f_{cf} = 0.843\, f_m V_m + 2.93 V_f \frac{L_f}{D_f} \quad \text{[MPa]} \qquad \text{---------- (2-7)}$$

(b) The ultimate composite flexural strength;

$$f_{cu} = 0.976V_m + 3.41V_f \frac{L_f}{D_f} \text{ [MPa]} \quad \text{---------- (2-8)}$$

where

V_m, V_f The volume fraction of the matrix and fiber respectively.

L_f, D_f The length and diameter of the fiber respectively [mm].

f_m The tensile strength of the matrix [MPa].

(Al-Ta'an 1978) used the finite element method for the non-linear analysis of reinforced concrete fibrous beams. The reinforced concrete beams were assumed in a state of plane stress. The concrete and the steel reinforcement were represented by constant strain triangular element. Nonlinearities due to cracking, compressive behavior of concrete, steel and bond stress-slip were taken into account. The ultimate loads; deflection, crack propagation and crack patterns were predicted satisfactorily.

(Murugappan, et al. 1992**)** developed a non-linear finite element model for the analysis of reinforced fibrous concrete beams under predominant shear. The finite element formulation treated the crack reinforced fiber concrete as an orthotropic non-linear elastic material, based on smeared rotating crack model. Appropriate constitutive relation for the cracked fiber reinforced concrete, accounting for the post-cracking tensile strength and softening in compression were used in the principal stress-strain directions to define the secant module.

(**AL-Ta'an** 1992**)** described a method for nonlinear flexural analysis of concrete beams, with both longitudinal steel bars and steel fibers. The method took into account the nonlinear response of the fiber concrete in compression and the stiffening effect of steel fibers in the tension zone in the pre and post crack stages. The analysis was performed under monotonic increasing loads and capable of tracing the behavior of

members in the post peak stages. The analytical results obtained such as deflection, curvature, strains, neutral axis position, maximum crack width, and ultimate loads showed good agreement with the published test results.

(Allose 1995**)** extended the work of (**Al-Sha'arbaf** 1990) by analyzing steel fiber reinforced concrete beams in torsion. The 8 and 20-nodded brick element were presented to model the concrete. while the steel bars were simulated as axial members embedded within the concrete. Perfect bond was assumed between steel bars and concrete. Also some effects were studied such as warping restraint, hollowing out the cross-section and adding a small amount of discrete steel fiber to the concrete on the post-creaking behavior and the ultimate torque.

(Gencoglu, et al. 2002) studied several methods which have been developed to predict the flexural strength of beams reinforced with both bars and fibers. Fig. (2-4) shows that one of these methods was developed by Ezeldin and Shiah and presented as follows:

$$f_{tu} = 0.00772 \times F_{be} \times (L_f \times D_f) V_f \text{ [MPa]} \quad \text{---------- (2-9)}$$

where

F_{be} The bond efficiency factor of fibers, which varies from 1.0 to 1.2 depending upon fiber characteristics.

V_f The percent of fibers by volume.

After the cross-section is cracked, by using the compressive stress strain and tensile stress–strain relationship of SFRC, the moment equilibrium equation can be written with respect to the location of Cc and is given in expression (2-10).

$$M = A_s f_{st}(d - \lambda_c) + A_s' f_{sc}(\lambda_c - d') + C_T(\lambda_T - \lambda_C) \quad \text{--- (2-10)}$$

where

S_T The tensile force of As,

S_C The compressive force of As,

C_C The compressive force of SFRC,

C_T The tensile force of SFRC,

f_{St} The steel tensile stress of As,

f_{Sc} The steel compressive stress of As$^{\backslash}$,

y_c The neutral axis depth.

λ_C, λ_T Are the locations of C_C and C_T force, respectively.

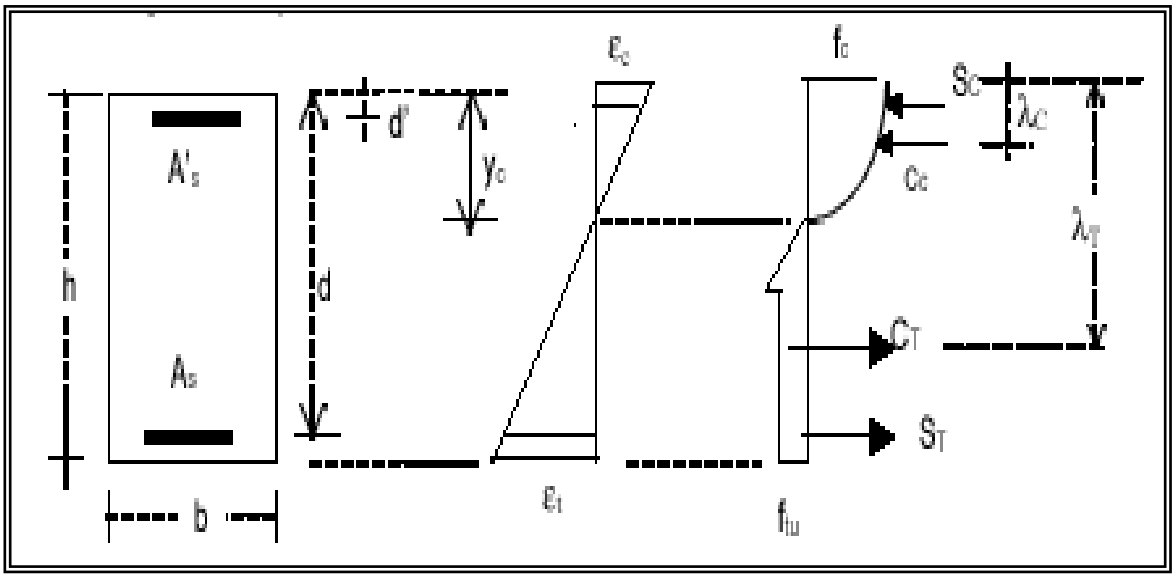

Fig. (2-4) bending behavior of SFRC beams (Gencoglu 2002)

(Lee, et al. 2002**)** proposed empirical equation and studied the effects of steel fibers and/or steel hoops in fly ash concrete. The proposed equation fitted well in various concrete mixtures including steel fibers and/or hoops, and can be found useful in studying the behavior of fly ash

concrete structures reinforced with steel fibers in addition to the standard steel reinforcing bars and stirrups. It is found that the addition of steel fibers improves the post peak behavior. This proves that addition of steel fiber is good for ductility improvement. As indicated in Fig. (2.5), the ductility of concrete can be significantly improved by adding steel fibers and/or hoops in concrete.

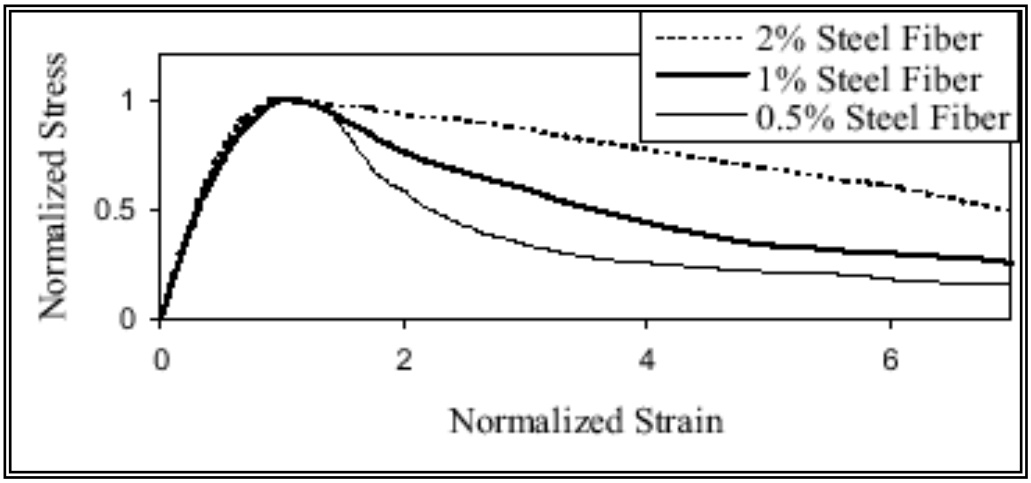

Fig. (2-5) Normalized Stress-Strain Curve for Steel Fiber Concrete,20% Fly Ash Replacement**, (Lee** and **Punurai** 2002**)**

(R. Santhakumar, et al. 2007**)** presented a numerical study on unretrofitted and retrofitted reinforced concrete beams subjected to combined bending and torsion. Different ratios between twisting moment and bending moment were considered. The finite elements adopted by ANSYS were used in this study. For the purpose of validation of the finite element model developed, the numerical study was first carried out on the unretrofitted reinforced concrete beams that are experimentally tested and reported in the literature. Then, the study was extended for the same reinforced concrete beams retrofitted with carbon fiber reinforced plastic composites with ±45o and 0/90o fiber orientations. The study revealed that the CFRP composites with ±45o fiber orientations were more

effective in retrofitting the RC beams subjected to combined bending and torsion for higher torque to moment ratios.

2.4 SUMMARY:

It is clear from the preceding review that there are a few detailed studies that deal with the inelastic non-linear behavior of reinforced fibrous concrete members with openings under combined shear and torsion. This problem is treated in this study, by using 20-node brick element with 60 degrees of freedom is employed to model the concrete. Steel reinforcement is represented by embedded bar through the brick element with perfect bond between concrete and steel.

The hardening rule, flow rule, tension stiffening and crushing state are taken into account. Also, Material non-linearity is taken into account.

Chapter One

INTRODUCTION

1.1 GENERAL

Reinforced concrete (R.C) has become one of the most important construction materials and is widely used in many types of engineering structures. The economy, efficiency, strength and stiffness of the reinforced concrete make it an attractive material for a wide range of structural applications. For its use as a structural material, concrete must satisfy the following conditions (**Kwak** 1997):

1. The structure must be strong and safe. The proper application of the fundamental principles of analysis, the laws of equilibrium and the consideration of the mechanical properties of the component materials should result in a sufficient margin of safety against collapse under accidental overloads.
2. The structures must be stiff and appear unblemished. Care must be taken to control deflections under service loads and to limit the crack width to an acceptable level.
3. The structures must be economical.

Reinforced concrete structures are commonly designed to satisfy criteria of serviceability and safety. In order to ensure the serviceability requirements, it is necessary to predict the cracking and the deflections of RC structures under service loads. In order to assess the margin of safety of R.C structures against failure, an accurate

estimation of the ultimate load is essential and the prediction of the load-deformation behavior of the structure throughout the range of elastic and inelastic response is desirable.

The development of analytical models of the response of RC structures is complicated by the following factors (**Kwak** 1997):

- Reinforced concrete is a composite material made up of concrete and steel, two materials with different physical and mechanical behavior.
- Concrete exhibits nonlinear behavior even under low level of loading due to nonlinear material behavior, environmental effects, cracking, biaxial stiffening and strain softening.
- Reinforcing steel and concrete interact in a complex way through bond-slip and aggregate interlock.

The present study is part of this continuous effort and concerns the analysis of steel fiber reinforced concrete member with openings under combined shear, bending and torsion.

1.2 FIBER REINFORCED CONCRETE

Fiber reinforced concrete is a concrete mix that contains short discrete fibers that are uniformly distributed and randomly oriented. Fiber material can be steel, cellulose, carbon, polypropylene, glass, nylon, and polyester (**Gebman** 2001). The amount of fibers added to a concrete mix is measured as a percentage of the total volume of the composite (concrete and fibers) termed volume fraction (Vf). Vf typically ranges from 0.1 to 3% (**Gebman** 2001). Aspect ratio (L_f/D_f) is calculated by dividing fiber length (L_f) by its diameter (D_F). For fibers with a non-circular cross section, an equivalent diameter for the calculation of aspect ratio is usually used.

This research focuses on steel fibers. Steel fiber length ranges from 1.5 to 75 mm and aspect ratio ranges from 30 to 100 (**Gebman** 2001). Fiber shapes are illustrated in Fig. (1-1).

The typical applications for fiber reinforced concrete include (**Radmix**):

- Explosive and impact resistant structures.
- Shotcrete in mining/tunneling.
- Slabs and pavements on ground.
- Refectory shotcrete and castables.
- Dam and water course lining.
- Pipeline coatings.
- Airport taxiways.
- Chemical containment requirements.
- Highways and roadways.
- Seismic resistant structures.
- Precast elements.
- Bored piers.
- Spillways.

Fibers work with concrete utilizing two mechanisms (**Gebman** 2001), the spacing mechanism and the crack bridging mechanism. The spacing mechanism requires a large number of fibers which are well distributed within the concrete matrix to arrest any existing micro-crack that could potentially expand and create a sound crack. For typical volume fractions of fibers, utilizing small diameter fibers or micro fibers can ensure the required number of fibers for micro crack arrest.

The second mechanism termed crack bridging requires larger straight fibers with adequate bond to concrete. Steel fibers are considered a prime example of this fiber type that is commonly referred to as large diameter fibers or macro fibers. Benefits of using discrete steel fibers, Fig. (1-2),

includes impact resistance, flexural and tensile strengths, ductility, and fracture toughness.

The shortcoming of using steel fibers in concrete is reduction in workability. Workability of steel FRC is affected by fiber aspect ratio and volume fraction as well as the workability of plain concrete. As fiber content increases, workability decreases, Most researchers limit Vf to 2.0% and L_f/D_f to 100 to avoid unworkable mixes (**Gebman** 2001). In addition, some researchers have limited the fiber reinforcement index [$V_f \times (L_f/D_f)$] to 1.5 for the same reason. To overcome the workability problems associated with SFRC, modification of concrete mix design is recommended. Such modifications can include the use of additives.

The steel fibers can be used on their own, or combined with other reinforcement to improve the energy absorbing capabilities and significantly increase spalling and impact resistance. The properties of steel fibers are listed in Table (1-1).

Table (1-1): Physical Property of S.F.R.C (**Radmix**)

Physical Property	**Beneficial Effect**
Modulus of Rupture	1 to 2 × plain concrete
Shear Strength	1.25 to 2 × plain concrete
Torsional Strength	1.25 to 2 × plain concrete
Impact Energy Absorption	2 to 15 × plain concrete
Fatigue Resistance	1.2 to 2 × plain concrete
Cavitations and Erosion	1 to 1.4 × plain concrete
Resistance Restrained Shrinkage Cracks	Reduced Crack widths

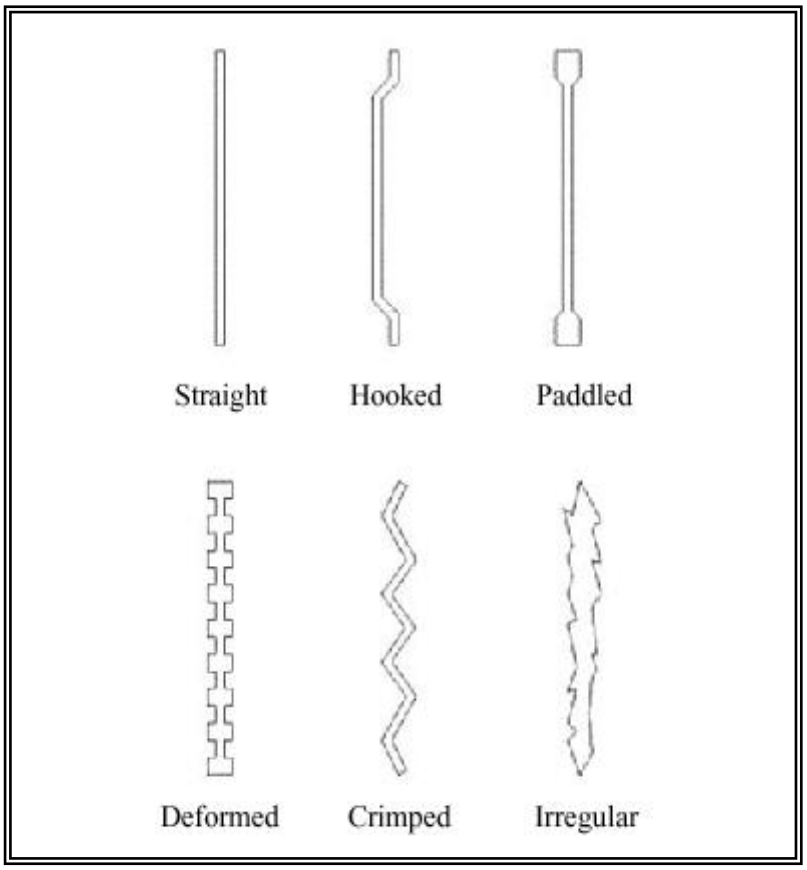

Fig. (1-1) Shapes of steel fibers

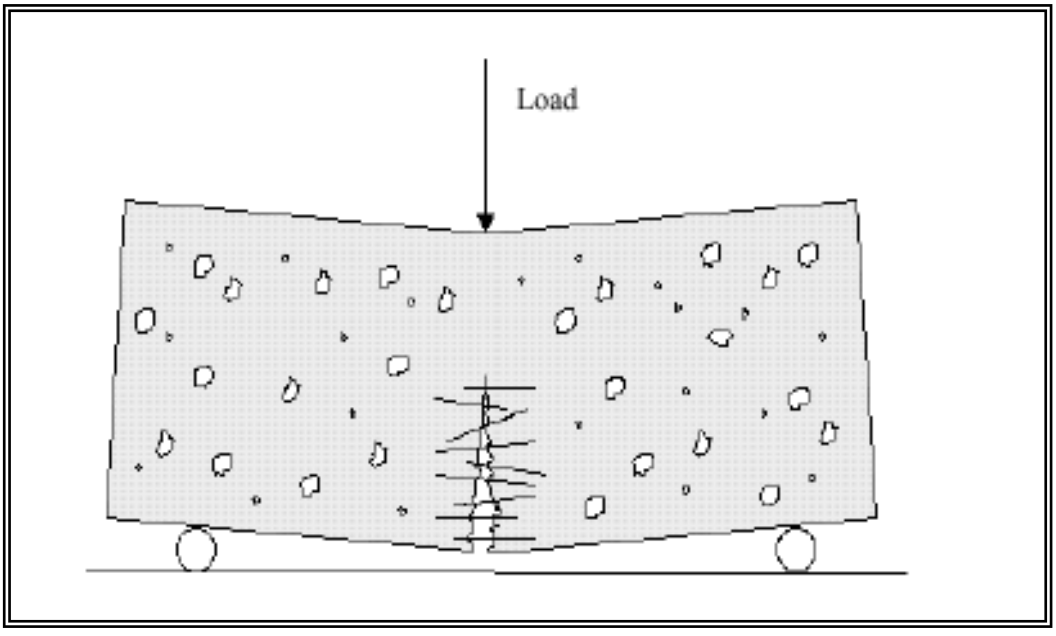

Fig. (1-2) Bridging action of steel fibers

1.3 OBJECTIVES AND SCOPE

The basic objective of the work is to study the effect of openings on strength and the overall behavior of steel fiber reinforced concrete beams under combined shear, bending and torsion.

The presence of openings in the steel fiber reinforced concrete beams in addition to nonhomogeneites of reinforced concrete, material nonlinearity and cracking patterns makes the problem more complex. Three-dimensional finite element method will be used to predict the overall behavior, stresses and strains components, at various stages of loading and to predict the cracking initiation and the failure load. Material nonlinearities due to cracking of the concrete, plastic flow or crushing of concrete and yield condition of reinforcement are considered. The maximum tensile strength of concrete is used as a criterion for cracking initiation. The tension stiffening of concrete will be used to describe post-cracking behavior of the concrete. The aggregate interlocking effect and the dowel action are incorporated in the model.

1.4 LAYOUT OF THE THESIS

This thesis consists of ***six chapters***. ***The first chapter*** gives an introduction to the subject of research and its objectivity. ***Chapter two*** introduces a literature review to the related previous studies. The basic concepts of the finite element method and the derivation of the governing equilibrium equations using the principle of virtual displacements are presented in ***chapter three***. The 20-noded brick element, the representation of concrete and steel, the integration rules, the incremental-iterative Newton-Raphson methods and nonlinear solution techniques are also presented in this chapter.

Material properties-modeling of fiber reinforced concrete in brief description are outlined in ***chapter four***. In ***chapter five*** several numerical examples are presented and verified with previous analytical and experimental studies. ***Chapter six*** gives the conclusions and suggestions for future research.

Chapter Six

CONCLUSIONS AND RECOMMENDATIONS FOR FUTURE WORKS

6.1 INTRODUCTION

The following conclusions are drawn with regard to the results of the present finite element analysis of reinforced concrete beams with steel fiber subjected to pure torsion and combined shear, bending and torsion with openings described in the previous chapter, are presented in this chapter. The suggestions for the future works are also presented in this chapter.

6.2 CONCLUSIONS

1. The three dimensional nonlinear finite element model and the proposed simulation of the material in the present study are capable of predicting the behavior of reinforced concrete beams subjected to pure torsion and for combined shear, bending and torsion. The results of the analysis are in good agreement with the experimental results, with a difference range (10%) of ultimate torque for pure torsion and while for beams subjected to combined shear, bending and torsion the difference in ultimate torque is (8.9%).

2. The effect of presence of discrete steel fiber on increasing ultimate torque has been studied. It can be concluded that, by adding (0.75%) of steel fiber the ultimate torque may increases by (35%, and 40%) for beams with or without openings respectively for the consider problems.
3. The results of the present finite element analysis shows that the location of openings has a large effect, where this effect is the largest when openings location is at tension zone and a small effect when openings location is at compression zone. The ultimate torque may decreased by amount (27.58%).
4. It is found that the ultimate torque increase with decrease for the area of openings, where the ultimate torque increase a bout (28%) as a compared with solid beam for opening's area (4%) and a bout (24%) for opening's area (2%).
5. The effect of opening shape on the ultimate torque depends on the size of tension zone. Therefore, if the designer has to provide an opening in a reinforced concrete beam, he should keep it in the compression zone.
6. The results of finite element analysis indicate that the tension stiffening parameters (α_1 and α_2) have a significant effect on the torque – twist behavior and the ultimate torque capacity of reinforced concrete beams under pure torsion and combined shear, bending and torsion. While, the shear retention parameters (γ_1, γ_2, and γ_3) have small effects on the behavior and ultimate torque capacity.
7. The addition of steel fibers reduces the number of cracks and slow crack propagation during incremental loading. The cracking torque is a bout (18%) more than the case of no steel fiber.

6.3 RECOMMENDATIONS FOR FUTURE WORKS

1. Analysis of prestressed concrete beams containing steel fiber under combined shear and torsion with openings can be carried out by modifying the material model used in the present study.
2. Analysis of reinforced concrete beams with steel fiber under cycle load with openings.
3. Studying the effect of fiber on the light weight concrete.
4. More numerical research works is required for studying the interaction between shear, bending, and torsion for different shapes of reinforced concrete beams with steel fiber.